SINGLE-MOLECULE FLUORESCENCE RESONANCE ENERGY TRANSFER STUDY OF SNARE-MEDIATED MEMBRANE FUSION

BY

JIAJIE DIAO

DISSERTATION

Submitted in partial fulfillment of the requirements
for the degree of Doctor of Philosophy in Physics
in the Graduate College of the
University of Illinois at Urbana-Champaign, 2010

Urbana, Illinois

Doctoral Committee:

Assistant Professor Yann Chemla, Chair
Professor Taekjip Ha, Director of Research
Professor John Rogers
Assistant Professor Aleksei Aksimentiev

ABSTRACT

This is a comprehensive study of protein-mediated membrane fusion through single-molecule fluorescence resonance energy transfer (smFRET). Membrane fusion is one of the important cellular processes by which two initially distinct lipid bilayers merge their hydrophobic cores, resulting in one interconnected structure. For example, exocytosis, fertilization of an egg by a sperm and communication between neurons are a few among many processes that rely on some form of fusion. Proteins called soluble N-ethylmaleimide-sensitive factor attachment protein receptor (SNARE) play a central role in fusion processes which is also regulated by many accessory proteins, such as synaptotagmin, complexin and Munc18.

By a new lipid mixing method at the single-vesicle level, we are able to accurately detect different stages of SNARE-mediated membrane fusion including docking, hemi and full fusion via FRET value of single donor/acceptor vesicle pair. Through this single-vesicle lipid mixing assay, we discovered the vesicle aggregation induced by C2AB/Ca^{2+}, the dual function of complexin, and the fusion promotion role of Munc18/SNARE-core binding mode.

While this new method provides the information regarding the extent of the ensemble lipid mixing, the fusion pore opening between two vesicular cavities and the interaction between proteins cannot be detected. In order to overcome these limitations, we then developed a single-vesicle content mixing method to reveal the key factor of

pore expansion by detecting the FRET change of dual-labeled DNA probes encapsulated in vesicles. Through our single-vesicle content mixing assay, we found the fusion pore expansion role of yeast SNAREs as well as neuronal SNAREs plus synaptotagmin 1.

To my family

ACKNOWLEDGMENTS

Dr. Taekjip Ha has been a good advisor for his profound insights and continuous encouragement during my graduate study. It is needless to say that this work would not be possible without his outstanding guidance and support. I also want to thank Dr. Sua Myong, who kindly supported everyone in the lab.

I really appreciate Dr. Yeon-Kyun Shin in Iowa State University and Dr. Tae-Young Yoon in KAIST for guiding me into this interesting SNARE field.

I also want to say thanks to all lab members in Dr. Ha's, Dr. Shin's, and Dr. Yoon's Lab, especially, to Yuji Ishitsuka, Zengliu Su, Xiaobin Lu, Bin Lu, Jiansong Tong, Janghyun Yoo, and Han-Ki Lee, who used to work together with me. In addition, supports from Julia Wright, Salman Syed, and Chirlmin Joo are important for my work.

I would like to thank the committee of Professors Yann Chemla, John Rogers and Alek Aksimentiev for overseeing my graduate study.

I hope to thank all my friends and my homeland, China.

Most importantly, I would like to take this chance to thank my family. My grandparents, my mother, my uncles, and my brother always stand with me and give me their sincere supports.

Finally, I want to say that all glory belongs to an important person in my life, Ms. Chen Shen, who sacrificed a lot to support me.

This work was supported by the National Institutes of Health (NIH R21 GM074526)

grant, the pilot fund from the Siteman Center for Cancer Nanotechnology Excellence (SCCNE), and L.S. Edelheit Family fellowship.

TABLE OF CONTENTS

LIST OF ABBREVIATIONS

APD Avalanche photodiode

βME 2-mercaptoethanol

bp base pair(s)

Biotin-DPPE 1,2-dipalmitoyl-sn-glycero-3-phosphoethanolamine-N-(biotinyl)

BSA Bovine serum albumin

CCD Charge-coupled device

Cy Cyanine dye

DiD 1,1'-dioctadecyl-3,3,3',3'-tetramethylindodicarbocyanine perchlorate

DiI 1,1'-dioctadecyl-3,3,3',3'-tetramethylindocarbocyanine perchlorate

DNA Deoxyribonucleic acid

dsDNA Double-stranded DNA

DOPE 1,2-Dioleoyl-sn-glycero-3-phosphoethanolamine

DOPS 1,2-dioleoyl-*sn*-glycero-3-[phospho-L-serine]

E FRET efficiency

E_{app} Apparent FRET efficiency

EGTA Ethylene glycol tetraacetic acid

EPR Electron paramagnetic resonance

FRET Föster (Fluorescence) resonance energy transfer

HEPES A buffer solution containing 5 mM HEPES/KOH, 100 mM KCl (pH 7.4)

I_A Emission intensity of an acceptor molecule

I_D Emission intensity of a donor molecule

MW Molecular weight

MD Molecular dynamics

OG n-octyl-D-glucopyranoside

PEG Polyethylene glycol

PIP2 Phosphatidylinositol 4,5-bisphosphate

POPC 1-palmitoyl-2-oleoyl-*sn*-glycero-3-phosphocholine

smFRET Single-molecule FRET

SNARE Soluble N-ethylmaleimide-sensitive factor attachment protein receptors

ssDNA Single-stranded DNA

TIR Total internal reflection

Tris trishydroxymethylaminomethane

Trolox 6-Hydroxy-2,5,7,8-tetramethylchromane-2-carboxylic acid

T50 A buffer solution containing 10mM Tris/HCl, 50mM NaCl (pH 8.0)

CHAPTER 1

INTRODUCTION

1.1 Membrane fusion

A biological membrane is a lipid bilayer made of two layers of lipid molecules, which forms a continuous barrier around cells to keep ions, proteins and other molecules. Natural bilayers are usually made mostly of phospholipids with a hydrophilic head and two hydrophobic tails. When phospholipids are exposed to water, they arrange themselves into a two-layered sheet (a bilayer) with all of their tails pointing toward the center of the sheet. Membrane fusion is a process by which two initially distinct lipid bilayers merge their hydrophobic cores, resulting in one interconnected structure. When fusion proceeds completely through both leaflets of both bilayers, a water-filled bridge is formed and the solutions contained by the bilayers can mix. Many important cellular processes, such as exocytosis, fertilization of an egg by sperm and communication between neurons, rely on some form of membrane fusion.

Four fundamental steps are in the fusion process [1]. First, two membranes approach each other to within several nanometers. Second, the two membranes come into very close contact (less than one nanometer). Third, a destabilization nucleates at one point between the two membranes with a highly localized rearrangement of the two bilayers. Finally, as this point defect grows, the components of the two membranes mix and diffuse away from the site of contact. At this point, the internal contents of the membranes may start to mix.

Biological fusion is almost always regulated by the action of membrane-associated proteins with one of them called soluble N-ethylmaleimide-sensitive factor attachment protein receptors (SNAREs) which play a critical role in eukaryotic cell system. SNARE-mediated membrane fusion is a ubiquitous process involved in a wide variety of important life activities, such as neurotransmitter release [2]. Neurons communicate through molecules called neurotransmitters which relay messages across the synaptic cleft between two neurons at the synapse. Synaptic vesicles in the axon bulb containing neurotransmitters are produced by the neuron and are released in the submillisecond time scale by exocytosis into the synaptic cleft (Figure 1.1). This fast neurotransmitter release is triggered by calcium influx and is tightly controlled by a number of regulators, such as SNARE proteins, synaptotagmin, complexin, and Munc18 [3,4,5,6].

1.2 SNARE proteins

With extensive evidence of proving them as minimal fusion machinery [7,8], SNARE proteins have been accepted as the engine that can pull the opposing membranes together and then somehow merge them into one continuous bilayer structure [9,10]. We mainly focus on two SNARE systems; either yeast mediated post-Golgi protein trafficking on the plasma membrane or synapse mediated neurotransmitter release triggered by calcium ions. Both of these SNARE systems consist of three components. According to their compartment distribution in the cell, they are classified as v-SNARE including synaptobrevin in neuron and Snc2p in yeast, and t-SNARE, which are composed of SNAP-25 & syntaxin in neuron and Sec9 & Sso1p in yeast (Figure 1.2).

As shown in Figure 1.2, the three SNARE components can form a ternary complex in the ratio of 1:1:1 via the association of their 'SNARE motifs'. In this ternary complex, three 'SNARE motifs' from t-SNARE proteins and one 'SNARE motif' from v-SNARE assemble into a four-helix bundle composed of 15 hydrophobic layers [11,12].

1.3 SNARE-mediated fusion pathway

Membrane fusion involves a concerted assembly of proteins and an exquisite rearrangement of lipid bilayers. It has been suggested that multiple steps are needed to accomplish membrane fusion. First, the assembly of the SNARE ternary complex brings opposing membranes together and achieves the intimate contact of the outer leaflets. Then, the contacting outer leaflets merge and form a lipid 'stalk', an intermediate state called hemifusion in which the opposing outer leaflets merge together while the inner leaflets remain intact [13,14,15,16]. Next, the rupture of the hemifusion diagram leads to a fusion pore. At last, the expanding of the fusion pore enables content mixing and finishes the full fusion (Figure 1.3). The essence of this hemifusion model is that the initial connection of two merging outer leaflet is lipids. An alterative model suggests that there exists a protein hemi-channel lined with the SNARE transmembrane segments in each membrane [17,18]. The assembly of the trans-SNARE complex brings the two opposing membranes close and connects the protein channels to form a protein fusion pore, directly leading to the content communication.

The evidence of the protein pore was provided by combined amperometry capacitance measurements. Jackson's group suggested that a protein pore was formed by a circular arrangement of five to eight syntaxin transmembrane segments in the plasma

membrane [18]. However, in a previous study using the same PC12 cells, Hua and Scheller deduced that only three syntaxin-containing complexes are required for Ca^{2+}-triggered excocytosis [19]. Based on the protein pore model, a vesicle-membrane counterpart formed by VAMP transmembrane segments was needed to complete their model, the EPR data from Dr. Shin's laboratory in Iowa State University indicated that there is no strong interaction between the transmembrane domains of VAMP, which did not support the protein pore model.

Hemifusion to full fusion transition is an accepted model for viral systems [20,21,22,23]. With viral fusion, proteins in only one of the opposing membrane were minimally required. Hemifusion intermediate was also visualized indirectly using x-ray diffraction [24]. By modifying the transmembrane domain or lowering the concentration of the fusion protein, a hemifusion intermediate was observed in Dr. Shin's laboratory [16]. After that, a large amount of evidence was provided in different laboratories to support that SNARE protein-mediated membrane fusion transits through a hemifusion intermediate state [15,25,26,27].

1.4 SNARE accessory proteins

It has widely accepted that SNARE proteins play a central role in membrane fusion. In living cells, the neurotransmitter release finishes in the submillisecond time scale upon coming to calcium ions. However, *in vitro* studies show that the lipid mixing induced by SNARE proteins needs hours to finish. Thus, it is reasonable to predict that the assembly of the SNARE complex and the fusion pathway are regulated extensively by other accessory proteins *in vivo* [3]. As identified by *in vivo* knockout method, three SNARE

accessory proteins, synaptotagmin, complexin, and Sec1/Munc18, are the most important regulators for the membrane fusion related to the fast neurotransmitter release (Figure 1.4).

1.4.1 Synaptotagmin

Synaptotagmin is a synaptic vesicle protein with a transmembrane domain on the N-terminal. It has been regarded as a calcium sensor to control the stimulus-coupled exocytosis. Synaptotagmin contains two cytoplasmic C2 domains, C2A and C2B, and both of them act as Ca ion binding sites [28]. These two C2 domains can also interact with negatively charged lipid membranes. With a membrane-associated SNARE complex, C2AB (C2A & C2B, the cytoplasmic part of synaptotagmin) can bind simultaneously to the lipid bilayer, as well as the SNARE complex, to form a quaternary SNARE-synaptotagmin-Ca^{2+}-phospholipids complex, which significantly increases the neuronal SNARE-mediated membrane fusion [29,30,31]. However, some *in vitro* experiments with full-length synaptotagmin have not been able to observe the Ca^{2+}-evoked acceleration of SNARE-mediated membrane fusion [32,33]. Through our single-vesicle lipid mixing technique, we found that C2AB and Ca^{2+} mainly induce vesicle aggregation [34].

1.4.2 Complexin

Complexin is a water soluble protein which can tightly bind to the SNARE complex to form an alpha helix [35]. It was suggested that the complexin works as a fusion clamp to the membrane-anchored SNARE complex. With the help from calcium ions, synaptotagmin can replace complexin and induce the synchronization membrane fusion

[36,37,38]. However, some results show that complexin plays a positive role in membrane fusion as well. Recently, our lab revealed a dual function of complexin, as, on one hand, it inhibits the formation of SNARE complexes, while on the other hand, once SNARE complexes are formed, it enhances membrane fusion [39].

1.4.3 Sec1/Munc18

Sec1/Munc18 is crucial for SNARE-mediated membrane fusion. Neurotransmitter release was totally abolished in Munc18 knockout mice [40,41]. Munc18 binds tightly to the closed conformation of syntaxin, which stabilizes the syntaxin during its transportation process to the plasma membrane *in vivo* [42,43]. In addition, it has been suggested that the N-terminal segment of syntaxin, Habc domain, is necessary for interacting with Munc18 to promote SNARE complex assembly [44,45,46,47,48]. Most recently, our single-pair vesicle-vesicle lipid mixing experiments indicated that Munc18 could increase the lipid mixing both for full-length syntaxin and syntaxin without Habc domain [49].

1.5 Questions

As summarized by Table 1, the main players of fast neurotransmitter release have been identified so far. Almost all membrane proteins for fusion have been identified, however, a detailed mechanism still remains ambiguous. Through the single-vesicle and -molecule technique, we hope to solve some important questions for SNARE-mediated membrane fusion, such as

1. The fundamental role of SNARE proteins,

2. The regulation of accessory proteins,

3. The interaction between SNARE and accessory proteins.

Table 1. Key proteins involving in the SNARE-mediated membrane fusion.

Name	Family	Location	Function
synaptobrevin	SNARE	Synaptic vesicle	To form SNARE complex, which is known as the minimum fusion machinery
SNAP-25	SNARE	Target membrane	
syntaxin	SNARE	Target membrane	
complexin		Free	Dual-functional regulator
synaptotagmin		Synaptic vesicle	Calcium sensor
Munc18	SM	Free	Docking and priming regulator

Chapter 1 Figures:

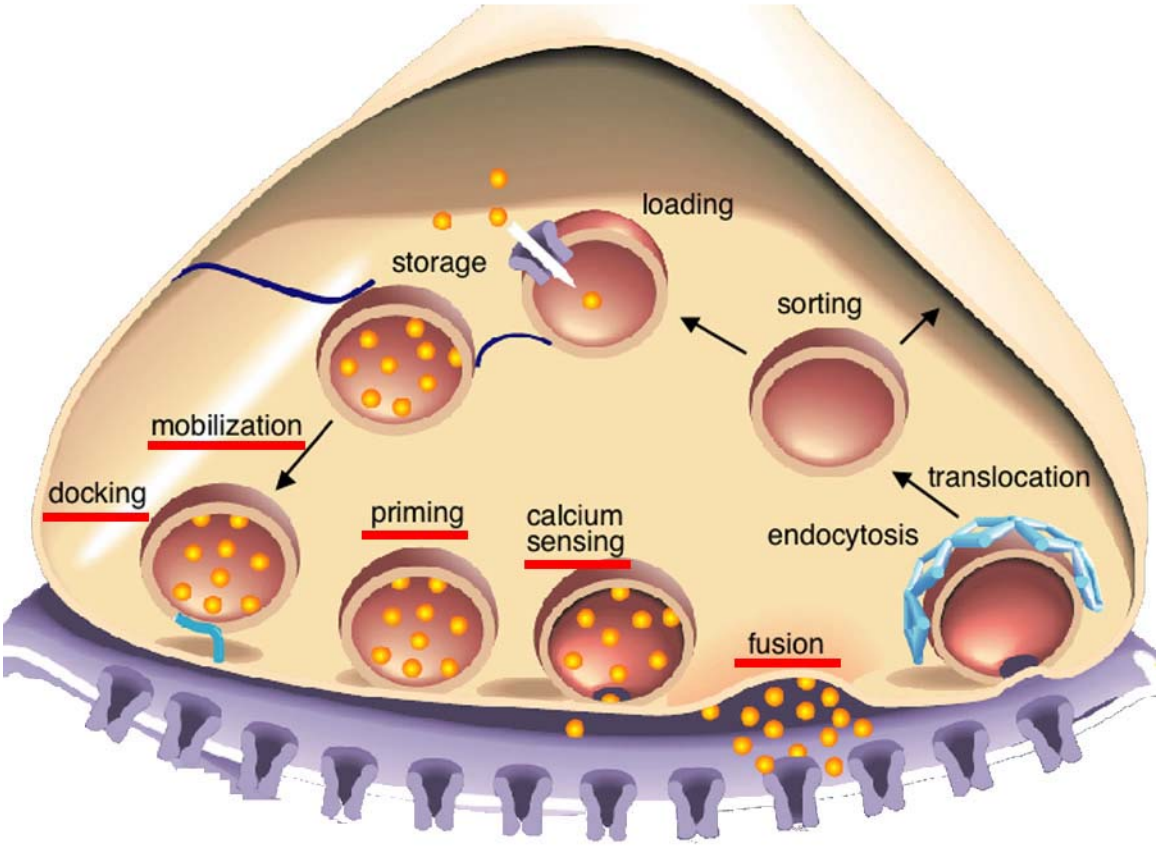

Figure 1.1. Neurotransmitter release cycle. Steps highlighted by red lines are regulated by SNAREs and accessory proteins involved in the thesis. (Modification based on: http://www.wormbook.org/chapters/www_synapticfunction/synapticfig1.jpg)

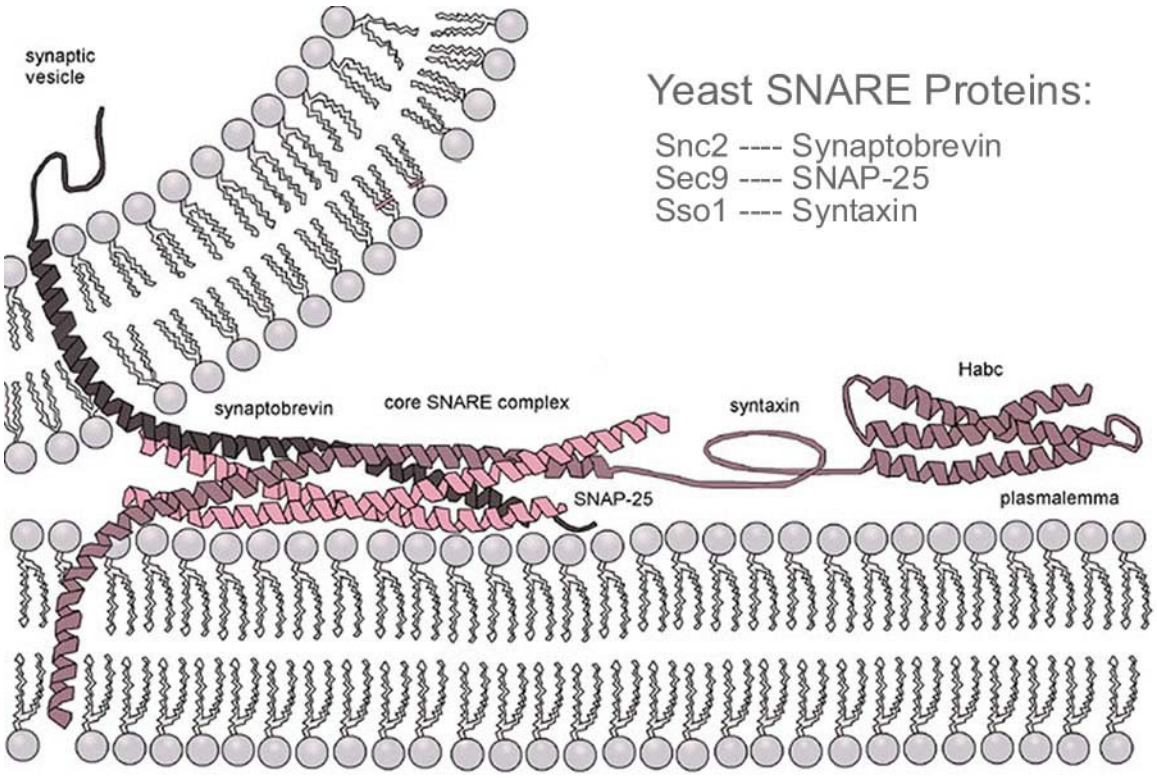

Figure 1.2. Neuronal SNARE proteins. (Modification based on: http://en.wikipedia.org/wiki/File:Exocytosis-machinery.jpg)

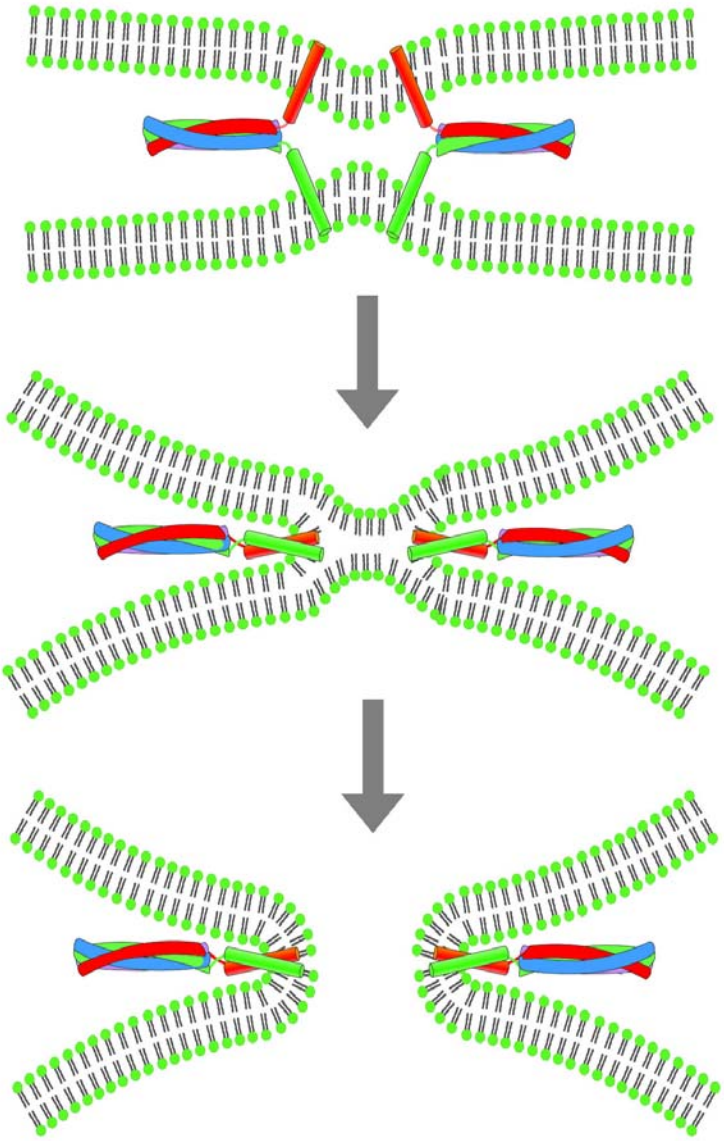

Figure 1.3. SNARE-mediated membrane fusion pathway.

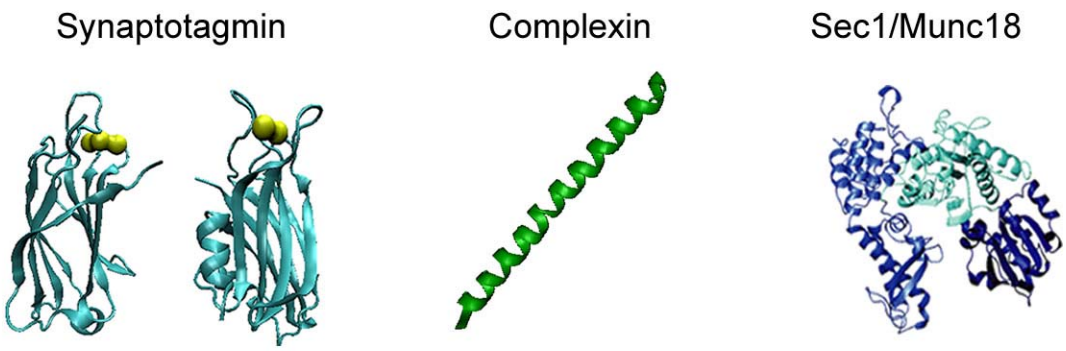

Figure 1.4. Neuronal SNARE accessory proteins.

CHAPTER 2

METHODOLOGY

2.1 Biological aspect

Traditionally, most studies rely on two major techniques, *in vivo* knockout and *in vitro* reconstitution methods [3,9]. While these two methods have many advantages, they come short in either isolating the function of the single contributing factor or revealing the fast and transient fusion dynamics.

2.1.1 Yeast SNARE proteins

Plasmid construction, protein expression and purification for yeast SNAREs were described in detail previously [50]. In brief, Sso1pHT (amino acids 185-290), which the N-terminal α-helical Habc domain was truncated and full-length Snc2p (amino acids 1-115) were expressed as the N-terminal glutathione S-transferase (GST) fusion proteins. Sec9c (amino acids 401–651 of Sec9) was expressed as a C-terminal His6-tagged protein. Recombinant proteins were expressed in *E. coli* Rosetta (DE3) pLysS (Novagen). The glutathione-agarose beads (Sigma) were used to purify Sso1pHT and Snc2p. The protein-bound GST beads were washed excessively with washing buffer (PBS, pH 7.4) containing 0.2% (v/v) Triton X-100. Following the buffer exchange with (PBS, pH 7.4) containing 0.8% (w/v) n-octyl-D-glucopyranoside (OG, Research Product International), the protein of interest was cleaved on column by thrombin in cleavage buffer (50 mM Tris/HCl, 150 mM NaCl, 0.8% OG, pH 8.0). His6-tagged Sec9c was purified using the Ni-NTA agarose beads (QIAGEN). The beads were washed with washing buffer (25 mM

HEPES, 100 mM KCl with 20 mM immidazole, pH 7.4), and then the protein was eluted out by the elution buffer (25 mM HEPES, 100 mM KCl with 150 mM immidazole, pH 7.4).

2.1.2 Neuronal SNARE proteins

Recombinant neuronal SNARE proteins syntaxin 1A (amino acids 1-288), SNAP-25 (amino acids 1–206), and VAMP2 (amino acids 1-116) are from rat. All of these proteins were expressed as N-terminal GST fusion proteins in *E. coli* Rosetta (DE3) pLysS. The cells were grown at 37 ^{o}C in LB medium with 100 mg/ml ampicillin until OD600 reached 0.6-0.8. The cells were further grown for 6 hours after adding IPTG (0.5 mM final concentration) at 16 ^{o}C for syntaxin 1A and VAMP2 or at 24 ^{o}C for SNAP-25. Cell pellets were resuspended in 10 ml PBS buffer, pH 7.4, containing 0.5% (v/v) Triton X-100, with a final concentration of 1 mM 4-(2-aminoethyl)-benzenesulfonyl fluoride (AEBSF), 2mM DTT. Cells were lysed by the sonication in an ice bath and centrifuged at 13,000 g for 20 minutes at 4 ^{o}C. The supernatant was mixed with glutathione-agarose beads in PBS buffer and nutated in the cold room (4 ^{o}C) for 2 hours. Proteins were cleaved by thrombin in cleavage buffer (50mM Tris/HCl, 150 mM NaCl, pH 8.0) with 0.8% OG.

2.1.3 Accessory proteins

Complexin 1: The plasmid for complexin 1 (amino acids 4-134) from rat was kindly provided by Dr. Josep Rizo (University of Texas Southwestern Medical Center). Complexin 1 was expressed as a glutathione S-transferase fusion protein. Recombinant

proteins were expressed in *E. coli* Rosetta (DE3) pLysS (Novagene, Madison, Wisconsin). The cells were grown at 37 °C in LB with 100 g/ml ampicillin until OD600 reached 0.6-0.8. The cells were further grown for 4-6 hours after adding isopropylthio-b-d-galactopyranoside (0.5 mM) at 24 °C. Recombinant proteins were purified using glutathione-agarose chromatography. Cell pellet was resuspended in 10 ml PBS buffer (phosphate-buffered saline with 0.5% (v/v) TritonX-100, pH 7.4) with the final concentrations of 1 mM AEBSF, 5 mM DTT. Cells were broken by sonication on the ice bath and centrifuged at 13000 g for 20 minutes at 4 °C. The supernatant was mixed with 2 mL glutathione-agarose beads in PBS and nutated in cold room for 2 hours. The proteins were then cleaved by thrombin in HEPES buffer (25 mM HEPES, 100 mM KCl, pH 7.4). Purified proteins were examined with 15% SDS-PAGE, and the purity was at least 90%.

C2AB: The plasmid for C2AB (amino acids 140-421) of rat Synaptotagmin 1 was a kindly gift from Dr. Josep Rizo (University of Texas South Western Medical Center). The C2AB was inserted into PGEX-KG expression plasmid and expressed in *E. coli* Rosetta (DE3) pLysS (Novagen). To purify C2AB, cell pellet was resuspended in 10 mL PBS buffer (pH 7.4, with 0.5% (v/v) TritonX-100) with the final concentrations of 2 mM AEBSF, 2 mM EDTA, and 2 mM DTT. The cell was broken by sonication on the ice bath and centrifuged at 13000 g for 20 minutes at 4 ºC. The supernatant was mixed with 2 ml glutathione-agrose beads and nutated in cold room for 2 h. After nutation, the beads were washed with a high salt buffer (25 mM HEPES, 1 M NaCl, PH 7.4) four times. In the high salt buffer, 1 mM $MgCl_2$, DNase (20 lg/ml) and RNase (4 lg/ml) were added and incubated for 6 h at 4 ºC. After washing by high salt buffer twice and low salt buffer (50

mM Hepes, 0.1M NaCl, PH 7.4) five times, the protein was cleaved from GST beads by thrombin in low salt buffer.

Munc18-1: C-terminal His6-tagged Munc18-1 plasmid is a kind gift from Dr. James McNew at Rice University. The Mucn18-1 protein was expressed in *E. coli* Rosetta (DE3) pLysS (Novagene). The cells were grown at 37 ^{o}C in LB medium with 30 μg/ml of kanamycin until the A600 reached 0.6-0.8. Isopropyl-β-D-thiogalactopyranoside (IPTG) was added to a final concentration of 0.5 mM. The cells were grown further for three more hours at 37 ^{o}C, and then collected by centrifugation at 6000 r.p.m. for 10 minutes. The cell pellets were resuspended in lysis buffer (25 mM HEPES/KOH, 100 mM KCl, 20 mM immidazole, 2 mM AEBSF, and 2 mM dithiothreitol (DTT), pH7.4). After sonication on ice, the cell lysate was centrifuged at 15000 g for 20 minutes at 4 ^{o}C. The supernatant was mixed with nickel-nitrilotriacetic acid-agarose beads (Qiagen) and nutated for binding at 4 ^{o}C for one hour. After binding, the beads were washed with washing buffer (25 mM HEPES/KOH, 100mM KCl, and 20 mM immidazole, pH 7.4). Then the protein was eluted out by elution buffer (25 mM HEPES/KOH, 100mM KCl, 150 mM immidazole, pH 7.4). Purified proteins dialyzed overnight against dialysis buffer (25 mM HEPES/KOH, 200 mM KCl, 10% glycerol, and 1mM DTT, pH 7.4).

2.1.4 Lipid mixing protein reconstitution

Unilamellar vesicles containing 45:15:40 (mol/mol/mol) 1-palmitoyl-2-oleoyl-sn-glycero-3-phosphocholine (POPC):1,2-dioleoyl-sn-glycero-3-[phospho-L-serine] (DOPS):cholesterol (Avanti Polar Lipids) and 2 mol% DiI (1,1'-dioctadecyl-3,3,3',3'-tetramethylindocarbocyanine perchlorate, Molecular Probes/Invitrogen, Carlsbad,

California) were formed by the extrusion method (Mini-Extruder, Avanti Polar Lipids). The t-SNARE protein complexes, 1:1 (mol/mol) Syntaxin:SNAP-25, were then reconstituted in the unilamellar vesicles through dialysis. The v-SNARE protein (VAMP2) was reconstituted in a different population of unilamellar vesicles that were doped with 2 mol% DiD (1,1'-dioctadecyl-3,3,3',3'-tetramethylindodicarbocyanine perchlorate, Molecular Probes) and 0.1 mol% biotinylated lipids 1,2-dipalmitoyl-sn-glycero-3-phosphoethanolamine-N-(biotinyl) (Biotin-DPPE, Avanti Polar Lipids). In both t- and v-SNARE vesicles, the lipid to protein ratio was kept at 200:1.

2.1.5 Content mixing protein reconstitution

One tube of mixture of POPC, DOPS, and cholesterol (molar ratio of 45:15:40) in chloroform was dried to form a lipid film on the wall of the glass tube. The same procedures and lipid components were applied to prepare another tube of lipid mixture except containing 0.1 mol% biotinylated lipid. The dried lipid film was resuspended with Tris-HCl buffer (10 mM Tris/HCl, 50 mM NaCl, pH 8.0) containing 10 μM target DNAs or 2 μM Cy3-Cy5 dual-labeled DNA probes (Integrated DNA Technologies), separately. After 5 freeze-thaw cycles, unilamellar vesicles were prepared by extrusion through polycarbonate filters (100 nm pore size, Avanti Polar Lipids).

For yeast SNARE system, Sso1pHT and Snc2p proteins were mixed with vesicles containing target DNA or vesicles containing dual-labeled DNA probes, separately, at a lipid/protein molar ratio of 200:1. The concentration of OG was kept at ~0.8% (w/v) during the reconstitution. After 4 ^{o}C incubation for 20 minutes, the protein/lipid mixtures were diluted two times to make the concentration of OG below the critical micelle

concentration (~0.6% w/v). The mixtures were then dialyzed overnight against HEPES buffer (25 mM HEPES/KOH, 100 mM KCl, pH 7.4) at 4 ^{o}C.

For neuronal content mixing, syntaxin and SNAP25 were mixed together to pre-form the t-SNARE complex for 1 hour at room temperature. Then, t-SNARE complex was mixed with vesicles containing target DNAs and v-SNARE proteins were mixed with vesicles containing dual-labeled DNA hairpin probes at a lipid/protein molar ratio of 200:1 at 4 ^{o}C for 20 minutes (~0.8% OG). The protein/lipid mixtures were diluted two times. The t-vesicle mixture was dialyzed overnight against HEPES buffer (25 mM HEPES/KOH, 100 mM KCl, pH 7.4) at 4 ^{o}C. However, the v-vesicle mixture was dialyzed overnight against acetate buffer (20 mM HAc/KOH, 100 mM KCl, pH 4.5) and then transferred to the HEPES buffer (25 mM HEPES/KOH, 100 mM KCl, pH 7.4) for additional 5 hours of dialysis before use. For the synaptotagmin 1 study, DOPE and PIP2 were used to recover the Calcium respond *in vitro*.

2.2 Physical aspect

Since 90's, ensemble Förster Resonance Energy Transfer or Fluorescence Resonance Energy Transfer (FRET) [51] has been a standard *in vitro* tool for studying SNARE-mediated membrane fusion of protein-reconstituted liposomes. [7] Recently, the single-molecule FRET has been applied for protein-protein interactions and membrane fusion process [52,53].

2.2.1 Förster Resonance Energy Transfer or Fluorescence Resonance Energy Transfer (FRET)

FRET is a popular biological technique because it is a non-invasive and powerful method to help observe reactions in biologically relevant conditions. Since the FRET degree changes only when fluorophore-labeled molecules are within the range of several nanometers, this helps us understand molecular interactions, such as protein-protein, protein-DNA and antibody-antigen. FRET contributes to the understanding of structural properties and dynamics of biomolecules.

The basic mechanism of FRET is shown in Figure 2.1. When a fluorophore (dye 1) is excited by a photon, it enters an excited state when the photon brings enough energy. After a few nanoseconds, dye 1 emits another photon of longer wavelength due to the vibration levels of the molecule. This is called fluorescence. When another fluorophore (dye 2) is near dye 1 and the absorption spectrum of dye 2 significantly overlaps with the emission spectrum of dye1, dye 2 absorbs the energy of dye 1. This is called fluorescence resonance energy transfer (FRET). Dye 1 is called the donor, while dye 2 the acceptor. Then, the acceptor emits another photon with an even longer wavelength. The FRET efficiency follows the equation of $1/(1+(R/R_0)^6)$, where R_0 is characterized by the spectral overlap, the quantum yield of donor and other factors. In single-molecule measurements, cyanine dyes are widely used because of their photostability. In our study, donor molecules (Cy3 or DiI) are excited by a 530 nm solid-state laser. Acceptors (Cy5 or DiD) are excited by Cy3 or DiI through FRET. The FRET value is ranging from 0 (donor only) to 1 (100% efficiency) [54].

2.2.2 Single-molecule spectroscopy

There are numerous advantages of using a single-molecule spectroscopy. By watching the motion of single molecules, we can see all details that would have been averaged out in the ensemble measurement. Since different states in individual fluorescence traces can be distinguished, we can synchronize brief states during post-experiment analysis, even when they are not synchronized during the measurement. This is called post-synchronization**,** which is one of the great advantages of the single-molecule spectroscopy.

The single-molecule detection requires that signals from background should be negligible compared to the intensity of the single molecule fluorescence. Thus, we use total internal reflection (TIR) microscopy for our study. The laser light is reflected on the interface between the glass and the water by TIR, but the evanescent wave goes into the water up to ~200 nm and excites the molecules immobilized on the surface. The fluorescence signals from dye molecules are collected by objective lens. And the signals are separated by a dichroic mirror to producet two side-by-side images of the same spot for donor (green) and acceptor (red) on a CCD camera for smFRET measurements (Figure 2.2) [55,56].

The main advantage of single-molecule experiments is that they allow us to study the behaviour of a single or countable number of molecules. The observation of individual events allows us to perform statistical analysis of a population of individual trajectories that is not possible in bulk because of ensemble averaging [55,56].

Through single-molecule FRET technique, several groups have developed single-vesicle fusion assays in planar bilayers [53,57,58]. They were able to record single vesicle fusion events, however these studies based on planar bilayers suffered from

ineffectively reproducing the known physiology and biochemistry. For example, SNAP-25 was not required in the acceptor t-SNARE complex [53,58] or fusion depended on calcium without the calcium sensor synaptotagmin [57]. Recently, several groups recovered SNAP-25 dependence of single-vesicle fusion assays in planar bilayers by directly inducing polyethylene glycol (PEG), a biologically irrelevant molecule, into the fusion system [59,60].

The single vesicle fusion assay developed by our lab can unambiguously detect different stages of fusion including docking, hemi and full fusion via FRET, which was not able for previous ensemble assays (Figure 2.3). Comparing with single-vesicle fusion assays in planar bilayers, we have advantages on reproducing the known physiology and biochemistry, such as SNAP-25 dependence.

2.2.3 Lipid mixing measurement

Details of the single vesicle lipid-mixing FRET assay were previously reported [61]. A quartz slide is firstly processed with PEG molecules by the ratio of 99:1 (mol/mol) PEG:biotin-PEG (Laysan Bio) to eliminate non-specific binding of vesicles. The slide is then assembled into a flow chamber and coated with neutravidin in the concentration of 0.2 mg/mL. Through the specific interaction between biotin and neutravidin, the v-SNARE vesicles are immobilized on the PEG-coated surface by an incubation at vesicle concentration of 100~200 pM for 15 minutes. After washing the free v-SNARE vesicles in the chamber, the t-SNARE vesicles are diluted to a final vesicle concentration of 200 pM with preset amounts of accessory proteins, and injected into the flow chamber for the reaction at 37 (±2) °C in the buffer (25 mM HEPES and 100 mM KCl, pH 7.4). After

washing the free t-SNARE vesicles and accessory proteins, the FRET measurements by a dual-color TIR fluorescence microscope are performed with the surrounding temperature of 37 (±2) °C or at room temperature.

2.2.4 Content mixing measurement

A quartz slide was first coated with PEG molecules (99:1 (mol/mol) mPEG-SVA:biotin-PEG-SVA (Laysan Bio)) to eliminate non-specific binding of vesicles and DNAs [62]. The slide was then assembled into a flow chamber and coated with neutravidin by flowing in 0.2 mg/ml solution. Through the specific interaction between biotin and neutravidin, the v-SNARE vesicles with dual-labeled DNA hairpin probes encapsulated inside were immobilized on the PEG-coated surface by an incubation at vesicle concentration of 100~200 pM for 15 minutes. After washing out the free v-SNARE vesicles in the chamber, the t-SNARE vesicles containing unlabeled single-strand target DNAs were diluted to a final vesicle concentration of 200 pM with accessory proteins, and injected into the flow chamber for the reaction at 37 (±2) °C in the buffer (25 mM HEPES, 100 mM KCl, pH 7.4) for 30 minutes. After washing out the free t-SNARE vesicles and accessory proteins, the FRET measurements by a TIR fluorescence microscope were performed with an oxygen scavenger system (0.1 mg/ml glucose oxidase, 0.02 mg/ml catalase, and 0.4% (wt/wt) β-D-glucose) and Trolox to eliminate single-molecule blinking events [63]. The alternating laser excitation system (530 nm and 638 nm) was used for content mixing measurement (Figure 2.4A). The FRET histogram is plotted for green laser excitation while all spots are picked by red

laser excitation. The donor only peak at $E = 0$ can be excluded by using the green/red laser alternating excitation (Figure 2.4B and 2.4C).

2.2.5 Data acquisition

Experiments were monitored in a wide-field TIR fluorescence microscope (IX70, Olympus) using an electron multiplying charge-coupled device camera (iXon DV 887-BI, Andor Technology). Details of the wide-field TIR fluorescence microscope have been reported [62]. Briefly, the excitation beam was focused into a pellin broca prism (CVI Laser), which was placed on top of a quartz slide with a thin layer of immersion oil in between to match the index of refraction. Cy3 or DiI (donor) and Cy5 or DiD (acceptor) dyes were excited through a 530nm laser or the alternating laser excitation system (530 nm and 638 nm) via TIR. The fluorescence signals from donor and acceptor that were collected by a water immersion objective lens (60X, 1.2 N.A. Olympus) went through a notch filter to block out excitation beams. The emission signals of acceptor dyes were separated by a 630 nm dichroic mirror (645DCXR, Chroma Technology) and detected by the electron-multiplying charge-coupled device camera (iXon DV 887-BI, Andor Technology) with a time resolution of 100 ms. The fluorescence signal, recorded in real time by using software written in Visual C++ (Microsoft), was amplified before camera readout, which produced an arbitrary unit for the recorded fluorescence intensity.

2.2.6 Data analysis

For lipid mixing, single fusion events were visually identified by an IDL program (Research Systems). A program written in Matlab (Mathworks) generated the time

trajectories of the donor and the acceptor fluorescence intensities and calculated the corresponding FRET efficiency by using the equation, $I_A/(I_D+I_A)$, where I_D and I_A are the donor and the acceptor fluorescence intensities, respectively. The average donor and acceptor fluorescence intensities measured before docking were considered as the background fluorescence for each fusion event and subtracted uniformly from the fluorescence signals. The leakage of donor fluorescence into the acceptor channel (~17.5% of the total intensity) was then taken into account.

For content mixing, the data analysis was carried out by programs written in Matlab (MathWorks) and Origin (OriginLab). The FRET efficiency, *E*, was also calculated as the intensity of the acceptor channel divided by the total intensity, which is the sum of donor and acceptor channel intensities. To exclude donor only molecules, single-vesicle spots were identified by red laser excitation through software written in Visual C++ (Microsoft).

2.2.7 Electronic Paramagnetic Resonance (EPR)

EPR is a technique to measure the interaction between unpaired electrons. Since EPR signals are only from nitroxide spin labels, which are rare in biological systems, it is a sensitive technique for studying the macromolecular structure [64,65]. Through site-directed mutagenesis, unique cysteines are introduced into the target protein, which are covalently attached to highly stable nitroxide spin labels. The EPR signal generated from the spin label reflects the information of local structures and environments [66,67,68,69].

In our study, the seven cysteines in the wild-type Munc18-1 or four cysteine residues in wild type cytosolic part of synaptotagmin 1 (C2AB, amino acids 140-421)

were spin-labeled for EPR spectrum detection. After the cell lysate was incubated with beads and washed with HEPES buffer (25 mM HEPES/KOH, 100 mM KCl, pH 7.4) three times, DTT was added to a final concentration of 2 mM, and nutation was continued at 4 ^{o}C for another 30 min. The beads were then washed eight times with an excess volume of washing buffer to remove DTT. An approximately 20-fold excess of (1-oxy-2,2,5,5-tetramethylpyrrolinyl-3-methyl) methanethiosulfonate spin label (MTSSL) was added into the column, and nutation at room temperature was continued for 40 min. The spin-labeled proteins were eluted by elution buffer and dialyzed overnight against dialysis buffer (25 mM HEPES/KOH, 200 mM KCl, 10% glycerol, pH 7.4).

EPR spectra were obtained using a Bruker ESP 300 spectrometer (Bruker) equipped with a low-noise microwave amplifier (Miteq) and a loop-gap resonator (Medical Advances). The modulation amplitude was set to be no greater than one-fourth of the line width. Spectral data were collected at room temperature in first-derivative mode with 1 mM microwave power.

2.2.8 Molecular dynamics (MD) simulations

In order to calculate the size of our DNA probes for content mixing in Chapter 4, we performed MD simulations. Two independent MD simulations were performed on single strand DNA with different sequences corresponding to Cy3/Cy5 dual-labeled DNA hairpin and unlabeled target DNA to probe their radius of gyration in equilibrium. Both starting structures were generated using 3D-DART [70] and VMD [71] with CHARMM27 topology [72]. The DNA hairpin was solvated using 22043 TIP3P water molecules and neutralized with 100 mM KCl in a water box of 89 Å × 89 Å × 89 Å. The

unlabeled target DNA was immerged in a simulation box of 100 Å × 100 Å × 100 Å including a POPC lipid patch, water, and 100 mM KCl. The DNA was kept in close with lipid using a virtual bond connecting the sugar ring oxygen of A_{30} at 3' end of target DNA and the phosphate of a lipid. The all-atom MD simulations were performed using the developing version of program NAMD 2.7 [73] with the TIP3P model for explicit water and the CHARMM27 force field including the CMAP correction [72]. In all simulations, periodic boundary condition was applied with a time step of 1 fs. Non-bonded energies were calculated using particle mesh Ewald full electrostatics and a smooth (1.0-1.2) cutoff of the van der Waals energy. Constant temperature was maintained using Langevin thermostat with a damping coefficient of 1 ps^{-1}. A Nosé-Hoover Langevin piston barostat was employed to maintain a constant pressure with a period of 200.0 fs and damping timescale of 100.0 fs. Each system was simulated for 75 ns, where the last 25-ns data were taken to calculate the radius of gyration.

The DNA hairpin probe composes of a 6bp stem and a poly-thymidine (T_{20}) loop. The unlabeled target DNA has a complementary sequence of poly-adenosine (A_{30}). The DNA hairpin stem was modeled with B-DNA-type geometry with a random conformation for the poly-T loop. K^+ and Cl^- ions were added to the water box to obtain a 100 mM KCl solution. Additional K^+ ions were added to neutralize the system. The resulting system contains 67229 atoms including DNA, water, and ions. The starting structure of target DNA was modeled by removing the complementary strand from a B-form double helix DNA. A patch of POPC with 274 lipids was added to the system with the membrane normal along the z-axis. The distance between the oxygen of A_{30} at 3' end of target DNA and the phosphate of one of lipids was harmonically restrained to be 10 Å

through a virtual bond. Such restrain mimic the 3'-cholesteryl TEG used in the experiment to prevent the target DNA from moving away from membrane while allow the target DNA diffuse along with the bonded lipid. Solvent was then added to both sides of the membrane, and the system was neutralized with 100 mM KCl using the Solvate and Autoionize plugins of VMD. The simulated system has about 183,000 atoms.

The simulated system of DNA hairpin was subject to 4000 steps of conjugate gradient minimization and 500-ps NPT (constant pressure and temperature) equilibration with DNA harmonically restrained. The system then was subject to 10-ns annealing at 500 K with the 6bp stem harmonically restrained in the NVT (constant volume and temperature) ensemble. After cooling the system down, the 75-ns production run was performed in the NVT ensemble at T = 310 K. The simulated system of unlabeled target DNA was subject to 4000 steps of conjugate gradient minimization first. Then, lipid tails were melted in a 1-ns NVT simulation at 310 K during which all other atoms were fixed. The system was then equilibrated in the NPT simulation at 1 atm and 310 K for 1 ns with DNA harmonically restrained and followed by 1-ns simulation with all restraint released. Finally, the 75-ns production run was performed in the NPT ensemble with constant area of the lipid bilayer and a constant normal pressure of 1 atm.

Chapter 2 Figures:

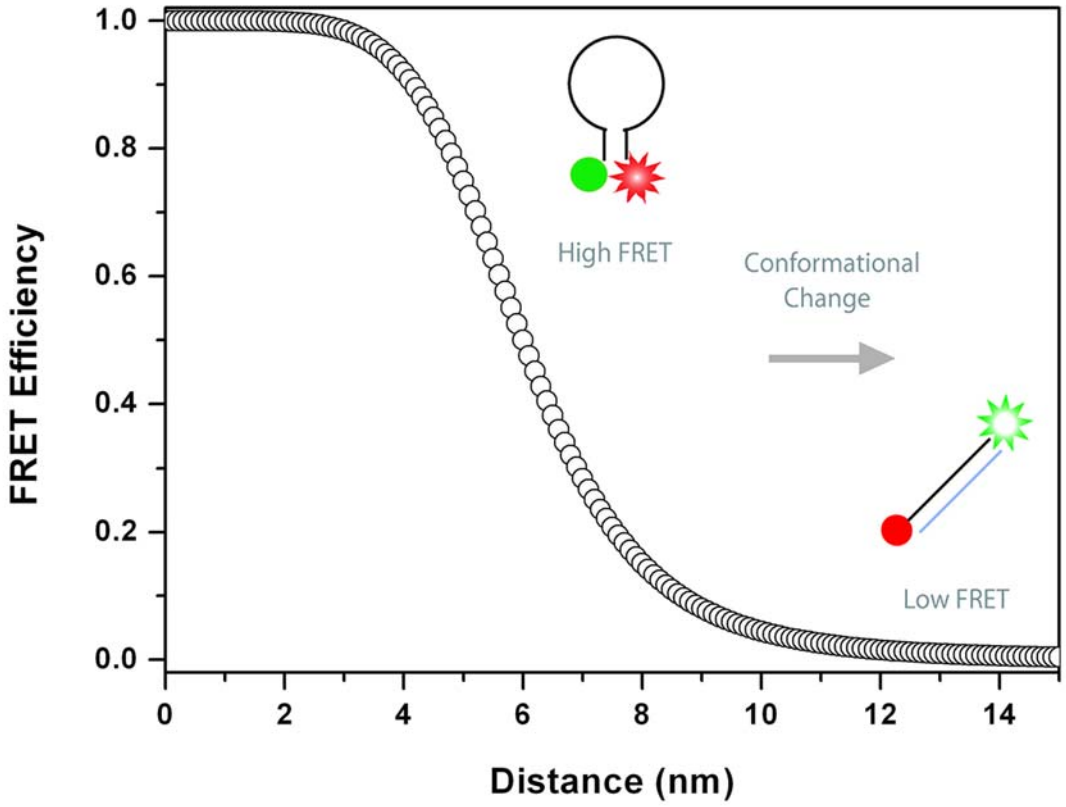

Figure 2.1. The FRET efficiency *v.s.* distance between donor and acceptor dye molecules. The FRET efficiency follows the equation of $1/(1+ (R/R_0)^6)$. R_0 is characterized by the spectral overlap, the quantum yield of donor and other factors.

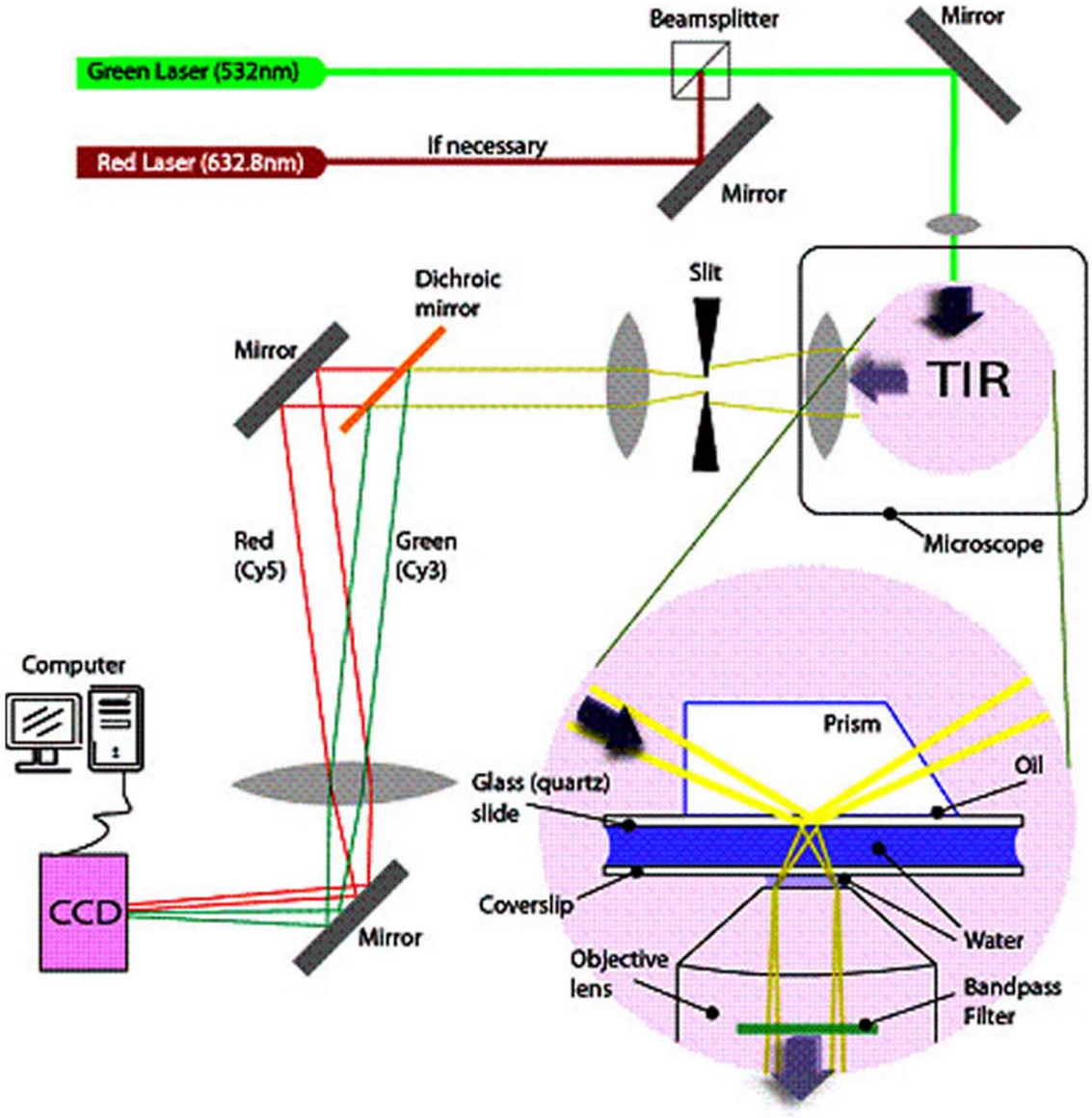

Figure 2.2. Total internal reflection (TIR) microscopy.

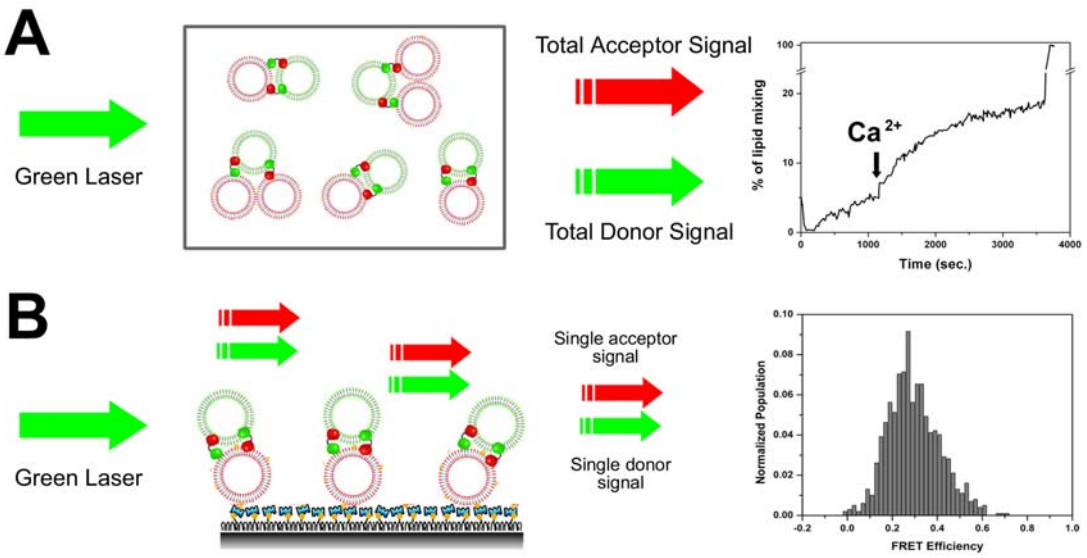

Figure 2.3. Schematics of the bulk fusion assay (**A**) and the single-liposome lipid mixing assay (**B**) for the mixture of vesicles and C2AB after 1 mM calcium. The FRET histogram is plotted by compiling FRET signals from over one thousand vesicles. Y-axis is normalized population, where we divided the distribution by the total number of vesicles measured and X-axis is FRET efficiency value.

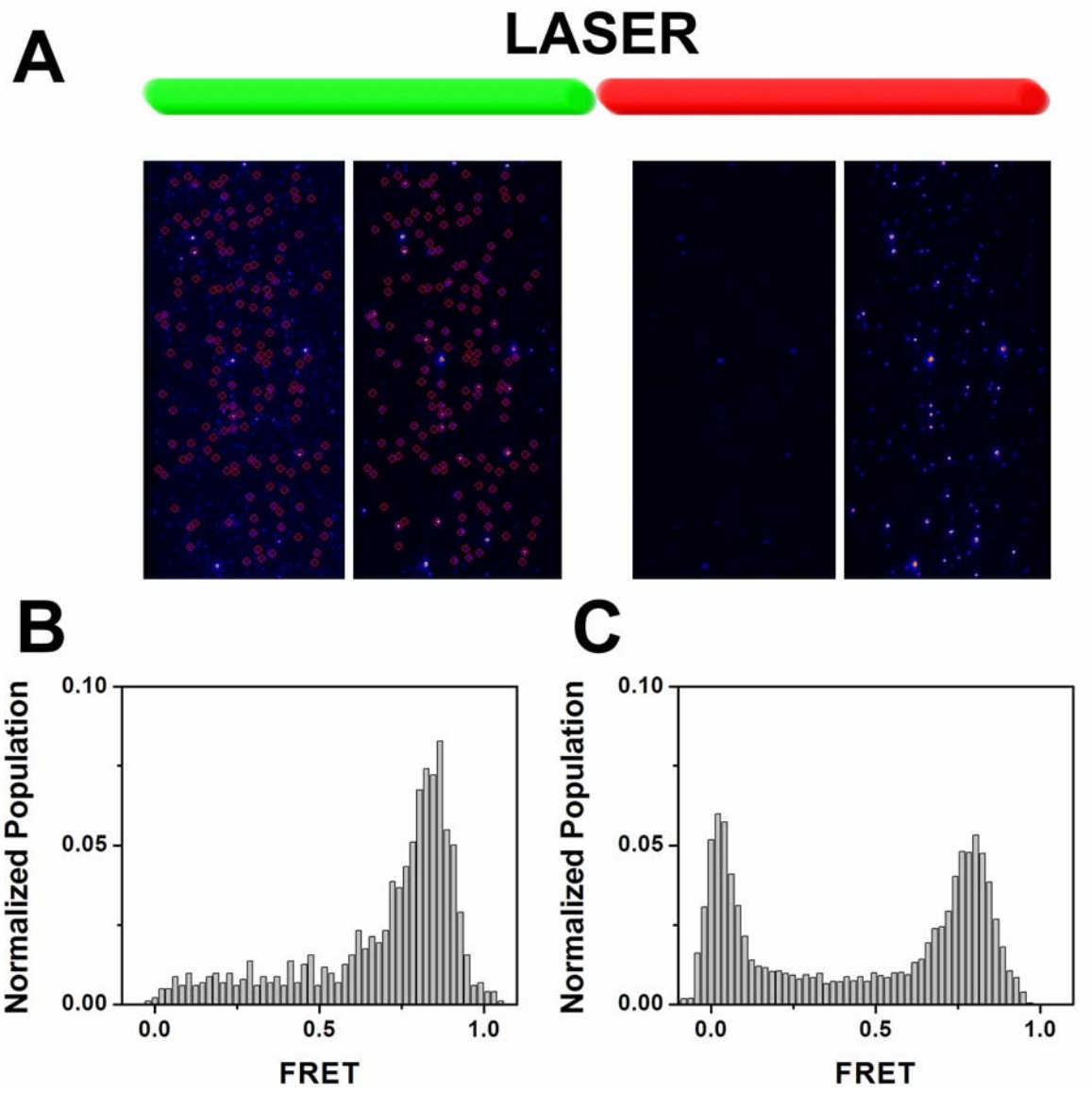

Figure 2.4. A, The alternating laser excitation system for content mixing measurement. The FRET histogram is plotted for green laser (530 nm) excitation while all spots are picked by red laser (638 nm) excitation. Green laser excitation FRET histograms with (**B**) or without (**C**) this system. The donor only peak at $E = 0$ can be excluded through the alternating laser excitation system.

CHAPTER 3

LIPID MIXING

3.1 Technique

In 2006, a single-liposome lipid mixing method based on FRET was developed in our lab [61]. The v- and t-SNARE proteins are reconstituted in two independent populations of liposomes that are labeled with acceptor (DiD) and donor (DiI) fluorophores, respectively. The liposomes containing v-SNAREs and acceptors (v-SNARE liposomes) are tethered to the bottom surface of a flow chamber, which is also an imaging surface of TIR microscopy. Then, the liposomes containing t-SNAREs and donors (t-SNARE liposomes) are flowed into the chamber to induce assembly of SNARE complexes and membrane fusion between a single pair of t- and v-SNARE liposomes. Real-time fusion intermediates with different degrees of lipid mixing are reported via increasing values of the FRET efficiency. For example, the highest FRET value is obtained when full fusion occurs in which both leaflets, inner and outer, mix. An intermediate FRET is obtained for hemifusion where only the outer leaflets mix. From the hemifusion state, a fusion pore opens to mix content as well as the inner leaflets. If the fusion pore closes prematurely, FRET increase can stall until the pore opens again which we have observed as additional intermediates in single liposome fusion. Comparing with bulk fusion method, this new technique can separate intermediate states of docking, hemi-fusion, and full fusion, and detect the kinetic transition between individual intermediates, and post-fusion pathway such as the kiss-and-run event.

The detailed scheme of this single-liposome lipid mixing method is shown in Figure 3.1. A quartz slide is firstly processed with PEG molecules to eliminate non-specific binding of liposomes. The slide is then assembled into a flow chamber and coated with neutravidin. Through the specific interaction between biotin and neutravidin, the v-SNARE liposomes are immobilized on the PEG-coated surface by a 15-minute incubation. After washing the free v-SNARE liposomes in the chamber, the t-SNARE liposomes are diluted with preset amounts of accessory proteins, and injected into the flow chamber for the reaction at 37 °C in the buffer. The low concentration of t-SNARE liposomes can dramatically reduce the probability of multiple liposome interactions to warrant this method in single-liposome level. After washing the free t-SNARE liposomes and accessory proteins, the FRET measurements by a TIR microscope are performed.

3.2 Study on complexin

[Related publication: Yoon, T.-Y., Lu, X., Diao, J., Lee, S.-M., Ha, T. & Shin, Y.-K. Complexin and Ca^{2+} stimulate SNARE-mediated membrane fusion. *Nat. Struct. Mol. Biol.* **15**, 707-713 (2008).]

The physiological studies of complexin, overexpression and knock out, yielded conflicting observations, initiating a debate as to whether complexin is a fusion inhibitor or stimulator. The three reports published in the 2006 primarily supported an inhibitory role and positioned complexin as a clamp for SNARE-driven membrane fusion [36,37,38]. Our single-vesicle FRET assay enables us to probe how individual fusion steps are modulated by regulatory factors, during parallel imaging of over 100 fusion events. We now directly show complexin 1 has indeed both inhibitory and stimulatory

effects on SNARE complexes: Inhibition of trans-SNARE complex formation and stabilization of once assembled SNARE complexes. However, only the stimulation effect becomes visible at physiologically relevant complexin concentrations, which accelerates SNARE-mediated fusion by two orders of magnitude via an externally applied Ca^{2+} wave. Our results suggest the existence of a 'primed' complex-consisting of trans-SNARE assemblies, complexin, and lipid membranes-providing an essential substrate for Ca^{2+} and Ca^{2+} sensors in the neurotransmitter release.

3.2.1 Complexin inhibits docking between v- and t-SNARE vesicles

We included recombinant full-length complexin 1 (residues 2-134) and 1 mM EGTA in the t-SNARE vesicle solution. We mixed t-SNARE vesicles with different amounts of complexin 1 (0.2, 2 and 20 μM) and then injected the mixture into a flow chamber with surface-immobilized v-SNARE vesicles (t = 0) (Figure 3.2A). After 12 minutes incubation at 37°C, unbound t-SNARE vesicles and complexins in solution were removed by flow washing. We then counted the average number of t-SNARE vesicles per imaging area (50×100 μm^2) that docked to individual v-SNARE vesicles (Figure 3.2A). By dividing this average number of docked t-SNARE vesicles by the average number of v-SNARE vesicles per imaging area (Figure 3.2B), we obtained the probability that a surface-tethered v-SNARE vesicle would be docked by a t-SNARE vesicle (Figure 3.2A). No docking was observed in the absence of v-SNARE vesicles or without SNARE proteins. Without complexin, the docking probability was 0.27. This probability was maintained up to the complexin concentration of 2 μM, but notably reduced to ~0.1 when 20 μM complexin was used (Figure 3.2A). Therefore, complexin at this high

concentration inhibits SNARE complex formation, which may explain the phenotype of complexin overexpression.

3.2.2 Complexin binding to SNARE complex stimulates fusion

For the docked vesicle complexes, however, the FRET distribution analysis shows that an increasing amount of complexin 1 significantly enhances the full fusion population at $E \approx 0.7$ (Figure 3.3A-3.3C). The normalized full fusion population was 0.18 at [Cpx I] = 0.2 μM and increased to 0.32 at 2 μM and 0.45 at 20 μM after 15 minutes reaction each. To probe whether the complexin/SNARE complex interaction is directly involved in this fusion reaction, we engineered double-point mutation in complexin 1 (C105A/R48C) to attach a nitroxide spin label at position 48, which is critically involved in complexin binding to the SNARE complex [35,74]. This spin labeled R48C mutant showed a minimal level of binding to the ternary SNARE complex. Consistent with this diminished binding, the stimulation effect was significantly reduced (Figure 3.3D) indicating complexin binding to the SNARE complex is essential for stimulation of fusion. Furthermore, the stimulatory effect is specific to the complete SNARE complex because drastically reduced full fusion population was observed without SNAP-25, even with reaction time of 60 minutes and 1 mM Ca^{2+} (Figure 3.3E). In addition, Ca^{2+}-independent stimulation of full fusion by complexin 1 continued beyond 15 minutes (Figure 3.3F).

3.2.3 Ca^{2+} accelerates complexin-assisted fusion events

The data described above suggests complexin is likely an independent fusion

stimulator, capable of directly lowering the fusion energy barrier without resorting to other proteins including synaptotagmin 1. Then, one immediate question is if such an independent stimulatory function of complexin even confers a Ca^{2+} sensitivity to the SNARE-mediated fusion. To probe potential Ca^{2+} responses, we used real-time tracking of single-vesicle fusion events. Here, we employed the vesicles of a physiologically relevant lipid composition containing 15 mol% PS (phosphor-L-serine) and 40 mol% cholesterol [75]. We incubated a solution of t-SNARE vesicles and complexin 1 (1-2 μM) with surface-immobilized v-SNARE vesicles for 5~7 minutes and introduced 1 mM Ca^{2+} in the imaging area at $t = 0$ (at the speed of 2 ml/min), while donor and acceptor signals from single-vesicle complexes were being recorded with the time resolution of 150 or 200 ms. Surprisingly, we observed a substantial fraction of vesicle complexes showing fusion synchronized with the Ca^{2+} flow (Figure 3.4).

In a typical real-time trace of Ca^{2+}-evoked fusion (Figure 3.4A), the vesicle complex begins with the initial E value of ~0.35 that corresponds the hemifused state and starts lipid mixing at $t = 0.4$ second (orange arrow) that reaches the full fusion state at $E \approx 0.75$. Likewise, many vesicle complexes start to show FRET increase following the arrival of the Ca^{2+} buffer (Figure 3.4C, orange arrows). The cumulative time histogram of these instances of initial FRET increase shows a rapid increase in number with the primary time constant of 8.8 seconds (Figure 3.4B, green symbols with a red curve). Overall, in the first 25-second window, 212 out of total 835 vesicle complexes imaged show the initiation of fusion, indicating a significant fraction of vesicle complexes (~25 %) undergoes Ca^{2+}-evoked membrane fusion events synchronized on the seconds time scale. When the Ca^{2+} concentration is reduced to 20 μM, that is a conservative estimate on the

Ca^{2+} concentration at the presynaptic active zone during neuronal stimulation [76], more than 10 % of the total vesicle complexes show Ca^{2+}-triggered fusion within the first 25 seconds. These percentages of Ca^{2+}-responding vesicle complexes, 26 and 11%, are underestimated values because we note that only ~30% of total vesicle complexes are available for Ca^{2+}-triggered fusion at the moment of the Ca^{2+} addition. In the in vitro fusion assay, we find that on average 35% of total vesicle complexes are fusion-inactive probably due to the absence of the auxiliary proteins, and at the same time, 36% of total vesicle complexes become already fully fused before Ca^{2+} is added. Therefore, nearly 90 and 35% of the remaining "fusible" pool of vesicle complexes respond to 1 mM and 20 μM Ca^{2+} respectively, within the first 25-second window. In addition, the control experiment of introducing a different type of divalent ion, 1 mM Mg^{2+}, showed minimal fusion activity (Figure 3.4B, red symbols).

This Ca^{2+}-triggered fusion mode should be attributed to the stimulatory effect of complexin because the fusion process mediated by solely SNARE proteins does not show any progression towards full fusion in response to 1 mM Ca^{2+}. It is highly likely that the fusion energy barrier is first lowered by ternary SNARE complexes and complexin, and the addition of Ca^{2+} ions enables many vesicle complexes to finally overcome the fusion barrier, accelerating the fusion kinetics by additional two orders of magnitude (Figure 3.4B, green *v.s.* blue symbols). The distribution of the initial *E* values for the vesicle complexes showing Ca^{2+}-induced fusion has a major population between 0.2 and 0.5 (Figure 3.4D), and this FRET range approximately corresponds to the hemifusion state [61].

Reducing negatively charged PS (phospho-L-serine) lipids from 35 mol% to 15

mol% largely abolishes Ca^{2+}-evoked fusion (Figure 3.4E, blue symbols), although the stimulation by complexin I in the absence of Ca^{2+} is still present. However, addition of 40 mol% cholesterol while keeping PS concentration at 15 mol% to emulate the lipid composition of the native synaptic vesicle fully restores the Ca^{2+}-triggered fusion (Figure 3.4E, red symbols; see Figure 3.4F for real-time traces). Even when the Ca^{2+} concentration is reduced to 20 μM, which is close to the low level of intracellular Ca^{2+}, more than 10% of the vesicle complexes show Ca^{2+}-triggered fusion. Our observations suggest that high concentration cholesterols in synaptic vesicles potentiate the Ca^{2+}-responsiveness [75].

3.2.4 Fusion step-specific switching of complexin function

As shown in Figure 3.5, we suggest a model of different complexin functions for each stage of the Ca^{2+}-triggered neurotransmitter release along with the possible molecular mechanisms. Firstly, to gain a further insight into the inhibitory effect of complexin on the docking step, we produced double mutation in complexin 1 (C105A/R56C) and attached a nitroxide spin label at position 56. The EPR spectrum of this construct shows relatively narrow peaks, typical of freely moving spin labels (Figure 3.5A, left; black curve). However, when mixed with t-SNARE vesicles, the spectrum shows a broad spectral component, now reflecting the slow motion of the nitroxide side chain (Figure 3.5A left; blue arrow). No broadening is observed either when the same construct is mixed with syntaxin-only vesicles or when the spin label is attached to the native cysteine at 105 and incubated with t-SNARE vesicles (Figure 3.5A, right). It is thus highly likely that this spectral broadening probes tertiary contacts between

complexin and the t-SNARE proteins, consistent with a recent finding of the complexin/t-SNARE interaction using a floatation assay [77]. Spectral subtraction analysis [78] gives the dissociation constant of ~50 μM, which is much weaker than that of the complexin binding to the ternary SNARE complex [37,74]. This weak interaction would lead to competition between v-SNARE and complexin for binding to t-SNAREs (Figure 3.5B). When highly expressed, complexin outnumbers v-SNARE thereby inhibiting SNARE complex assembly. This observation may explain the inhibitory phenotypes observed in complexin overexpression and *in vitro* assays [36,37,38,79,80].

However, it appears that the primary function of complexin is to stimulate SNARE-mediated fusion using the specific binding mode to the ternary SNARE complex (Figure 3.5C-F) [35,74]. Earlier structural studies positioned complexin as a potential fusion stimulator because complexin was thought to stabilize assembly of SNARE complexes [35,74]. By tracking the number of the docked t-SNARE vesicles in time, we indeed observed stabilization of the number of single vesicle complexes in the presence of complexin (Figure 3.6A). Without complexin 1, the number of docked t-SNARE vesicles significantly decreases with time (Figure 3.6A, green circles), reflecting disassembly of *trans*-SNARE complexes probably due to repulsion between t- and v-SNARE vesicles. In contrast, we observe even a moderate concentration of complexin 1 (2 μM) has a noticeable effect of keeping *trans*-SNARE complexes from being disassembled (Figure 3.6A, blue triangle). Such complexin-stabilized SNARE complexes may more effectively transmit the tensions created during SNARE complex formation to fusing membranes.

Our observation demonstrates that complexin is neither a simple inhibitor nor a stimulator, but has both functions in the same sequence. We note such dual roles have

been recently proposed for important presynaptic fusion regulators. A SM protein, Munc18-1 was long anticipated to be a fusion inhibitor by stabilizing closed syntaxin 1, but in vitro reconstitution experiments found Munc18-1 stimulates SNARE-mediated fusion through direct interaction with assembled SNAREpins [45,46,47]. It was also recently reported that complexin domains contribute differentially to rescuing its KO phenotype [81], attributing different functions to different domains. Remarkably, we observe both inhibition and stimulation of complexin in "one round" of single fusion events–not in two independent experimental designs–and show that the transition from inhibition to stimulation takes place "in phase with" SNARE complex assembly. Such dual roles could be a common and salient feature of presynaptic fusion regulators considering high degree of controllability required for neuronal exocytosis. Our observation that the switching between dual roles is a sharp function of SNAREpin assembly could be crucial because 1) as implied in the zippering model [82,83], the degree of SNARE complex assembly is one of the physical parameters that define the fusion step, 2) fusion regulators could then swap interaction modes across synergetic cooperation to negative feedback loop for different fusion steps, tightly regulating fusion progression to next steps and 3) our observation may provide a clue for understanding the previous conflicting complexin phenotypes.

A noteworthy aspect of our results is the observation that the Ca^{2+} influx synchronizes fusion of single vesicle complexes on the seconds time scale (Figure 3.4), a totally unexpected finding that has been hidden in physiological analysis and in vitro ensemble measurements. The stringent control experiments involving the single point mutation in complexin, the SNAP-25-dependence of fusion, the different lipid

compositions, and the Ca^{2+}-specificity test using Mg^{2+} ions argue that the observed Ca^{2+}-evoked fusion mode occurs in a way that is highly selective to physiologically relevant conditions. We cannot rule out the possibility that complexin is an active Ca^{2+}-sensor and especially, the first 26 residues of complexin could play an active role upon Ca^{2+} influx [81]. However, we find the Ca^{2+}-response diminished in the absence of cholesterol (Figure 3.4E) can be largely restored by increasing the PS concentration in the vesicle lipid composition, indicating the fusion triggering is in part largely mediated through interactions between divalent Ca^{2+} ions and negatively charged lipid membranes. On the basis of our data, we suggest that the supramolecular complex consisting of ternary SNARE complexes, complexin, and lipid membranes directly reacts with Ca^{2+} ions to achieve fusion triggering.

This fusion mechanism is well described in the viewpoint of fusion energetics [84,85,86]. Although our observation of the inhibitory effect is reminiscent of the fusion clamp model [36,38], the underlying energetics suggested by our results is fundamentally different from that of the clamp model. In the fusion clamp model, SNARE complex assembly is thought to release sufficient free energy to overcome all the fusion energy barriers, so its energy release needs to be spring-loaded by a 'clamp' to gain control over the timing of fusion (Figure 3.6B, left). Our data suggest that the SNARE complexes dramatically decrease the free energy barrier of a fusion event that would otherwise exhibit negligible fusion progression on practical time scales (Figure 3.6B, right). The single vesicle FRET imaging does show even with the molecular action of SNAREs, there remains a significant energy barrier, giving the growth of the full fusion peak on the time scale of tens of minutes. Complexin further lowers the energy barrier, and the

interaction of Ca^{2+} ions and lipid membranes helps vesicle complexes finally pass the transition state on the seconds time scale (Figure 3.6B, right).

How then do Ca^{2+} ions lower the fusion energy barrier? Ca^{2+} ions condense on a surface of a negatively charged membrane, attracted by the electrostatic interaction. Theoretical works suggest when the ion valency is higher than two, correlations between charges can drive the amount of the condensed charges to be larger than that of the membrane negative charge, making the membranes positively charged when looked from outside [87,88]. This charge inversion induces undulations of membranes, and entails dynamic instability and membrane fusion above a critical threshold. We observed Ca^{2+} ions effectively induce fusion events at concentrations as low as 20 μM, suggesting the threshold is smaller than 20 μM for our single vesicle complex. Moreover, plotting the percentages of the Ca^{2+}-responding vesicles (in the 25-second window) at three Ca^{2+} concentrations higher than the threshold (20, 200, and 1,000 μM) gives a small cooperativity coefficient of ~0.25 to this fusion triggering mechanism (Figure 3.6C). In protein-free vesicles, the threshold is reported to be in a few millimolar range [88], so the molecular action of SNAREs and complex is essential in obtaining such a low cooperativity.

3.2.5 Conclusion

In summary, we demonstrated that complexin has both inhibitory and stimulatory effects and switching between these dual roles crucially occurs as a function of SNARE complex assembly. We also observed vesicle complexes primed by SNAREs and complexin can directly react with Ca^{2+} ions. Single vesicle fusion data enables novel

analyses, including assessing the synchrony level of given vesicle pools and finding the Hill cooperativity coefficient, which can be directly compared with physiological findings, positioning this new Ca^{2+}-triggering pathway in relation to asynchronous release. Incorporation of full-length synaptotagmin 1 in our system may further accelerate our Ca^{2+}-response and reveal the molecular details of synchronous release. The methodology established in this work can be used to study a wide range of membrane fusion regulators and uncover previously hidden molecular function.

3.3 Study on Munc18-1

[Related publication: Diao, J., Su, Z., Lu, X., Yoon, T.-Y., Shin, Y.-K. & Ha, T. Single vesicle fusion assay reveals Munc18-1 binding to the SNARE core is sufficient for stimulating membrane fusion. *ACS Chem. Neurosci.* **1**, 168-174 (2010).]

Munc18-1 interacts with SNARE proteins at least in two different modes, namely binding to Habc domain (amino acids 28–146) of syntanxin and binding to the SNARE core complex. In the first mode, Munc18 interacts with monomeric syntaxin through the N-terminal helical segment of syntaxin called the Habc domain to form a Munc18/syxntaxin binary complex [40,41,42,43]. This Habc binding mode stabilizes the closed conformation of syntaxin during its transportation to the plasma membrane *in vivo*. Without this stabilization effect, the syntaxin level in sensory neurons was reduced by 70% in Munc18 knockout mice [89]. In the second mode, Munc18 also binds to the SNARE core, a four helical bundle formed by syntaxin, VAMP and SNAP25 [44,45,46,47]. Ensemble proteoliposome fusion experiments showed that Munc18 binds preassembled SNARE complexes, and effectively promotes SNARE-mediated fusion

with full-length syntaxin [45]. An interaction called N-peptide binding between Munc18 and N-terminal peptides (amino acids 1-24) of syntaxin besides this SNARE core/Munc18 interaction is believed to be critical for this fusion promotion effect [44,45]. However, how Munc18 activates fusion remains unclear in part due to the inability of the ensemble in vitro fusion assay to dissect different steps of fusion reaction.

3.3.1 Munc18-1 promotes lipid mixing with SNARE core complex

The resulting single vesicle FRET efficiency histograms of the reaction product showed that Munc18-1 promotes full fusion represented at the FRET efficiency > 0.5 in a concentration-dependent manner whether the full-length syntaxin 1A (syntaxin-full, amino acids 1-288) or the truncated syntaxin 1A lacking N-peptide and Habc domain (syntaxin-HT, Habc-truncated, amino acids 168-288) was used. After 20 minutes reaction, we observed more than 50% full fusion populations (Figure 3.7), which is much faster than the previous report of several hours [45]. The fusion promotion activity of Munc18-1 is dependent on SNAP-25 for both syntaxin-full and syntaxin-HT cases because omitting SNAP-25 led to a significant reduction in full fusion population (Figure 3.7A and 3.7B). Because SNAP-25 is required for the formation of the complete SNARE complex, it is likely that the interaction between Munc18-1 and the SNARE core complex promotes fusion. Furthermore, this fusion promotion activity of Munc18-1 does not seem to require additional interactions with the N-peptide of syntaxin 1A.

3.3.2 Munc18-1 interacts with the SNARE core complex reconstituted on vesicles

Spin labeling EPR has proven effective in detecting the intermolecular interaction such the one between syntaxin 1A and Munc18-1. The seven native cysteines in wild-type Munc18 hamper the site-specific attachment of the nitroxide spin labels. However, we could at least non-selectively spin-label native cysteines to primitively probe the putative intermolecular interaction. For this purpose, wild type Munc18-1 was labeled with the methanethiosulfonate spin label. The EPR spectra for spin labeled Munc18-1 in solution, with syntaxin 1A (full length and HT), and with the SNARE complex in membrane were measured respectively at room temperature (Figure 3.8). The broadened line shape of the EPR spectrum indicates that the Munc18-1 bind to full-length syntaxin directly (Figure 3.8B, left panel). The EPR spectrum did not show any change when incubated with syntaxin-HT only (Figure 3.8C, left panel). These data are consistent with the previous conclusion that the Habc domain of syntaxin plays an important role in the interaction between monomeric syntaxin and Munc18 in solution.

We found a different result when the EPR spectrum from Munc18 was measured with the SNARE complex in the context of membrane. After full-length syntaxin or syntaxin-HT was reconstituted into membrane and formed a ternary complex with SNAP-25 and soluble VAMP 2 (amino acids 1-89), spin labeled Munc18-1 was added to the complex. The EPR spectra of Munc18-1 were broadened for both SNARE complexes containing full-length syntaxin and syntaxin-HT, indicating that the N-peptide of syntaxin 1A is not necessary for Munc18-1 interaction with the membrane associated SNARE complexes (Figure 3.8B and 3.8C, right panels). Interestingly, Rothman's group [45] also found that Munc18-1 still binds to the membrane associated SNARE complex even with the Habc domain removed (syntaxin-HT) or the N-peptide mutated (L8A). Overall, our

work shows that Munc18-1 could bind to the SNARE core complex reconstituted into the lipid membrane even in the absence of the N-peptide interaction, and this SNARE core/Munc18 binding mode is likely to be responsible for fusion acceleration by Munc18-1. Meanwhile, the EPR analysis showed that there is no direct interaction between the membrane and Munc18-1 (Figure 3.8A, right panel) which rules out the possibility that the spectral broadening observed in the presence of SNARE complex (Figure 3.8C, right panel) was caused by lipid molecules. We note here that we not only have the EPR line broadening (Figure 3.8, indicated by arrows) due to the quaternary interaction between Munc18 and SNAREs, but we also see some extra line broadening (Figure 3.8, indicated by circles) due to the spin-spin interaction. The spin-spin interaction is most likely due to the clustering of spin labeled Munc18, perhaps reflecting the binding of several Munc18 molecules to the oligomeric supramolecular SNARE complex [90].

3.3.3 Conclusion

In conclusion, Munc18-1 promotes neuronal SNARE-mediated fusion not only with the full-length syntaxin 1A but also with Habc-truncated syntaxin 1A. The SNARE complex/Munc18 interaction is mainly responsible for this effect. Furthermore, Munc18-1 accelerates vesicle fusion significantly more rapidly than previously observed. With the advent of new single molecule imaging technologies, these protein-protein interactions critical for fusion may also become observable.

3.4 Study on C2AB

[Related publication: Diao, J., Yoon, T.-Y., Su, Z., Shin, Y.-K. & Ha, T. C2AB: a molecular glue for lipid vesicles with negatively charged surface. *Langmuir* **25**, 7177-7180 (2009).]

C2AB, is the cytosolic part of synaptotagmin I, believed to be the primary calcium sensor in synaptic vesicle exocytosis, and has two C2 domains referred as the C2A- and C2B-domains [91,92]. C2A domain binds three calcium ions whereas the C2B domain binds two calcium ions with their calcium binding pockets formed by two protruding loops at the top of the beta sandwiches. The C2AB molecule interacts with both SNARE (soluble N-ethylmaleimide-sensitive factor attachment protein receptor) complexes, which is an essential part of the intracellular membrane fusion machinery, and negatively charged phospholipids, such as phosphatidylserine (PS). In response to the calcium, C2AB partially penetrates the membrane to deform the lipid bilayer and lower the activation barrier to assist the membrane fusion [93]. The detailed mechanism of C2AB binding on membrane with assistant from calcium ions has been studied by Rizo's group [93]. Simply, after calcium ion binding, C2AB molecules containing multiple binding sites become very positively charged, which has a high affinity with negatively charged lipid molecules.

3.4.1 C2AB and Ca^{2+} cause vesicle aggregation

As shown in Figure 3.9A, in the absence of Ca^{2+}, we could not see appreciable docking of the DiI-labeled donor liposomes. However, as this mixture was washed out by subsequent injection of 0.1 mM Ca^{2+}, DiI-labeled liposomes began to dock to surface-immobilized, DiD-labeled liposomes rapidly with a time constant of hundreds of

milliseconds. The negative stain transmission electron microscopy also verified that the separated liposomes containing 35 mol% PS plus 65 mol% PC clustered together quickly after adding 1 μM C2AB and 0.1 mM Ca^{2+} (Figure 3.9B and 3.9C).

The negatively charged PS molecules play an important role in the interaction between C2AB molecules and calcium ions. When we reduced PS concentration from 35 mol% to 5 mol%, the gluing of DiI liposomes was extinguished (Figure 3.10A). Since only 5 calcium ion-binding sites are associated with each C2AB molecule, the 0.1 mM Ca^{2+} was saturating for 1 μM C2AB. When calcium concentration was increased to 1 mM, the docking number of DiI liposomes, which is the number of donor spots in each image area with the size of 25 μm × 50 μm, remained the same (Figure 3.10B). Under the calcium-saturated condition, we can control the results by adjusting the amount of C2AB. As shown in Figure 3.10B, the DiI-liposome docking number was greatly reduced when C2AB concentration was lowered to 0.1 μM.

3.4.2 Factors influence C2AB and Ca^{2+} effect

The effect of the C2AB is specific in terms of the response to calcium ions and the interaction between charged membranes. When we replaced calcium ions with the same concentration of magnesium ions, the glue function of C2AB totally vanished (Figure 3.11A). This result indicates that this molecular glue is not simply caused by the electrostatic interaction of any divalent ion and specific binding of calcium to C2AB molecules is required [93]. When we partially destroyed pre-docked DiD liposome layer by an air bubble before DiI liposomes were injected, as demonstrated in the upper part of Figure 3.11B, no DiI liposome attachment was observed after calcium washing while the

lower part with intact DiD liposomes worked normally. We concluded that no DiI liposome docking was observed without DiD liposomes. This experiment illuminates the specificity of this molecular glue, which hints at wide applicability.

This abrupt and stable appearance of the DiI-labeled liposomes is ascribed to specific docking to DiD-labeled liposomes because the FRET distribution peaked at a non-zero efficiency value, $E = I_A/(I_A+I_D) = 0.3$, where I_A and I_D are the sensitized emission intensity of the acceptor and donor, respectively (Figure 3.11C). This FRET efficiency value, strongly suggests that a close packaging state of vesicles, in which the outer leaflets are about to mix, is induced by C2AB and calcium ions. As shown in Figure 3.9C, this close packaging state is also observed through the negative stain transmission electron microscopy. After calcium ion binding, C2AB molecules become positively charged, which has a high affinity with negatively charged lipid molecules of the membrane [93]. We found that interaction between C2AB molecules with calcium ions and charged membranes is strong and stable. Even after ten-rounds buffer washing, 150 μL for each round, more than 80% of the DiI liposomes still remained bonded on the surface (Figure 3.11D).

3.4.3 Conclusion

In conclusion, we reported on C2AB molecules containing calcium ions, specifically for aggregating negatively charged lipid vesicles. A high local concentration of lipid vesicles can be achieved rapidly.

Chapter 3 Figures:

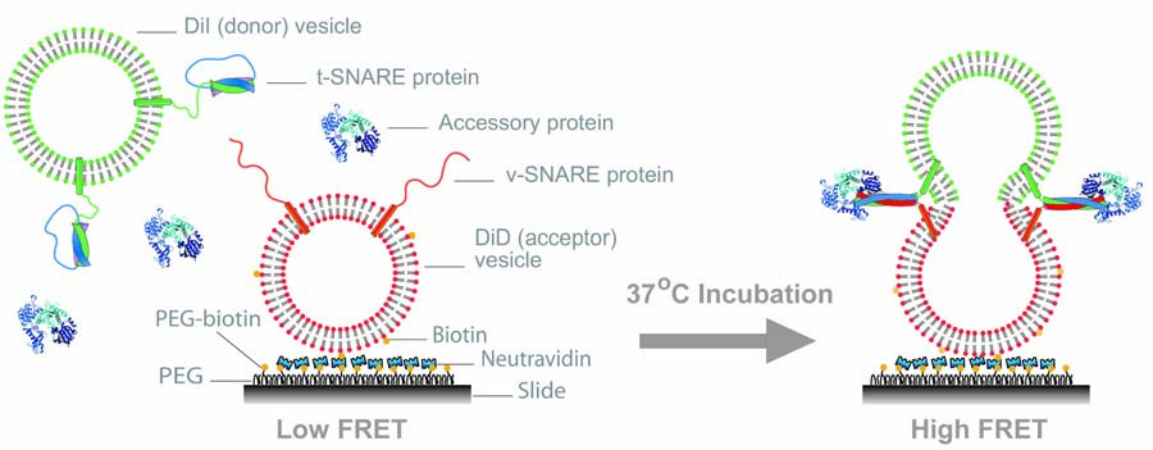

Figure 3.1. Schematics of the single-vesicle lipid mixing assay. (*Left*) DiD (acceptor) labeled v-SNARE vesicles are immobilized on the bottom surface of a flow chamber, which is also the imaging surface of the TIR microscopy. DiI (donor) labeled t-SNARE vesicles and accessory protein are introduced to the chamber space using a flow system. (*Right*) After a 37 ^{o}C incubation, some t-SNARE vesicles dock to single v-SNARE vesicles through formation of trans-SNARE complexes, and accessory protein binds to the trans-SNARE complexes. Membrane fusion between t- and v-SNARE vesicles and resultant lipid mixing will entail an increase in the FRET efficiency.

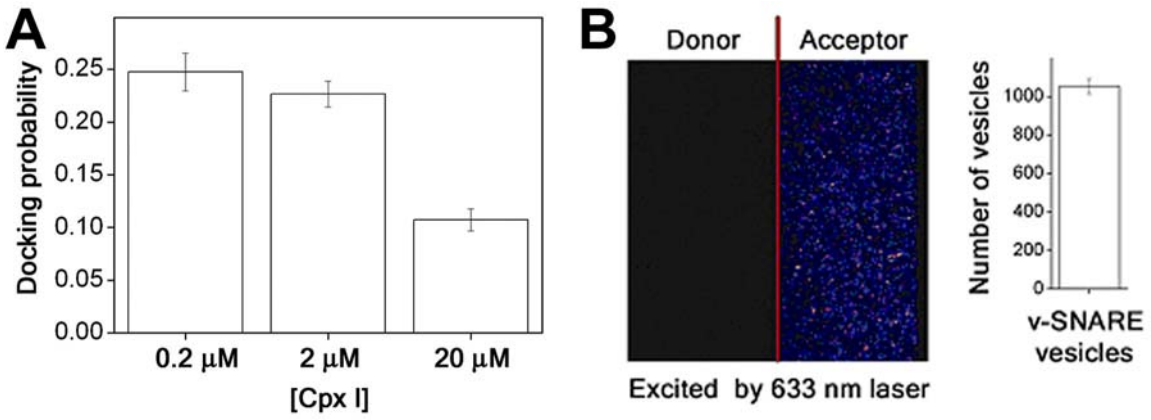

Figure 3.2. A, Docking probability of a single v-SNARE vesicle measured at t = 15 min as a function of the Cpx I concentration. Error bars, s.d. **B**, The number of v-SNARE vesicles in an imaging area can be counted by selectively exciting v-SNARE vesicles using a 633 nm red laser. (*Left*) An example image, directly obtained from TIR imaging, shows excited v-SNARE vesicles in the acceptor channel. (*Right*) The measured average is 1,052 ± 39 vesicles per imaging area. The docking probability of a v-SNARE vesicle can be simply obtained by dividing the number of docked t-SNARE vesicles with the average number of v-SNARE vesicles.

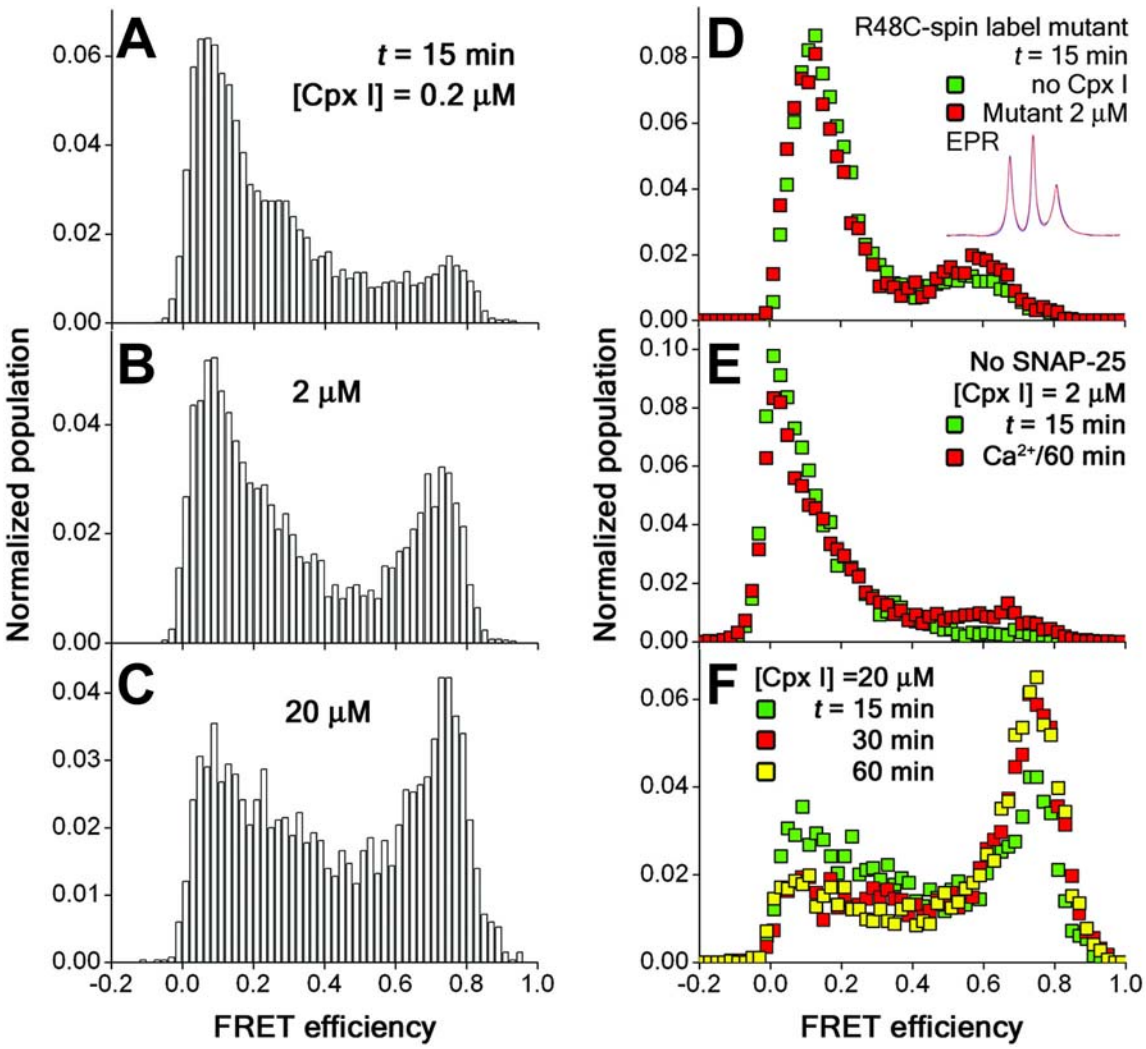

Figure 3.3. A-C, FRET histograms of single-vesicle complexes measured at t = 15 min at [Cpx I] = 0.2 (**A**), 2 (**B**), and 20 μM (**C**). **D**, Control data using the C105A/R48C-spin label complexin I mutant. The FRET population assay (green symbol: without complexin I, red: with 2 μM mutant; t = 15 min) shows the stimulation effect is largely diminished, coincident with the impaired complexin binding to ternary SNARE complexes. **E**, Control data without SNAP-25. t-SNARE vesicles with only syntaxin HT (lipid/protein ratio = 200:1) and [Cpx I] = 2 μM were used for incubation with v-SNARE vesicles. Green symbols show the FRET distribution measured at t = 15 min. (*Red*) 1 mM Ca^{2+} was injected subsequent to flow washing of t-SNARE vesicles and complexin I, and

FRET values were imaged at t = 60 min. **F**, Time-course change of the single-vesicle FRET histogram at [Cpx I] = 20 μM. Three FRET histograms, measured at t = 15 (green), 30 (red), 60 min (yellow), are shown.

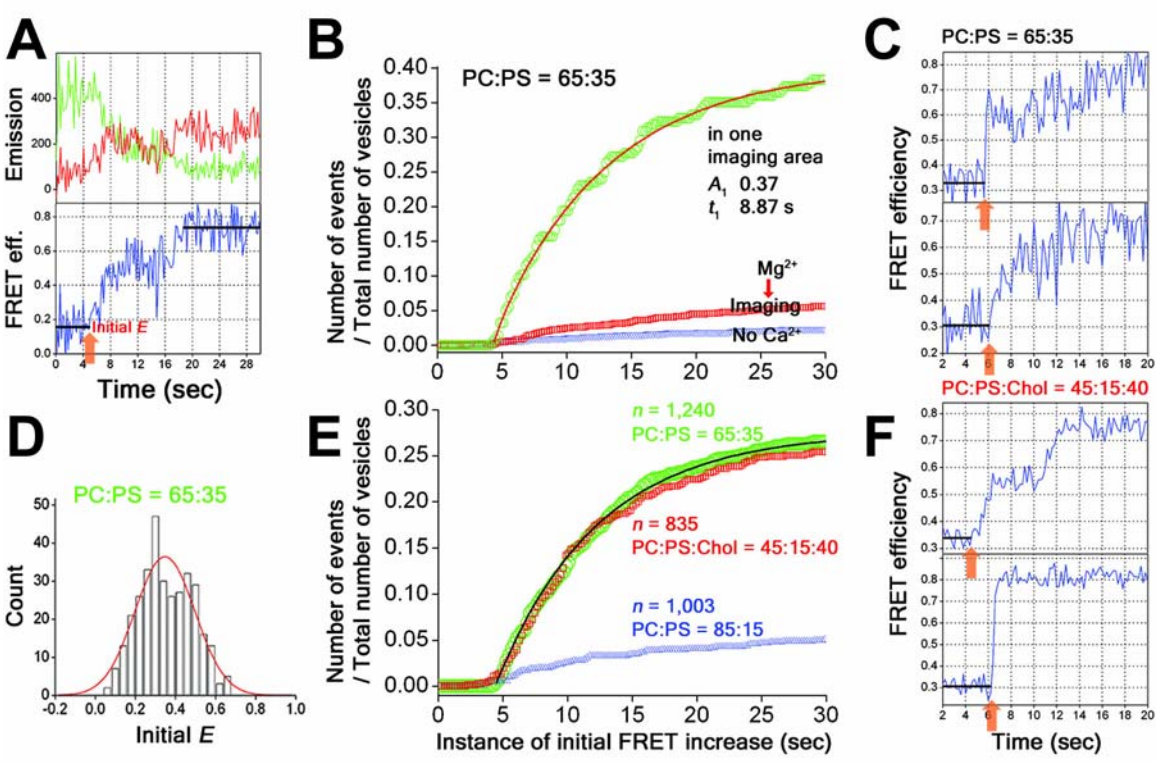

Figure 3.4. Ca^{2+}-accelatrates, complexin-assisted single vesicle fusion events. *t* denotes the time elapsed after start of real-time tracking. **A**, Exemplary real-time fusion trace of a single-vesicle complex. (*Upper panel*) Shown are the changes in the donor (green) and the acceptor (red) fluorescence intensities. (*Lower panel*) The corresponding changes in the FRET efficiency are shown in blue. The initial and the final FRET states are marked by black bars and the instance of initial FRET increase is marked by an orange arrow. The data in **A-D** were measured using the lipid composition of 65:35 (mol/mol) POPC:DOPS. **B**, (*Green symbol*) Cumulative plot of the instances of initial FRET increase for 217 vesicle complexes in one imaging area. With the first-order kinetics assumed, we used two exponentials, $A_1(1-\exp^{-t/t_1})+A_2(1-\exp^{-t/t_2})$, to fit the plot after the Ca^{2+} arrival at 4.4 sec (red curve). The time constants (t_1, t_2) and the corresponding normalized population (A_1, A_2) are (8.87 sec, 0.95 sec) and (0.37, 0.01), respectively. We

thus find that the cumulative plot exhibits mainly one time constant of ~8.9 sec. (*Red* and *Blue symbols*) Cumulative plots of the instances of initial FRET increase upon injection of 1 mM Mg^{2+} (Red) or fusion buffer without Ca^{2+} (Blue). Both cumulative plots are based on multiple numbers of flow experiments; Total number of vesicle complexes studied are 1,161 (Red) and 1,900 (Blue). **C**, Exemplary real-time traces showing synchronized FRET jumps. The instances of initial FRET increase, marked by orange arrows, are 5.8 and 6.2 sec (from upper to lower). **D**, Distribution of the initial *E* values for the single-vesicle complexes that show an FRET increase within the first 30 second window. Fitting with a Gaussian distribution gives the center at $E = 0.35$ and the standard deviation of 0.15 (red curve). Total 1,240 vesicles from five independent flow experiments are included in statistics, and the corresponding cumulative time plot is shown as green symbols in **E**. **E**, Cumulative plots of the instances of initial FRET increase for different lipid compositions: (green symbol) 65:35 (mol/mol) POPC:DOPS, (red) 45:15:40 (mol/mol/mol) POPC:DOPS:cholesterol, and (blue) 85:15 (mol/mol) POPC:DOPS. n = 1,240 (green), 835 (red), and 1,003 (blue). **F**, Exemplary real-time traces showing synchronized FRET jumps. The lipid composition of 45:15:40 (mol/mol/mol) POPC:DOPS:cholesterol was used. The instances of initial FRET increase, marked by orange arrows, are 4.8 and 6.2 sec (from upper to lower).

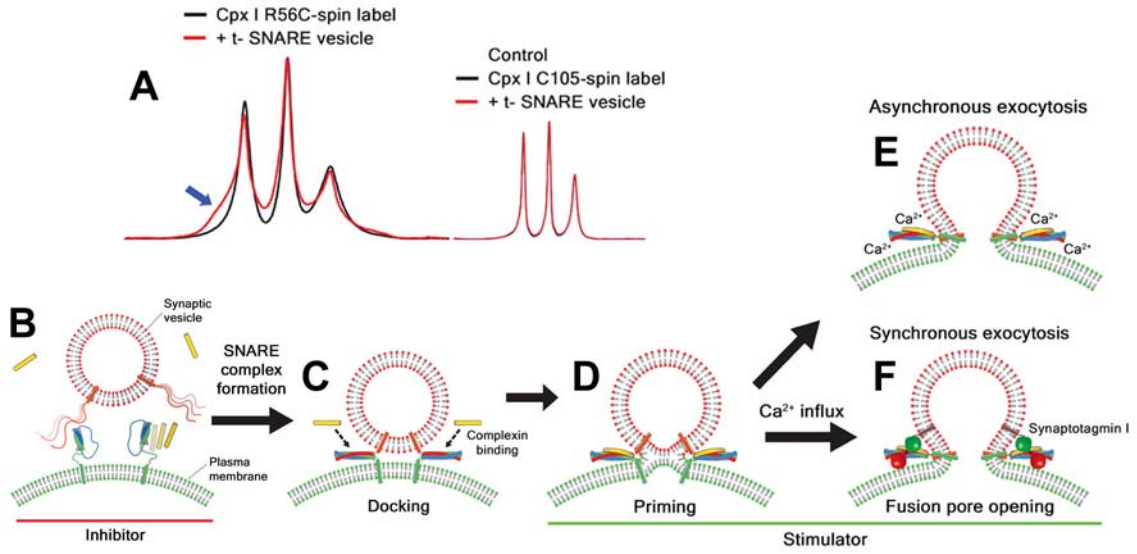

Figure 3.5. Molecular model of complexin function for Ca^{2+}-triggered neurotransmitter release. **A**, Room temperature EPR spectra of a spin-labeled complexin 1 mutant (C105A/R56C-spin label) when incubated in fusion buffer (black trace) or mixed with solution of t-SNARE vesicles (red trace). (*Inset*) For negative control, we attached a spin label to native cysteine at position 105 of complexin 1. The EPR spectra of the C105-spin label mutant do not show any change when incubated with t-SNARE vesicles, indicating the broadening observed for the R56C-spin label mutant specifically reflects the interaction between complexin 1 and t-SNARE proteins. **B**, Pre-docking stage: Through the direct interaction with t-SNARE proteins, complexin competes with v-SNAREs for binding to t-SNAREs. At a high expression level, complexin has the effect of suppressing formation of *trans*-SNARE complexes. **C**, Docking stage: Once *trans*-SNARE complexes are formed, synaptic vesicles are more tightly associated with the plasma membrane, and complexin binds to the ternary SNARE complexes. **D**, Priming stage: Complexin directly lowers energy barriers for synaptic vesicle fusion in cooperation with neuronal SNAREs. **E** and **F**, Fusion pore opening stage: The synaptic vesicles primed by complexin and

other non-synaptotagmin fusion stimulators directly react with Ca^{2+} to produce the asynchronous neurotransmitter release (**E**). The molecular action of Ca^{2+}-bound synaptotagmin 1 further accelerates fusion pore opening, achieving the synchronous release (**F**).

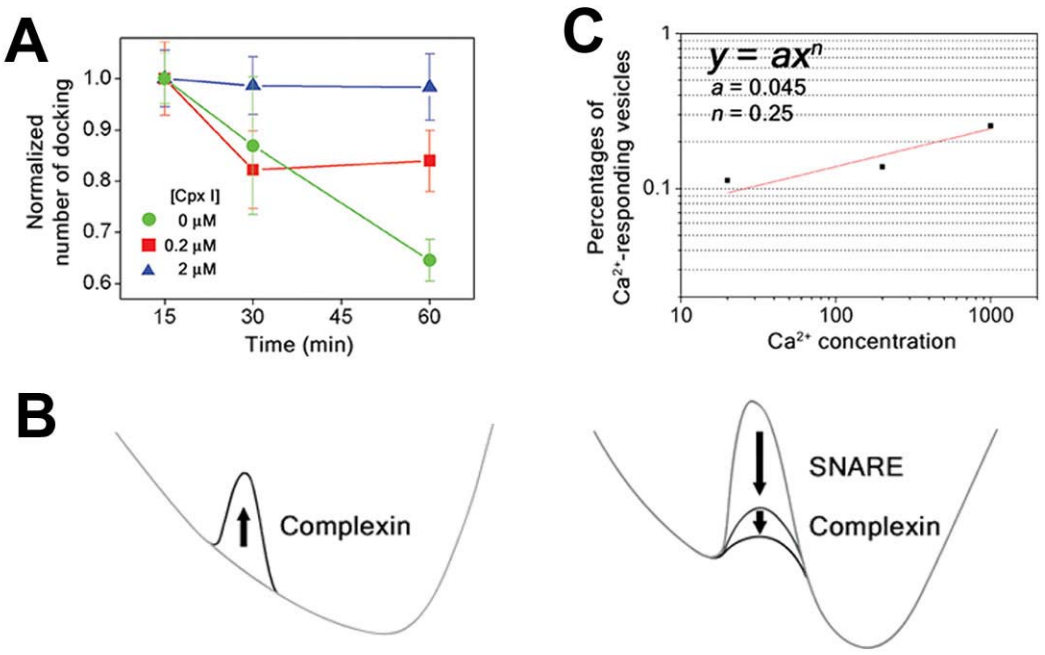

Figure 3.6. A, Time-course change of the number of docked t-SNARE vesicles. The sequence of experiments is the same as that for Figure 3.3. The numbers of docked t-SNARE vesicles at [Cpx I] = 0 (green circle), 0.2 (red square), and 2 μM (blue square) were measured at t = 15, 30, 60 min. Each case was normalized by the docking number measured at t = 15 min. **B**, Energy landscapes of SNARE-mediated fusion assisted by complexin for clamping model (left) and promotion model (right). **C**, Percentages of the Ca^{2+}-responding vesicles (in the 25-second window) at three Ca^{2+} concentrations higher than the threshold (20, 200, and 1,000 μM).

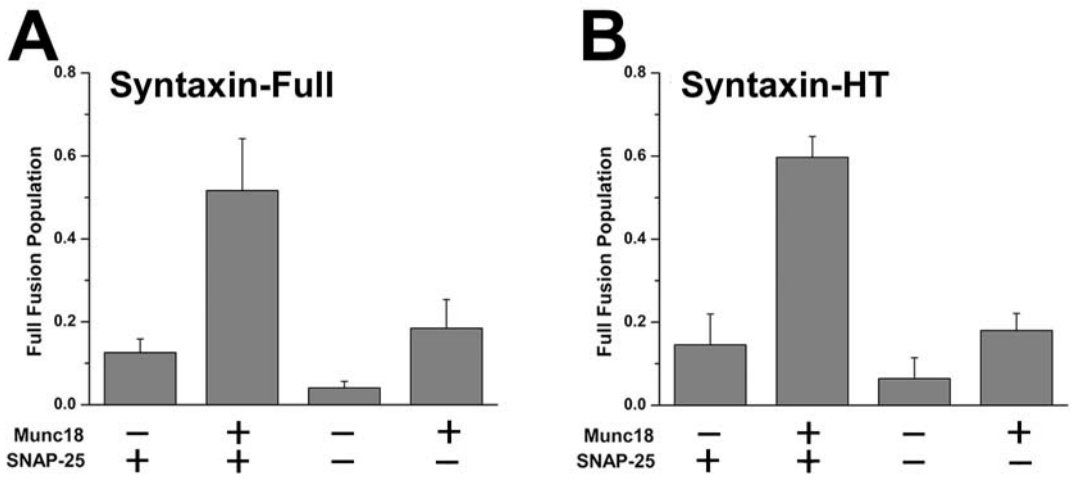

Figure 3.7. Fraction of vesicle complexes showing full fusion for various reaction conditions. 1 μM Munc18-1 was used. Results obtained with the full length syntaxin (**A**), and with a syntanxin-HT (**B**). Controls without SNAP-25 led to a significant reduction in full fusion, likely due to the formation of incomplete SNARE complexes, which cannot mediate efficient fusion. Full fusion population is calculated by summing all normalized populations with E values > 0.5. Error bars denote the s.d. of 3 to 5 independent experiments with different batches of SNARE and Munc18-1 proteins.

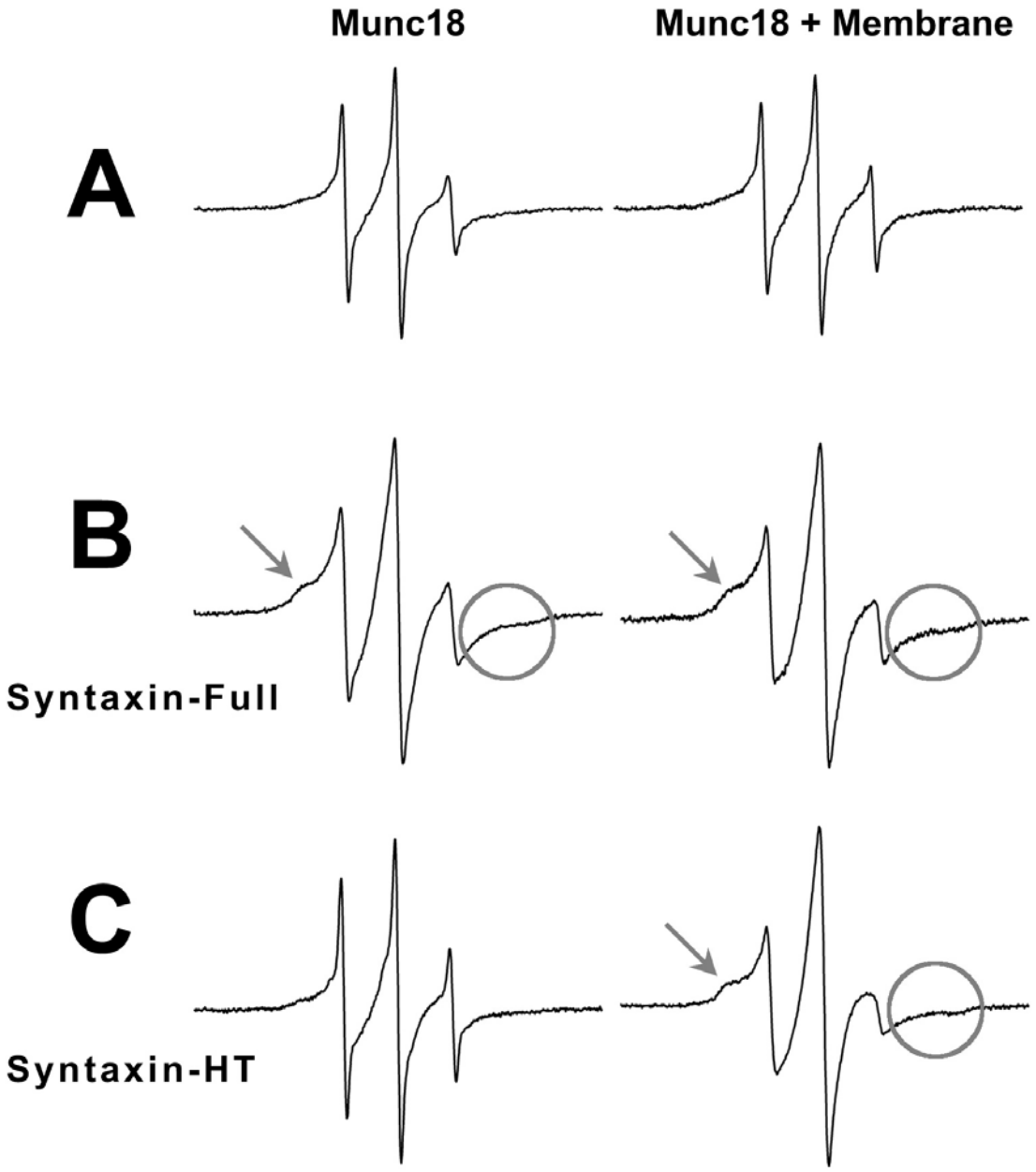

Figure 3.8. Electron paramagnetic resonance (EPR) spectra of Munc18-1. **A**, Munc18 only (left panel) and Munc18with protein free membrane in the fusion buffer (right panel). The same EPR sharp spectra indicate that there is no measurable interaction between Munc18 and membrane. **B**, Munc18 with syntaxin-full protein (left panel) and Munc18 with membrane-associated SNARE complex containing syxtaxin-full (right panel). Both

EPR spectra are broadened in comparison to the spectrum of Munc18 only (**A**, left panel) indicating interactions. **C**, Munc18 with syntaxin-HT protein (left panel) and Munc18 with membrane-associated SNARE complex containing syntaxin-HT (right panel). The sharp EPR spectrum on the left indicates that there is no interaction between Munc18 and syntaxin-HT, while the broadened EPR spectrum on the right suggests interactions. Arrows indicate the quaternary interaction between Munc18 and SNAREs, and circles show the spin-spin interaction due to the clustering of spin labeled Munc18.

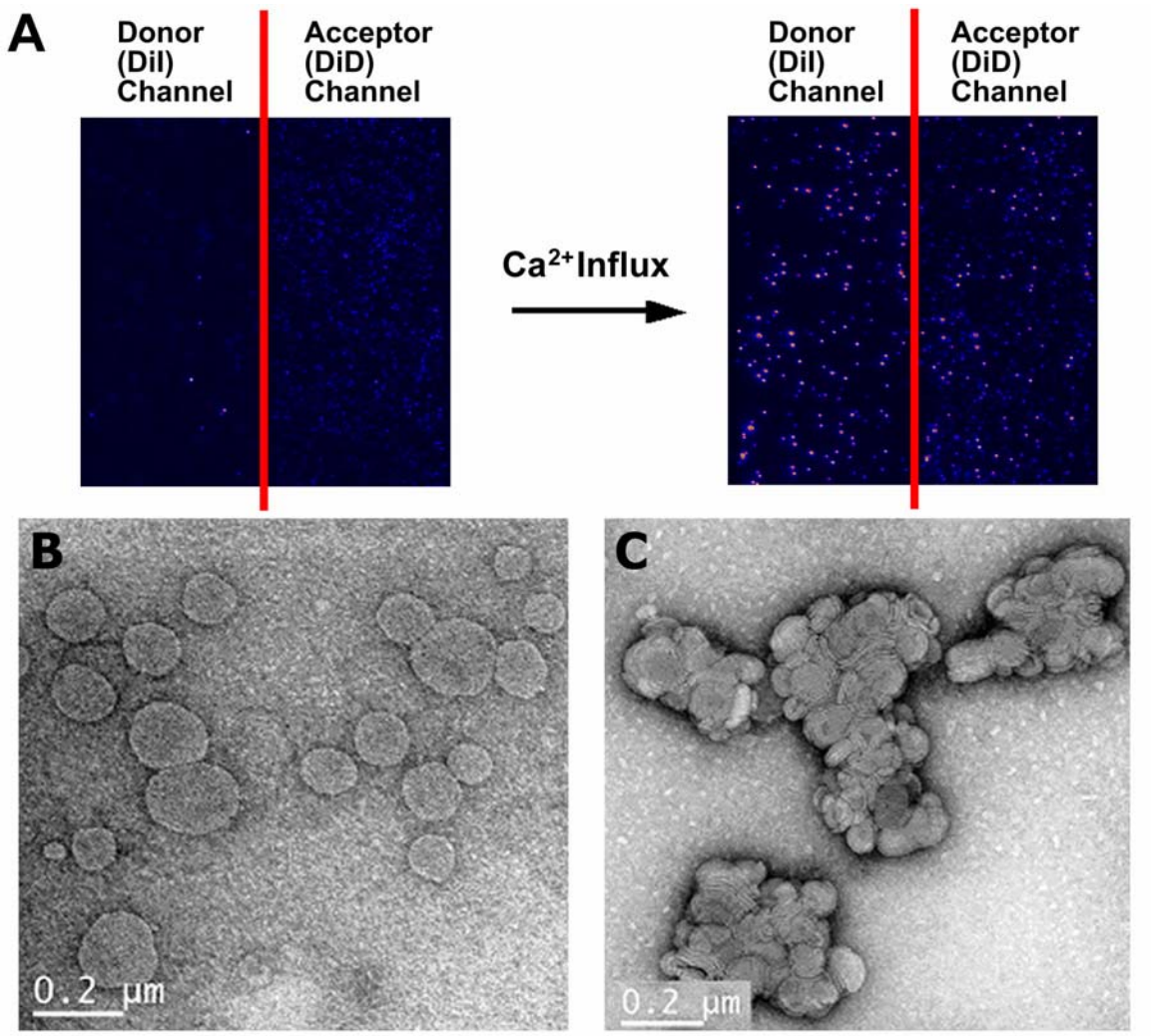

Figure 3.9. A, TIR images before and after 0.1 mM Ca^{2+} influx. The images are split into donor and acceptor channels. Only a few fluorescent debris molecules were visible in donor channel before calcium influx. A large number of bright donor spots in the TIR image appeared shortly after calcium influx indicating the docking of DiI liposomes to the surface-immobilized DiD liposomes. The negative stain transmission electron micrographs of liposomes (35 mol% PS : 65 mol% PC) without (**B**) and with adding 1 µM C2AB and 0.1 mM Ca^{2+}, (**C**).

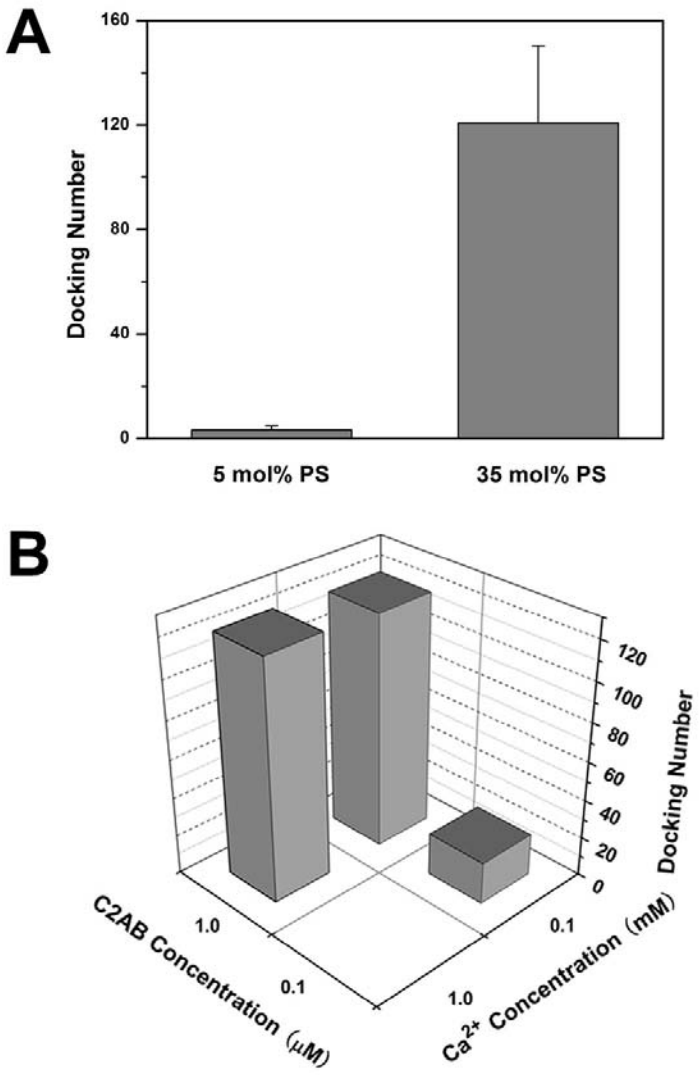

Figure 3.10. A, Average number of docked DiI-liposomes per imaging area (25 μm × 50 μm). We studied two different lipid compositions for vesicles, one with 5 mol% and the other 35 mol% PS molecules. When the PS concentration was reduced to 5 mol%, the portion of PC lipids was accordingly increased to 95 mol%. 15 to 20 imaging spots were used to get these average values. 0.1 mM Ca^{2+} and 1 μM C2AB were used. **B**, Average number of docked DiI-liposomes for various C2AB and calcium concentrations.

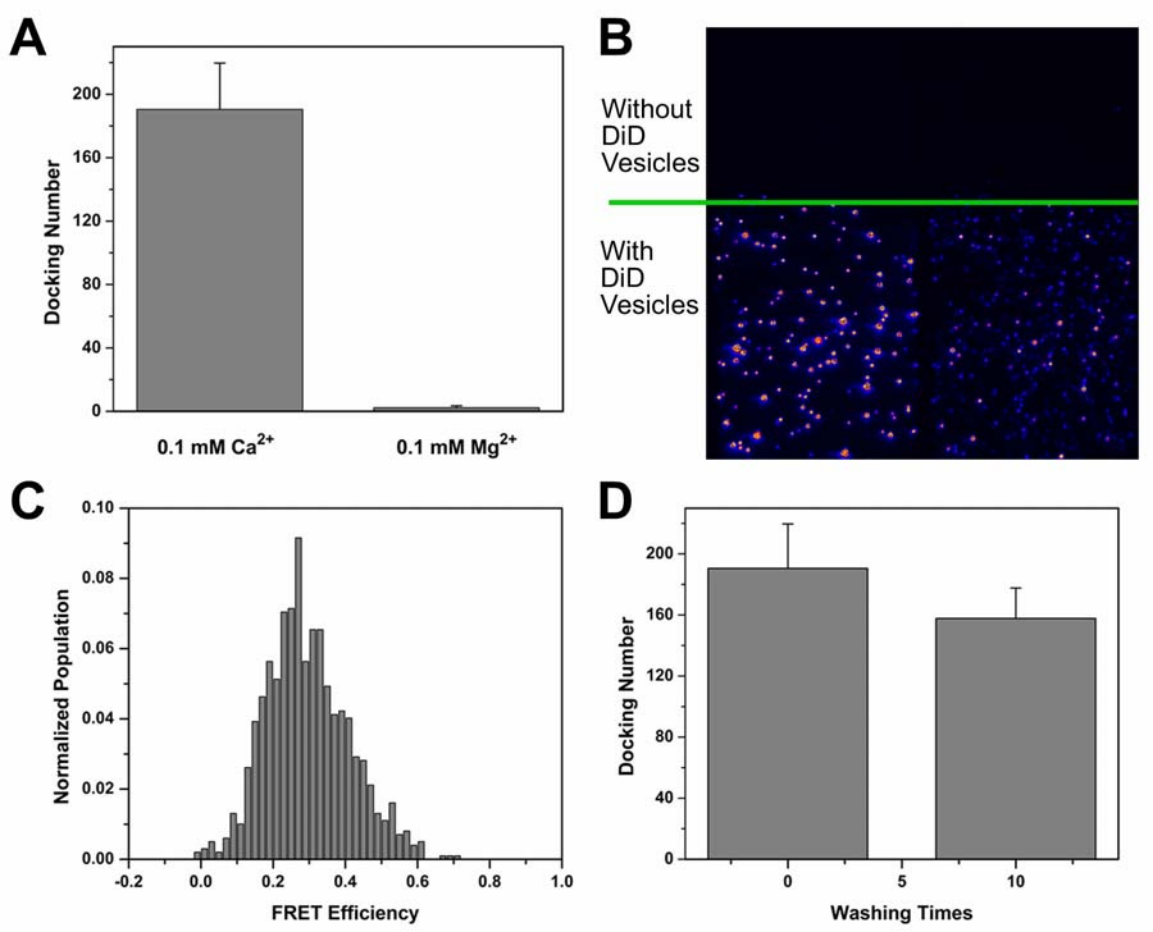

Figure 3.11. A, Average number of docked DiI-liposomes after 0.1 mM Ca^{2+} and 0.1 mM Mg^{2+} influx. **B,** A TIR image of a flow channel after 0.1 mM Ca^{2+} influx. The DiD vesicles on the upper part of this flow channel were removed by an air bubble before injecting DiI liposomes. **C,** The FRET distribution of DiI and DiD vesicle complexes after 0.1 mM Ca^{2+} influx. The FRET population peak at 0.3 represents close-docked state or the hemifusion state of vesicle complexes. **D,** Average number of docked DiI-liposomes before buffer washing and after ten-rounds of buffer washing, 150 μL for each round.

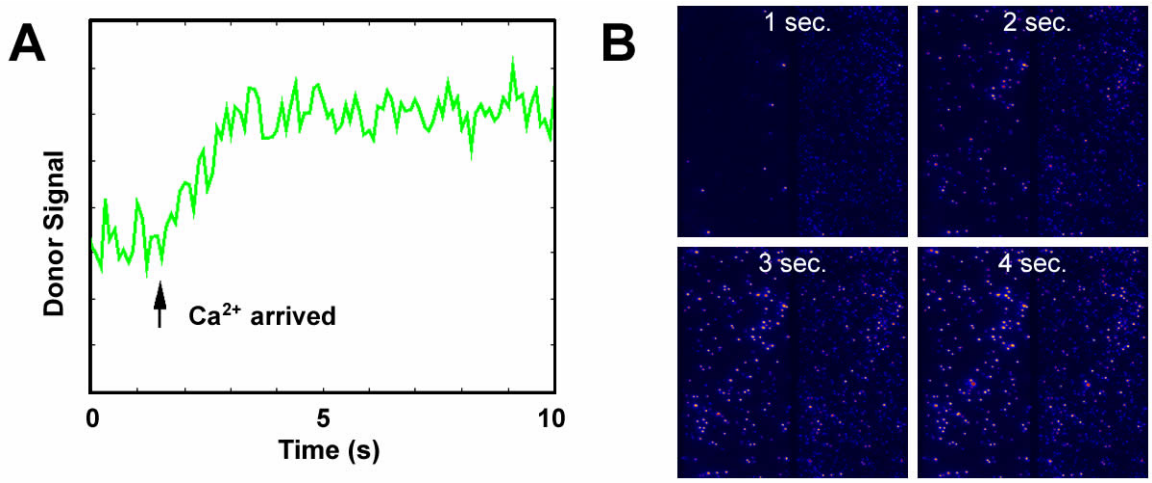

Figure 3.12. A, A real-time fluorescent trace of donor (DiI) channel, averaged over all liposomes, upon the arrival of Ca^{2+} influx. **B,** TIR images for both donor and acceptor channels of the same trace shown in part **A** at different times. For more information, see the movie in supporting materials.

CHAPTER 4

CONTENT MIXING

4.1 Motivation

The lipid mixing method developed in our lab has been shown as a useful technique through revealing the vesicle aggregation induced by C2AB/Ca^{2+}, a dual function of complexin, and the role of Munc18/SNARE-core binding mode [34,39,49]. This method clearly shows the fusion process by observing the mixing of two lipid bilayers. Despite the success with assays based on lipid-mixing, they cannot directly detect the content release, which is one of the most rigorous definitions of membrane fusion [94]. Cellular studies showed that the content release can proceed in two pathways, kiss-and-run, where a small fusion pore opens transiently upon docking of an incoming vesicle, but closes again as the vesicle 'runs' away, and the full-collapse fusion pathway, where the small opening of the pore continues to expand to a large pore [95,96]. Unfortunately, both current ensemble and single-vesicle lipid mixing assays are blind to the fusion pore formation and expansion and, therefore, unable to tell how the regulatory proteins are involved in this critical step.

There is a general assumption that the extent of lipid mixing between vesicles is directly proportional to the extent of the content release. However, a recent study on DNA-mediated vesicle fusion showed that high efficient lipid mixing (up to 80%) of both inner and outer leaflets can occur without mixing of content (less than 2%) [97]. A similar phenomena was observed with PEG-mediated membrane fusion [98]. These

studies suggest that lipid mixing is necessary for fusion, but lipid mixing alone is an insufficient indicator for content mixing.

The original *in vitro* reconstruction of SNARE-induced membrane fusion used ^{33}P-labeled oligonucleotides and led to the conclusion that SNARE proteins constitute the minimal machinery for membrane fusion [99]. However in that study, because the content mixing signal was indirectly measured after vesicles were lysed by the detergent, their result could not clearly separate fusion from vesicle docking and aggregation. Other attempts of using small reporters, such as carboxyfluorescein, for the content mixing studies have mainly failed due to the membrane leakiness after the SNARE protein reconstitution at a physiological protein to lipid ratio (> 1:500) [98], unless a very low protein and lipid ratio (< 1:1000) was used [100,101].

Thus, the formation of fusion pore, as well as the key factor of pore expansion, remains to be confirmed by a new content mixing method. We have developed a reliable and efficient single-vesicle content mixing assay for SNARE-mediated membrane fusion. The main advantage of single-molecule experiments is that they allow us to study the behaviour of a single or countable number of molecules. The observation of individual events allows us to perform statistical analysis of a population of individual trajectories that is not possible in bulk because of ensemble averaging [55,56,94].

4.2 Experimental design

To detect large fusion pores, with the inspiration from molecular beacons [102], we designed a DNA hairpin composed of five base-pairs stem and poly-thymidine loop (T_{20}) labeled with a donor (Cy3) and an acceptor (Cy5) fluorophores at either ends of the stem

(Figure 4.1A). When the loop region of this Cy3/Cy5 dual-labeled DNA probe hybridize with a second DNA strand having a complementary sequence (A_{30}), the formation of a longer double strand breaks apart the stem region, which moves apart the donor and the acceptor fluorophores from one another. As a result of this distance change, the FRET efficiency (*E*) switches from a high to a low value (Figure 4.1B and 4.1C). Dual-labeled DNA and the complementary poly-adenosine (poly-A) strands are encapsulated inside proteoliposomes reconstituted with vesicle SNARE (v-SNARE) and target membrane SNARE (t-SNARE), respectively, and the FRET signal is used to monitor the extent of the SNARE-mediated content mixing.

Because many earlier attempts suffered from probe leakage, we first tested the stability of our dual-labeled DNA probe inside the vesicle. Dual-labeled DNA probe encapsulated vesicles reconstituted with yeast v-SNARE protein (Snc2p) (1:200 protein to lipid ratio) were immobilized on the polymer-coated imaging surface. Non-specific binding of dual-labeled DNA probes outside the vesicle was prevented by the PEG molecule coating flow cell surface, and these DNA molecules were washed away with excess buffer (Figure 4.2A). Single molecule fluorescence signals from DNA molecules in individual vesicles were collected and plotted as a histogram showing a distinct high *E* as expected (Figure 4.3A left). In order to verify that these probes were inside the vesicle, Deoxyribonuclease I (DNase) was added to the system. The number of molecules showing the high FRET signal before and after the treatment did not show a significant difference (Figure 4.3A) and no shift of the FRET distribution was observed. This shows that DNA probes are inside vesicles and are protected by lipid bilayer from DNase digestion. In contrast, DNase treatment effectively eliminated DNA probes unprotected

by vesicles (Figure 4.3B). These DNA probes did not leak out of vesicles over the course of 60 minutes (Figure 4.3C), and showed stable high FRET distribution at 37 ^{o}C incubation as well as in the presence of free poly-A DNA outside the vesicles (Figure 4.2B). These control experiments show that Cy3/Cy5 dual-labeled DNA probe could be used as a reliable content mixing indicator [103].

A reliable and an efficient content-mixing assay based on the FRET switch caused by the DNA hybridization has been developed at the single vesicle level. The DNA hairpin probe used is thirty nucleotides long with a molecular weight of ~11 kD, whereas most neurotransmitters are much smaller (~0.1 kD). A transient opening of fusion pores allows passage of small molecules, but the larger molecular weight probes used here may be difficult to pass. Our assay is most likely to report the content mixing resulting from the stably expanded pore that results from the complete collapse of vesicle membranes.

4.2.1 Content probe size simulation

In order to estimate the minimal required fusion pore size, we performed a Molecular Dynamics (MD) simulation to calculate the radius of gyration of both Cy3/Cy5 dual-labeled DNA hairpin and unlabeled target DNA in equilibrium condition. The average Rg over the last 25 ns of simulation for DNA hairpin is 1.91 ± 0.53 nm, while 1.80 ± 0.28 nm for target DNA (Figure 4.4). We conclude that the radius of the pore has to be ~2 nm for either DNA to pass through. In principle, the single-stranded DNA can go through a narrow pore with a large Rg as in the case of stretched out. However, in our case, it is unlikely for the unlabeled target DNA to adopt such extended configuration without external force if one considers its high flexibility.

For a general membrane fusion process, the outer monolayer of a phospholipid vesicle coalesces with the contacting monolayer of the planar phospholipid bilayer membrane forming a trilaminar structure (hemifusion). A small fusion pore is formed in this area. Once formed, the fusion pore can close again or expand to some critical size when further expansion becomes irreversible [104]. For the critical size of pore, as estimated by Jackson, the lipidic fusion pore has an energy minimum at a radius of ~0.5 nm [105,106]. Since the minimal fusion pore size (2 nm radius) to pass through our content-mixing indicator is much larger than this critical size, fusion pore expansion, the very late step of membrane fusion, is most likely reported through this assay.

4.3 Study on yeast SNARE

[Related publication: Diao, J., Su, Z., Ishitsuka, Y., Lu, B., Lee, K.S., Lai, Y., Shin, Y.-K. & Ha, T. A single vesicle content mixing assay for SNARE-mediated membrane fusion. *Nat. Commun.* **1**, 54 (2010).]

We first applied our content mixing assay to the yeast SNAREs (Sso1p, Snc2p and Sec9c) that mediate constitutive fusion of transport vesicles to the plasma membrane [107]. Figure 4.5A shows the basic scheme of our assay. The v-SNARE vesicles, with Snc2p in the membrane and DNA hairpin encapsulated inside, are immobilized on a polymer-coated quartz surface via biotinylated lipids [61]. The t-SNARE vesicles containing Sso1pHT and harboring multiple poly-A DNAs with a cholesterol modification are added together with soluble Sec9c (1 μM), and the sample is incubated at 37 ^{o}C. The average number of dual-labeled DNA probes inside the v-SNARE vesicle quantified from the number of photobleaching steps is ~0.4 (Figure 4.6). Cholesterol

modification increases the incorporation efficiency of poly-A DNA in the t-SNARE vesicle membrane, thus increasing the probability of two vesicles with DNA probes to react (Figure 4.7). When two vesicles, both ~100 nm in diameter, dock and a large enough fusion pore forms between them, the two DNA molecules should hybridize to switch the FRET efficiency (*E*) between Cy3 and Cy5 from a high (Figure 4.3A) to a low value (Figure 4.1C).

Figure 4.5B and 4.5C show actual *E* distributions before and after addition of t-SNARE vesicle/Sec9c to the flow cell and incubated for 30 minutes at 37 ^{o}C. The *E* distribution measured from thousands of single DNA hairpin probes clearly switched from ~0.8 to ~0.2 (Figure 4.5B and 4.5C). We repeated the same experiment using DNA without the cholesterol link to the target DNA and observed a similar shift in the *E* distribution, but with a reduced extent of FRET population shift due to a lower DNA encapsulation efficiency (Figure 4.7). To further ensure that the DNA hybridizations are taking place inside vesicles, the sample was treated with DNase after the fusion reaction. The *E* distribution remained the same and the average number of fluorescent spots did not decrease, indicating that all observed signals came from DNA probes inside vesicles (Figure 4.8A).

The formation of these stable pores was not caused by the surface immobilization step. We verified this by first performing the fusion reaction in bulk solution, and then immobilizing the product onto the surface. As shown in Figure 4.8B, the major low FRET peak from DNA hybridization was observed as in the standard experimental scheme. This FRET shift was driven in the DNA sequence dependent manner - and not by protein or vesicle aggregation - for when we replaced target poly-A DNAs in t-

vesicles with non-complementary poly-T DNAs, no FRET switch was observed under the same reaction condition on the surface (Figure 4.8C).

4.3.1 Real time content mixing

Through our single vesicle content mixing assay, we can also monitor single content mixing event in real-time. For this experiment, we switched the surface immobilization configuration. t-vesicles with the target DNAs are surface immobilized and v-vesicles containing FRET beacons are flown into the solution. To eliminate DNA molecules outside vesicles, DNase I treatment was applied before reactions. A typical real-time content-mixing time traces are shown in Figure 4.9. Upper panel shows fluorescence intensities, green curve representing the donor and red curve representing the acceptor intensity. The lower panel shows the corresponding FRET efficiency in blue. Initially, the surface immobilized vesicles containing unlabeled target DNAs shows no donor and acceptor signals. Upon binding of the v-vesicle with FRET beacon is seen as a sudden appearance of the fluorescence signal associating to a high FRET value. After a certain time, DNA hybridization caused by content mixing decreases FRET value to ~0.2.

4.3.2 Yeast SNAREs are sufficient to induce content mixing.

The *E* shift we observed with our content mixing assay is SNARE dependent. A control experiment without Sec9c showed no change in *E*, while lowering the Sec9c concentration (0.1 μM) reduced the vesicle population with expanded pores (Figure 4.10A). Interestingly, 0.1 μM Sec9c, corresponding to ~2:1 Sec9/Sso1 ratio, showed a much lower degree of content mixing than lipid mixing [61]. This seems to suggest that

in some instances, lipid mixing could progress without formation of stable pores across the membrane. A time course study showed a progressive shift from *E*~0.8 population to *E*~0.2 population over 30 minutes (Figure 4.10B).

Two helices of Sec9c both contribute in formation of the four-helix bundle necessary for membrane fusion, but play slightly different roles. The N-terminal helix (SN1) plays more dominant role in the initial docking of the vesicle, while the C-terminal helix (SN2) drives the membrane lipid mixing [108]. Helix-breaking proline mutations (L626P, L647P) on SN2 helix showed significantly stronger inhibitory effect on the lipid mixing efficiency in comparison to the docking efficiency, but their effect on pore formation has been unclear [108]. We also tested these mutants using our content mixing assay and found a similar inhibitory effect on the pore formation efficiency (Figure 4.9C). The proline mutation close to the C-terminal end of the helix (L647P) showed a stronger inhibitory effect than what the L626P mutant did on both lipid and content mixing supporting that complete engagement of SN2 helix in the SNARE complex is necessary for completing membrane fusion.

4.3.3 Conclusion

Yeast SNARE proteins has been known to induce efficient and rapid lipid mixing [109]. Our results further show that yeast SNARE proteins are necessary and sufficient for expansion of the fusion pore.

4.4 Study on neuronal SNARE

[Related publication: Diao, J., *et al.* Ha, T. Protein facilitated membrane fusion pore expansion. (in preparation)]

We applied this single vesicle content mixing assay to neuronal SNAREs, which constitute the minimal machinery for membrane fusion [7]. However, the conclusion has being questioned due to its rather slow fusion rates and its inability to distinguish between various intermediate statuses and the full fusion for the release of vesicle contents.

4.4.1 Neuronal SNAREs are able to induce content mixing inefficiently

As shown in Figure 4.11, few FRET switch was observed after a 30-minute incubation of v- and t-SNARE vesicles at 37 ^{o}C, while a small low FRET peak corresponding to content mixing was observed after a 60-minute incubation. This indicates that neuronal SNAREs are much less efficient for fusion pore expansion, which an essential step for full collapse fusion, in the absence of the fusion regulators while one SNARE interaction is sufficient for vesicle docking [53]. It is still possible that a fusion pore opens, but the pore is either too transient or too small for passage of our large DNA probes.

Our previous results further showed that yeast SNARE proteins are necessary and sufficient for expansion of the fusion pore [103]. For the neuronal SNARE on the other hand, although a limited extent of lipid mixing does occur [39], SNAREs alone are inefficient to form stable pore for passage of our large DNA probes. SNARE complex has been regarded as the minimal machinery for membrane fusion [7]. However, the conclusion has being questioned due to its rather slow fusion rates, which is due to a slow

full complex formation rate or a block effect by a 2:1 (syntaxin:SNAP-25) t-SNARE complex [110]. Thus, how to effectively form fully-assembled SNARE complexes is essential for SNARE-mediated fusion. Recent studies showed that fully-assembled SNARE complexes facilitated by VAMP fragments or N-terminal mutant are able to induce fast full fusion [110,111].

For SNARE proteins only, a recent single molecule force study shows that breaks of only 7 N-terminal hydrophobic layers are required for rupture of the neuronal SNARE complex compared to 15 hydrophobic bonds for rupture of the Syntaxin1A-VAMP2 binary complex [112]. This study indicates some major differences in the layers of the SNARE complex between yeast and neuronal cases, especially, in the membrane-proximal half of the complex, which could affect the kinetics of assembly and driving full fusion events. As shown recently, these membrane proximal layers play an important role in Ca^{2+} triggered fusion assisted by synaptotagmin [113].

4.4.2 Synaptotagmin 1 expands fusion pores by facilitating SNARE formation

We also tested v-vesicle co-reconstituted with full-length synaptotagmin 1, an additional peak at E~0.2 emerged at the expense of the high E fraction (Figure 4.12A) after a 10-minute incubation with t-vesicles plus 10 μM Ca^{2+}. Due to a similar E value as the DNA hairpin hybridized to the target strand in solution and the FRET stoichiometry change (Figure 4.13), this new low FRET population is interpreted as the product of fusion reactions that proceeded through the expansion of large pore. The possibility of hybridization reaction taking place outside of the vesicles was rule out using the DNase I treatment (Figure 4.14). In contrast, incubating with the VAMP mutant without the

transmembrane region (6 μM, amino acids 1-92) or omitting synaptotagmin 1, during the SNARE complex formation step significantly inhibited the increase in the low *E* fraction (Figure 4.12B). A reduced low *E* fraction was observed when we removed Ca^{2+} ions (Figure 4.12A).

Most recently, using a single-vesicle lipid mixing assay, H.-K. Lee *et al.* showed that the membrane anchor synaptotagmin 1 and Ca^{2+} induce fast fusion through a trans-conformer [114], which is the first *in vitro* study showing the fusion promotion from full-length synaptotagmin 1 plus Ca^{2+}. *In vivo*, the neurotransmitter release happens in the submillisecond time scale and is induced by calcium with synaptotagmin 1 being the calcium sensor. However, *in vitro* experimental results with full-length synaptotagmin 1 showed a Ca^{2+}-independent promoted effect, while adding Ca^{2+} ions inhibits vesicle fusion [29,32]. Furthermore, recent studies using native synaptic vesicles from the rat brain showed that the final step in fusion is calcium independent even though the synaptic vesicles contained endogenous synaptotagmin 1 [33]. Here, through our new single-vesicle content mixing assay, we confirm that the fusion induced by synaptotagmin 1 and Ca^{2+} by a trans-conformer is also associating with mixing of large contents, which is a sign of expanded fusion pore. This observation agrees with previous *in vivo* studies showing that synaptotagmin 1 promotes full fusion while synaptotagmin 4 stimulates kiss-and-run events [115].

We observed some pore expansion processed by synaptotagmin 1 in the absence of calcium, which also agrees with previous *in vitro* studies for full-length synaptotagmin 1 [29,32,33]. Since fully-assembled SNARE complexes are able to induce fast full fusion [110] and synatotagmin 1 promotes SNARE complex formation through a Ca^{2+}-

independent interaction with t-SNAREs [116,117,118,119], we conclude that synaptotagmin 1 expands fusion pores by promoting SNARE complex formation. Ca^{2+} ions dramatically accelerate this interaction into a synchronized manner through a structure reformation [120,121]. By using SNARE proteins purified directly from the bovine brain, Rickman *et al.* also showed that synaptotagmin 1 binds to the SNARE complex in a calcium-independent manner [122]. Through Electron paramagnetic resonance (EPR), the Ca^{2+}-independent interaction between synaptotagmin and SNARE (Figure 4.15) is confirmed. Because of the Ca^{2+}-independent interaction, the synaptotagmin 1 binding blocked by complexin in the absence of Ca^{2+} is essential for the synchronized fusion process [37]. Furthermore, a doubled content mixing observed in the presence of Ca^{2+} ions (Figure 4.12A) also implies an additional fusion promotion by Ca^{2+}-bound synaptotagmin 1, for instance, membrane bending [30,123] or adhering [29,93].

4.4.3 Conclusion

Based on our content mixing current results presented in this paper, we suggest that synaptotagmin 1 expands fusion pore by facilitating SNARE complex formation. Calcium ions are important to synchronize the pore opening events by accelerating the synaptotagmin-facilitated SNARE complex formation.

Chapter 4 Figures:

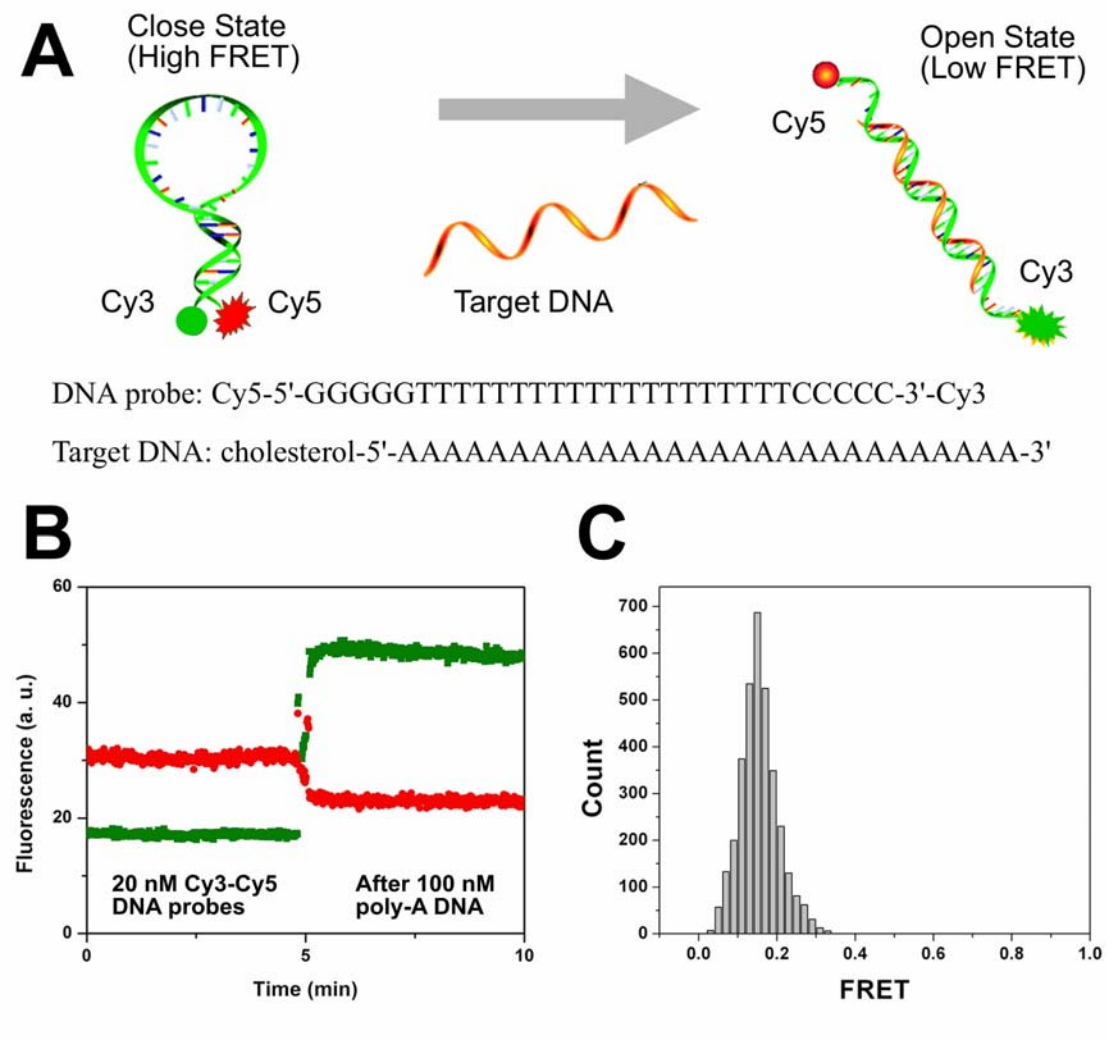

Figure 4.1. Dual-labeled DNA hairpin probes are single-stranded oligonucleotide hybridization probes that form a stem-and-loop hairpin structure. The loop contains a probe sequence (poly-T, 20mer long) that is complementary to a target sequence (poly-A, 30mer), and the 5 base pair stem is formed by the annealing of complementary arm sequences that are located on either side of the probe sequence (GGGGG & CCCCC). A Cy3 donor is covalently linked to the end of one arm and a Cy5 acceptor is covalently linked to the end of the other arm. **A,** Illustration of the configuration change for dual-

labeled DNA probes. **B,** Ensemble fluorescent trace for Cy3 (green) and Cy5 (red) channels of dual-label DNA probes before and after hybridization obtained in a cuvette via manual addition of the probe strand at 5th minute. **C,** The FRET efficiency, *E* distribution obtained outside vesicles with poly-A targets inserted into the membrane via the cholesterol link and externally added dual-labeled DNA hairpin probes. The peak at *E* = 0.15 corresponds to the DNA hairpin annealed to the target DNA.

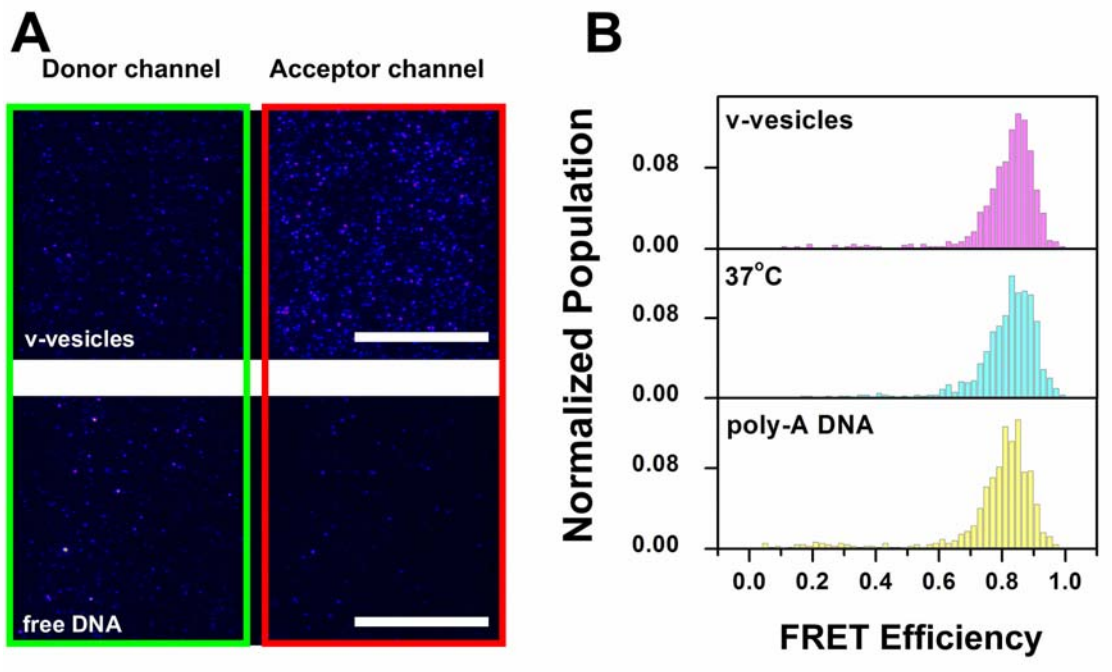

Figure 4.2. A, 532 nm laser excited images of experimental channels after 160 pM v-vesicles with DNA probes or 2 nM free DNA probes. Lower panel only shows dim spots in the donor and acceptor channels, demonstrating that the nonspecific adhesion of the free DNA probes to the surface is minimal. **B,** *E* distributions of v-vesicles at room temperature, at 37 ^{o}C, and after incubating with 2 μM poly-A DNA at 37 ^{o}C for 30 minutes. Vesicle encapsulated DNA probes are not sensitive to either temperature or free target DNA in solution. Scale bars are for 25 μm.

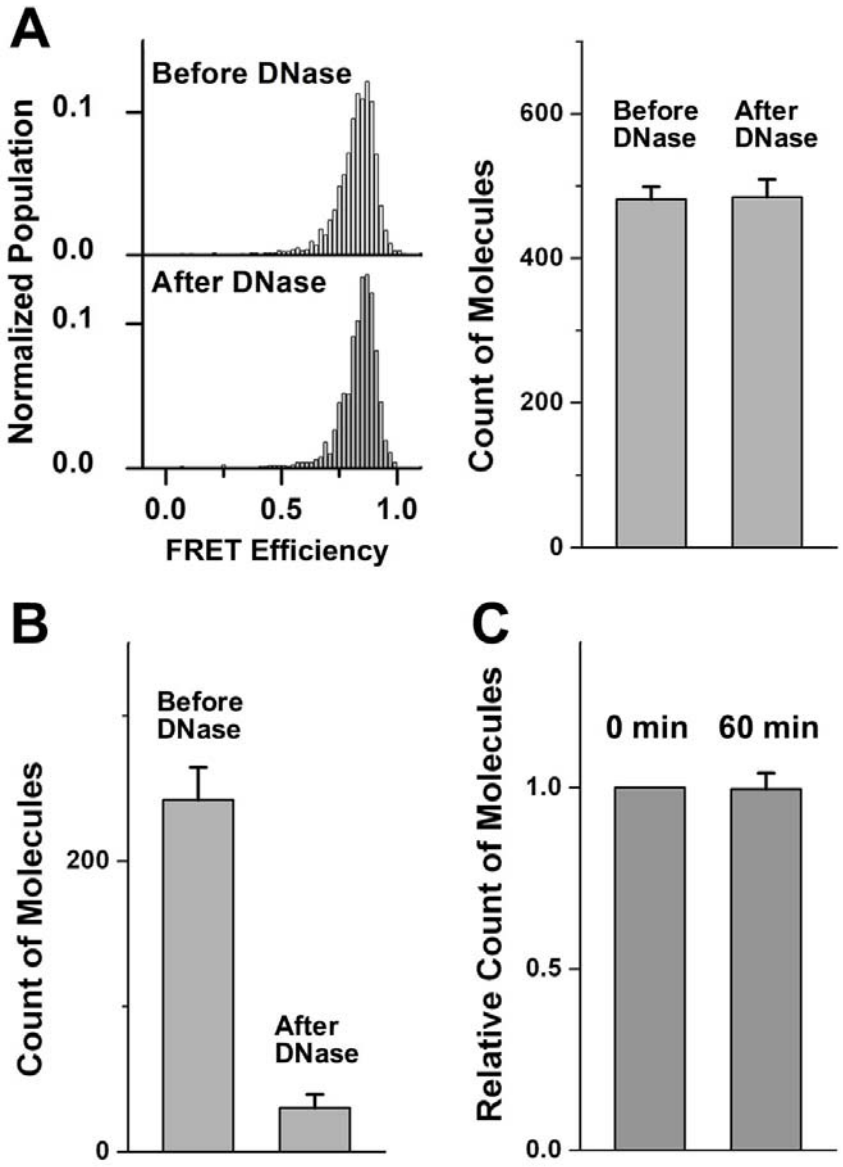

Figure 4.3. Stable encapsulation of DNA probes inside SNARE protein reconstituted vesicles. **A,** Histograms of FRET efficiency, *E*, (left) and average numbers (right) of molecules per imaging area (25 μm X 50 μm) before and after a DNase treatment of DNA probes encapsulated inside surface immobilized v-SNARE (protein:lipid = 1:200) vesicles. For histograms of FRET efficiency, Y-axis is normalized population, where we divided the distribution by the total number of vesicles measured and X-axis is FRET efficiency value. **B,** Average count of molecules per imaging area before and after a

DNase treatment of DNA probes immobilized outside vesicles. (Corresponding representative images for **A** and **B** are shown in Supplementary Fig. S2.) **C,** Relative count of molecules per imaging area for surface immobilized v-vesicle encapsulating DNA probes after incubating at 37 ^{o}C for 60 min. The number of molecules at 0 min was set as 1. Error bars denote the standard error.

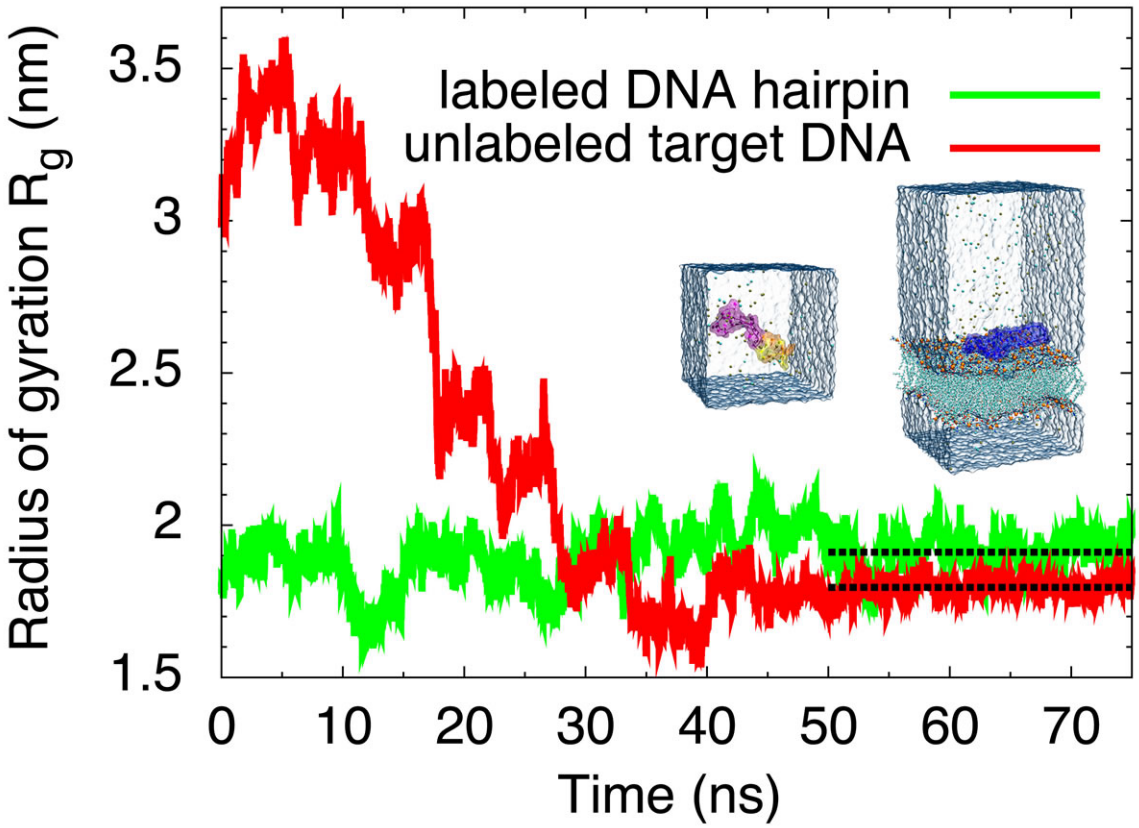

Figure 4.4. The time evolution of the gyration radius (Rg) for Cy3/Cy5 dual-labeled DNA hairpin (green) and unlabeled target DNA (red). The average R_g over the last 25-ns simulations for each DNA molecule is shown in black dash line yield a value of 1.91 ± 0.53 nm and 1.80 ± 0.28 nm for labeled DNA hairpin and unlabeled target DNA, respectively. The Rg of target DNA collapses rather quickly from a relatively extended configuration because the starting structure is similar to the one in double helix for minimizing the effect of initial condition. The results consist with the known high flexibility of single-stranded DNA (persistent length 1.5 nm). The insets are snapshots of equilibrated system of the dual-labeled DNA hairpin (left) and the unlabeled target DNA (right) resulting from 75-ns MD simulations. The simulated systems include waters (blue box), K^+ ions (brown spheres), Cl^- ions (cyan spheres), lipid bilayers (orange head and

cyan tails) and DNA molecules colored by type of nucleotide (yellow: G, orange: C, purple: T, blue: A). The water boxes have a dimension of 89 Å × 89 Å × 89 Å and 100 Å × 100 Å × 186 Å for the dual-labeled DNA hairpin and the unlabeled target DNA, respectively.

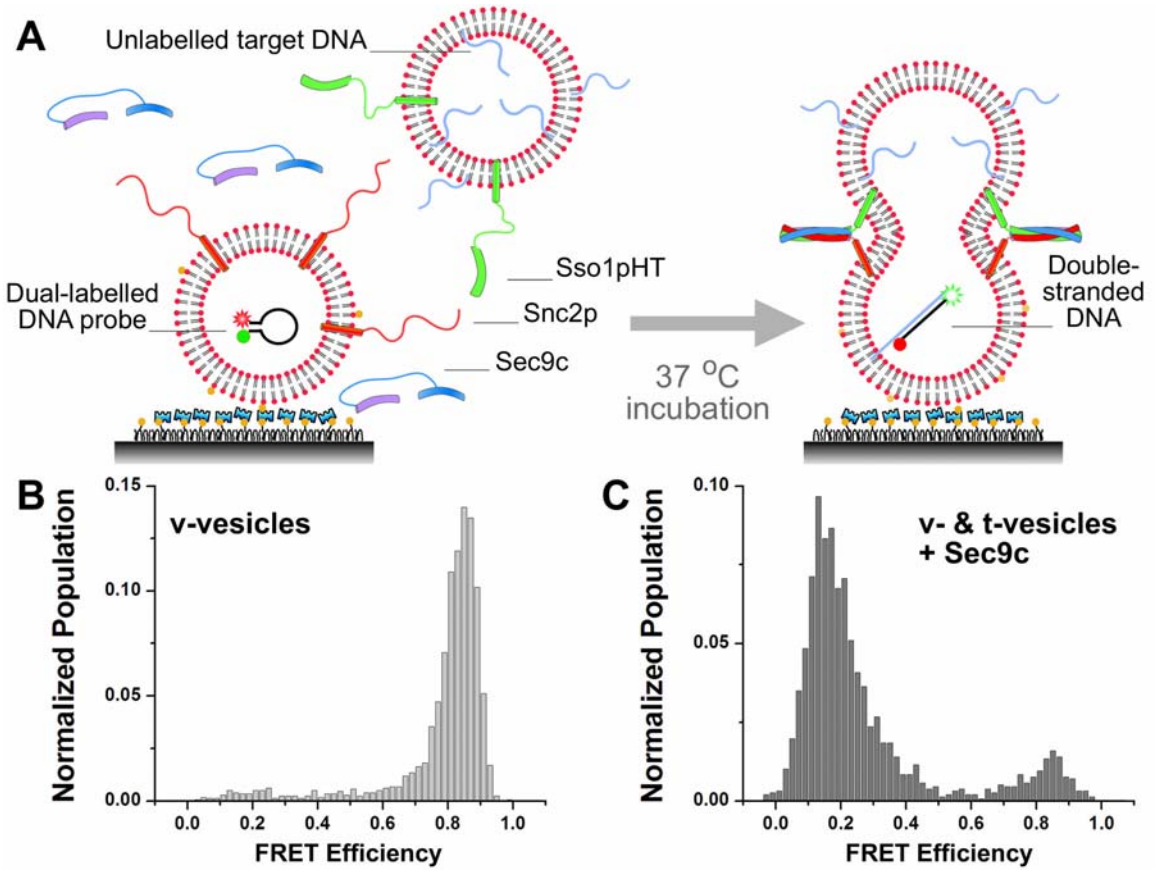

Figure 4.5. Single molecule content mixing assay for yeast SNARE-mediated fusion. **A,** Schematics of the assay. Vesicles reconstituted with Snc2p proteins (v-vesicles) and encapsulating dual labeled DNA probes are immobilized on the surface of the flow cell. Vesicles reconstituted with Sso1pHT proteins (t-vesicles) and encapsulating poly-A DNA strands are flown in along with soluble Sec9c proteins, and the sample is incubated at 37 ^{o}C. **B,** *E* distributions of v-vesicles before the reaction, and **C,** after incubating for 30 min with t-vesicles and 1 μM Sec9c protein.

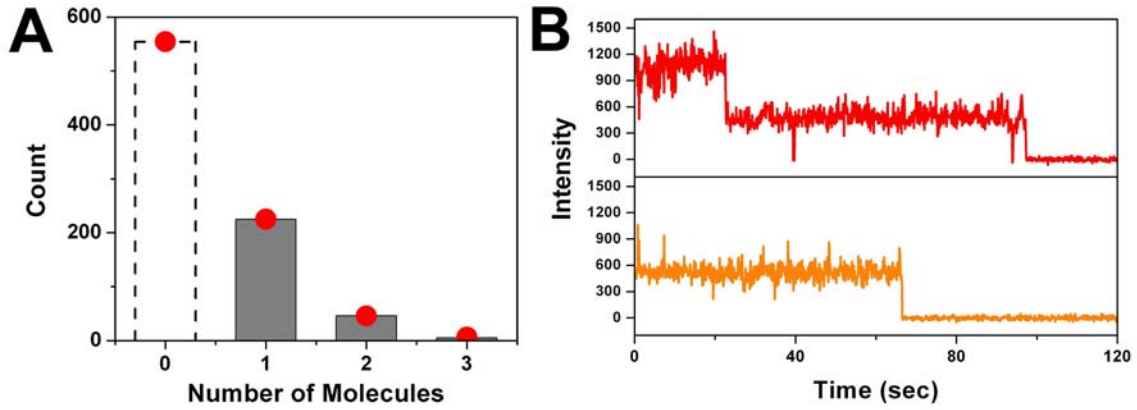

Figure. 4.6. Single-molecule analysis of encapsulated DNA after protein reconstitution. **A,** The distribution of the number of molecules inside a vesicle. Solid bars are experimental results. Red dots indicate the Poisson fitting, by which we obtain the bar represents 0 molecule. Based on that, we estimate that the average number of DNA probes inside a vesicle is ~0.4. **B,** Representative time records for two vesicles. The number of encapsulated DNA molecules can be determined by counting the digital photobleaching events. In the upper trace, the Cy5 intensity reduces to its background level in two discrete steps, which implies that there are two molecules entrapped within this vesicle, whereas in the lower trace photobleaching occurs in a single step, indicating occupancy by a single DNA molecule.

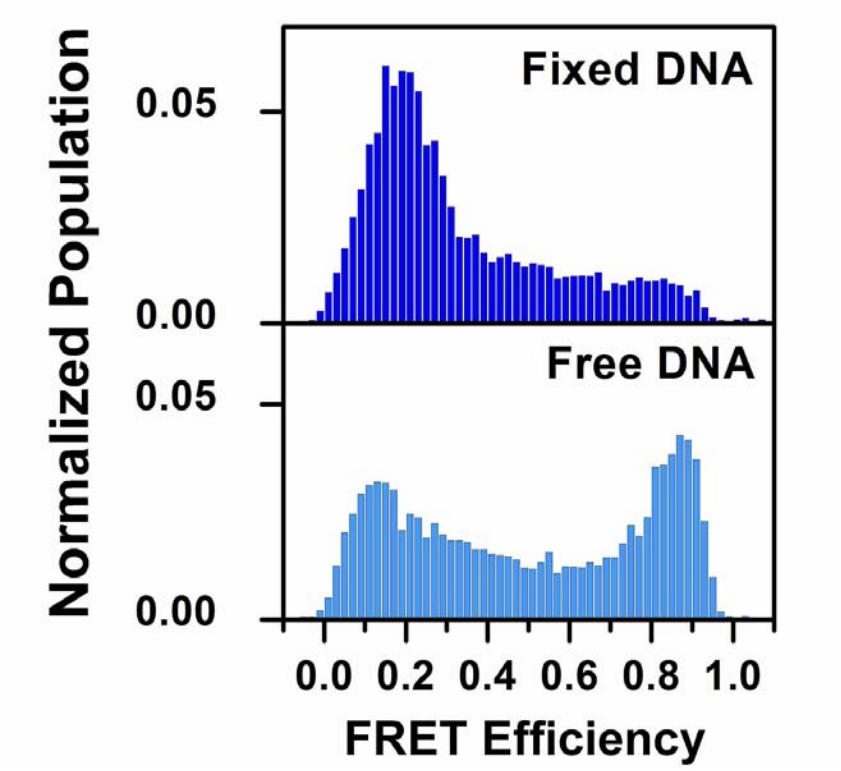

Figure 4.7. Yeast SNARE content mixing: *E* distributions of yeast SNARE-mediated fusion products for t-vesicles containing free poly-A DNA and fixed poly-A DNA through a cholesterol molecule. The distinction of low FRET peak change is due to the difference on DNA encapsulation rate. Cholesterol linked target DNA dramatically increases the degree of content mixing.

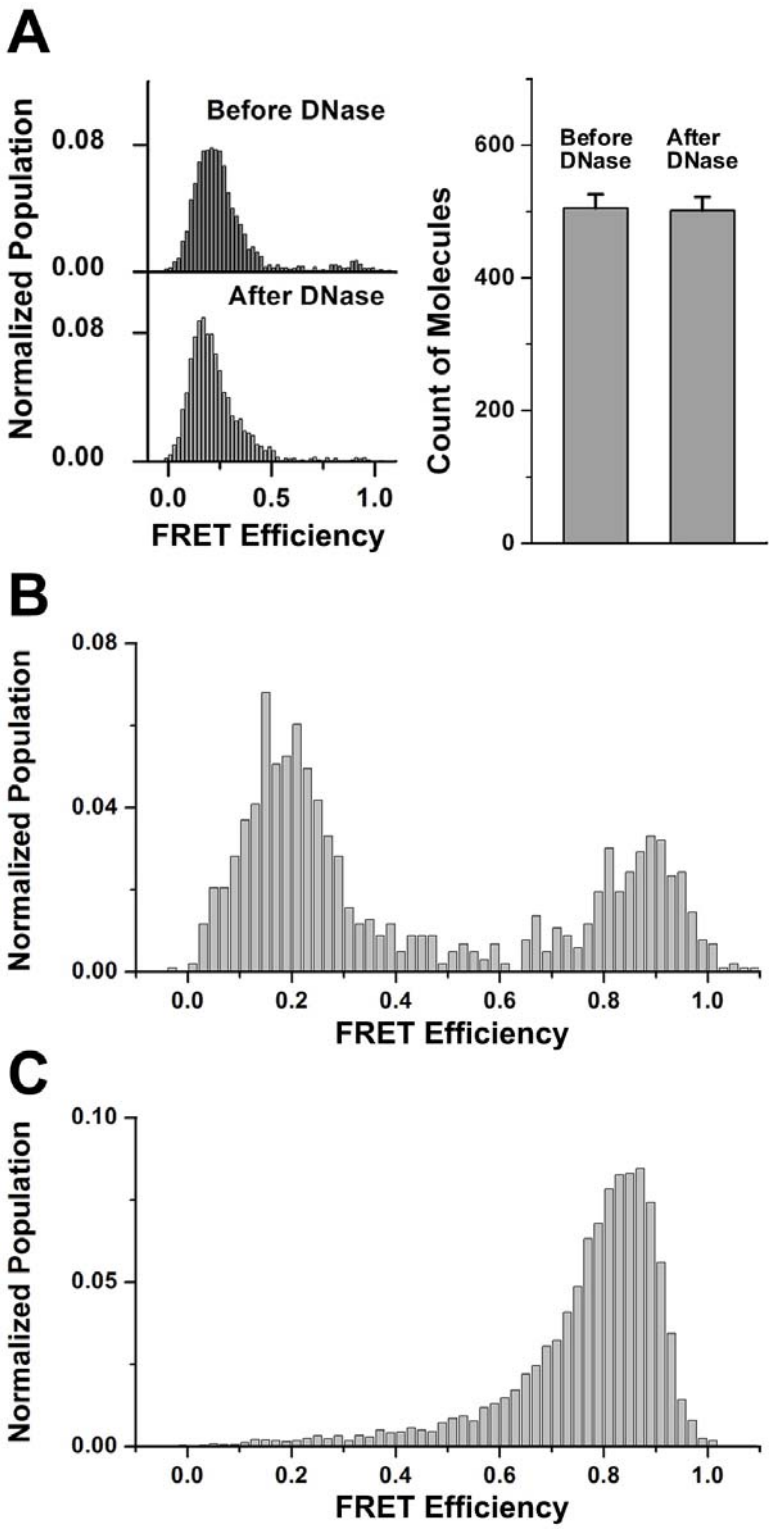

Figure 4.8. A, DNA annealing take place inside vesicles. *E* distributions (left) and average numbers (right) of molecules per imaging area (25 μm × 50 μm) of fusion

products before and after a DNase treatment. **B,** *E* distribution of the fusion product with 1 μM Sec9c performed in the bulk solution and subsequently immobilized on the quartz surface for observation. DNase treatment was applied to both v- and t-vesicles to eliminate free DNA molecules before reaction. **C,** *E* distribution after fusion reaction using non-complementary poly-T DNA inside t-vesicles.

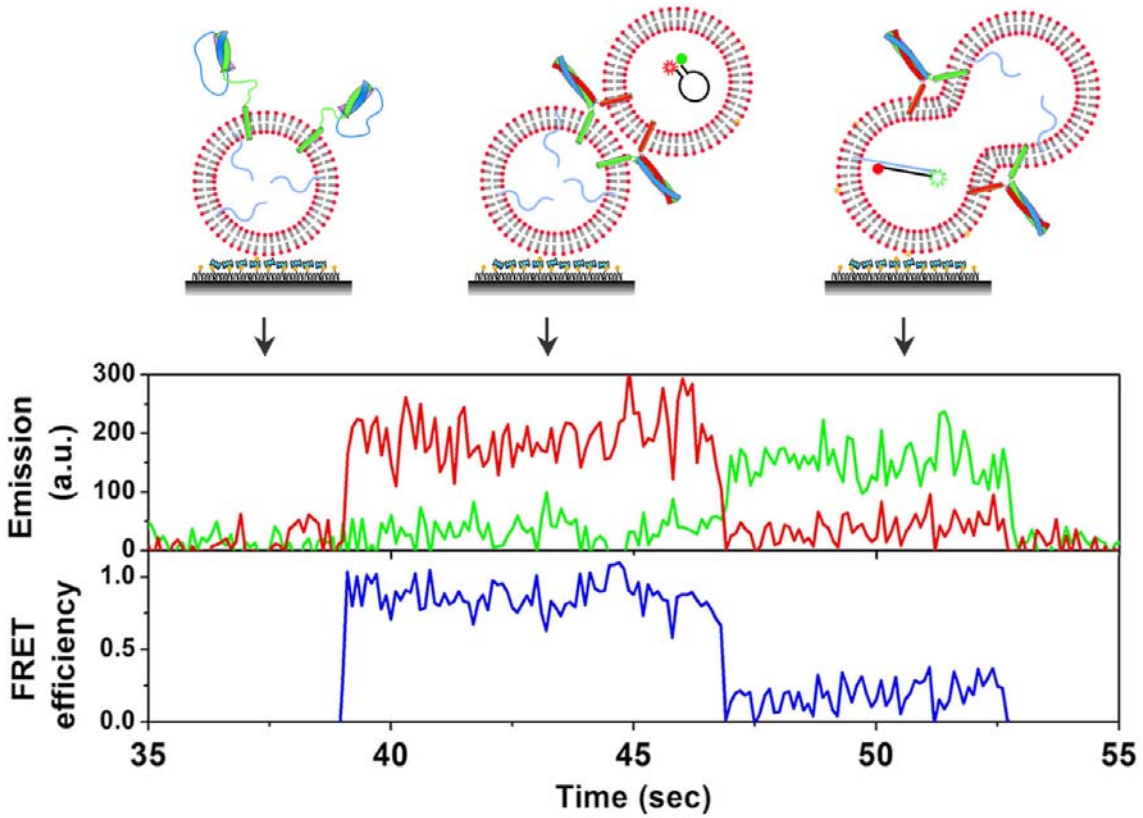

Figure 4.9. A typical real-time content-mixing time trace of fluorescence intensity (green curve for donor & red curve for acceptor) and corresponding FRET efficiency (blue curve). For this experiment, we switched the surface immobilization configuration. t-vesicles with the target DNAs are surface immobilized and v-vesicles containing FRET beacons are flown into the solution. To eliminate DNA molecules outside vesicles, DNase I treatment was applied before reactions. A typical real-time content-mixing time traces are shown here. Upper panel shows fluorescence intensities, green curve representing the donor and red curve representing the acceptor intensity. The lower panel shows the corresponding FRET efficiency in blue. Initially, the surface immobilized vesicles containing unlabeled target DNAs shows no donor and acceptor signals. Upon binding of the v-vesicle with FRET beacon is seen as a sudden appearance of the fluorescence signal associating to a high FRET value. After a certain time, DNA

hybridization caused by content mixing decreases FRET value to ~0.2. The dwell time in the high FRET state is designated as the fusion time.

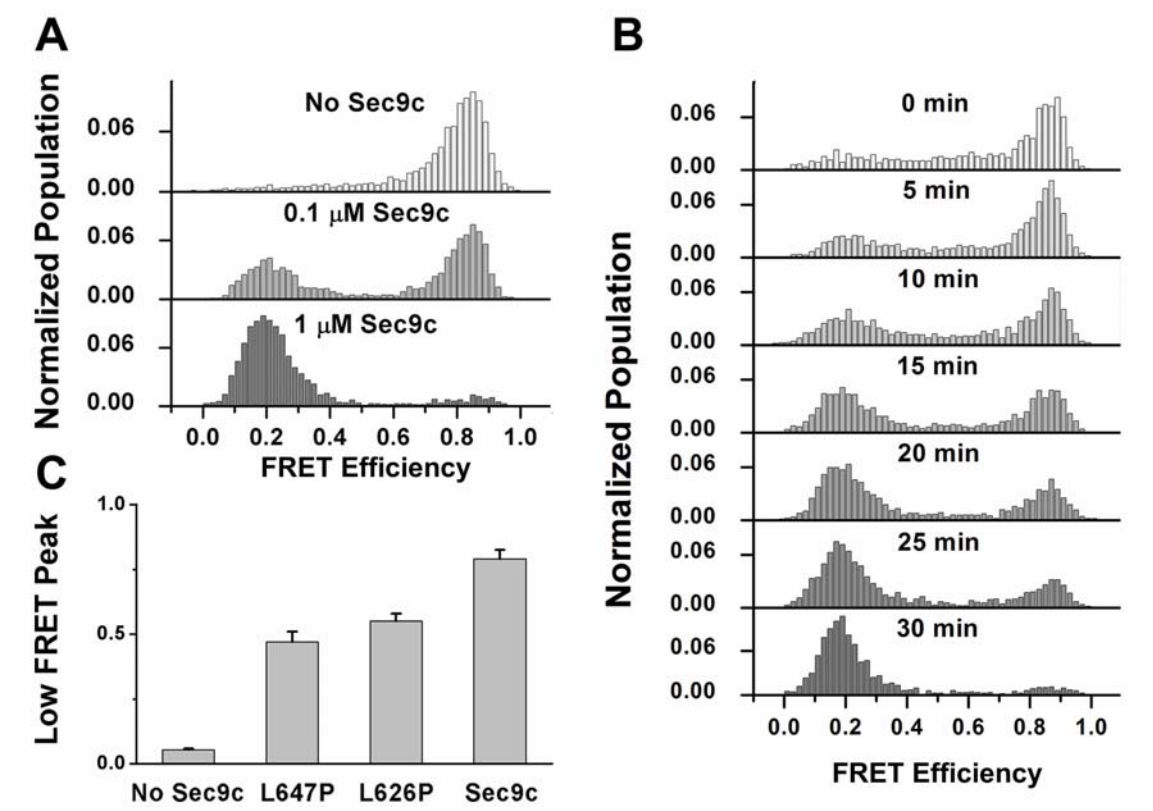

Figure 4.10. A, *E* distributions of fusion products for different Sec9c concentrations. **B,** *E* distributions of yeast SNARE-mediated fusion with different incubation times ranging from 0 min to 30 min with 1 μM Sec9c. **C,** Pore expansion efficiency quantified by low FRET peak (*E* = 0-0.4) percentage for wild type and mutant Sec9c, L626P and L646P. 1 μM Sec9c and its mutants were used. Error bars denote the standard deviation of three independent experiments. 30 min incubation at 37 ^{o}C was applied for all experiments in **A** and **C**.

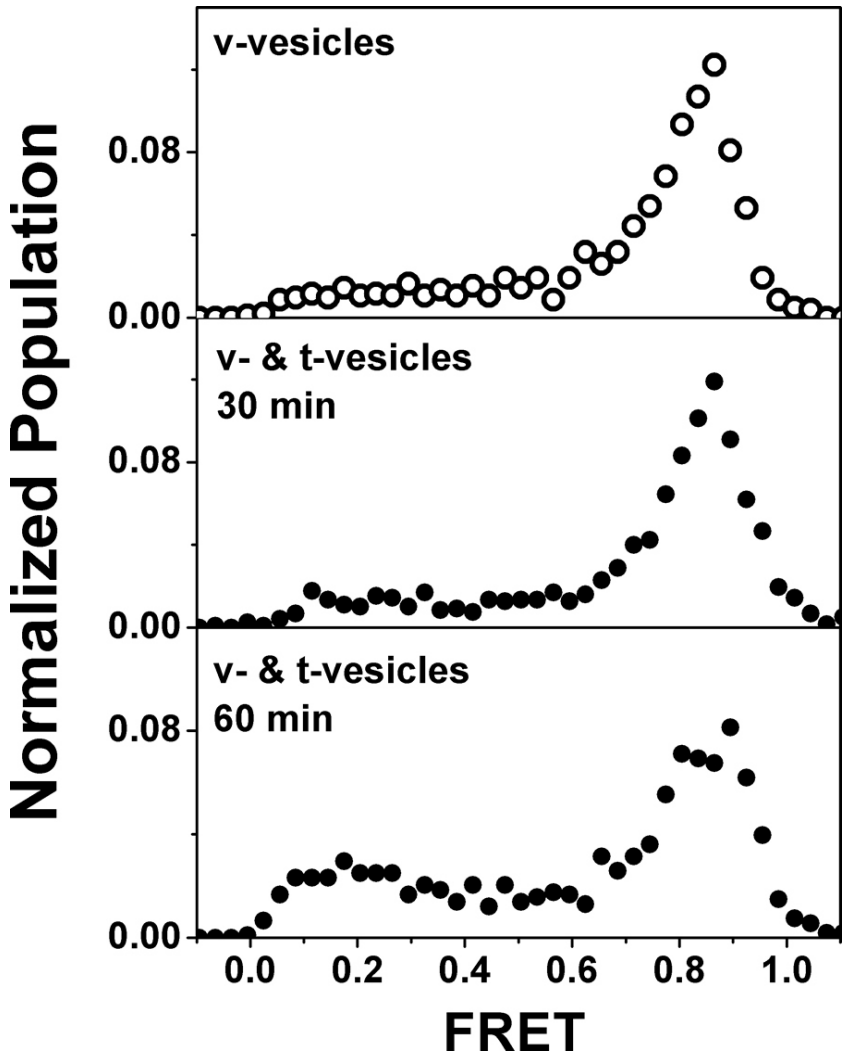

Figure 4.11. Neuronal SNARE-mediated membrane fusion. V-SNARE vesicles (Cy3/Cy5 dual-labeled DNA probes) reconstituted with VAMP2 proteins are immobilized on the surface. T-SNARE vesicles (poly-A DNAs) reconstituted with SNAP-25 and Syntaxin1A proteins were flown into the channel, followed by an incubation at 37 ^{o}C. *E* distributions for v-vesicles only and after incubating with t-vesicles for 30 minutes and 60 minutes are shown.

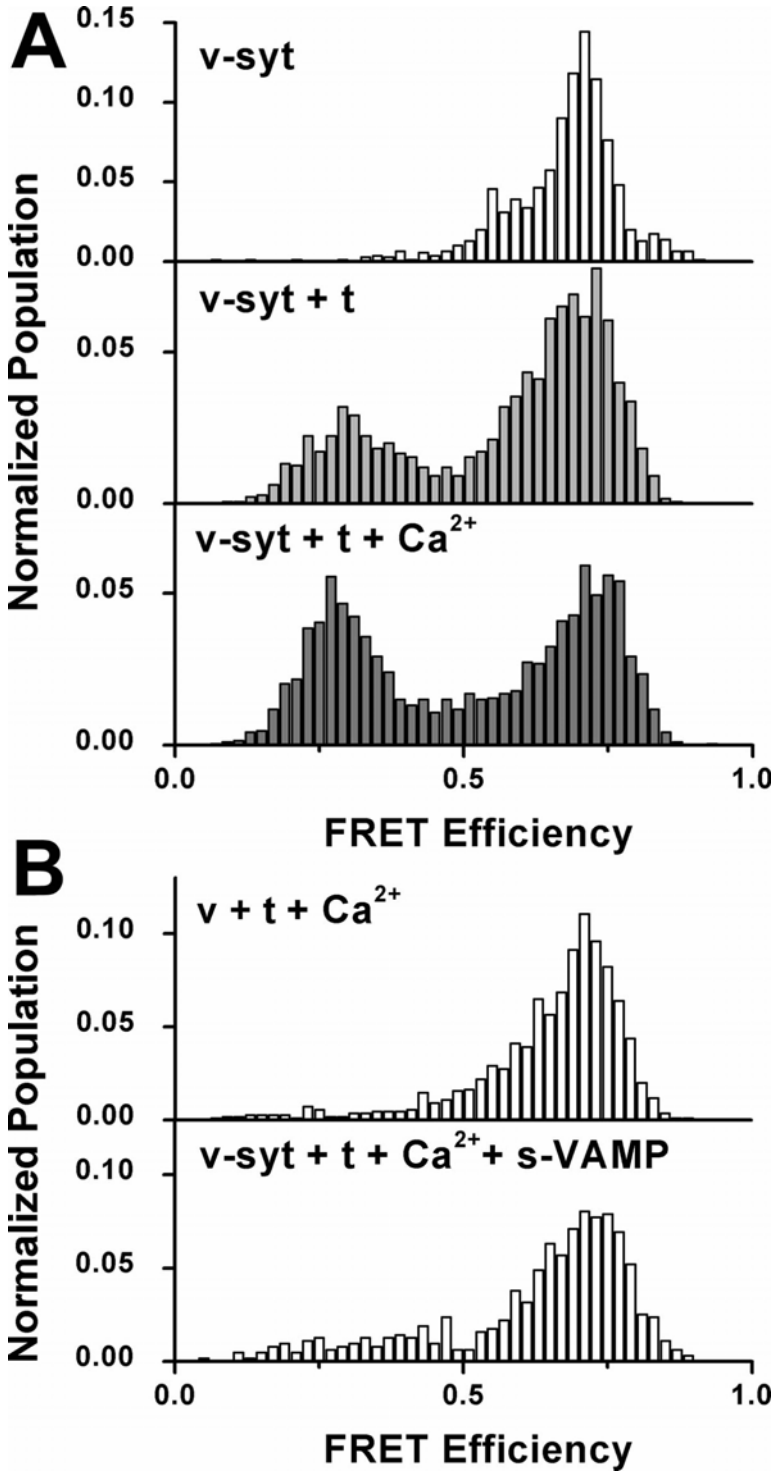

Figure 4.12. Synaptotagmin expands fusion pore by helping SNARE complex formation. **A,** *E* distributions of v-vesicles with synaptotagmin before the reaction, after incubating with t-vesicles, and after incubating with t-vesicles plus 10 μM Ca^{2+}. **B,** *E* distributions of

v-vesicles incubating with t-vesicles plus 10 μM Ca^{2+}, and v-vesicles with synaptotagmin incubating with t-vesicles, 10 μM Ca^{2+}, and soluble VAMP2.

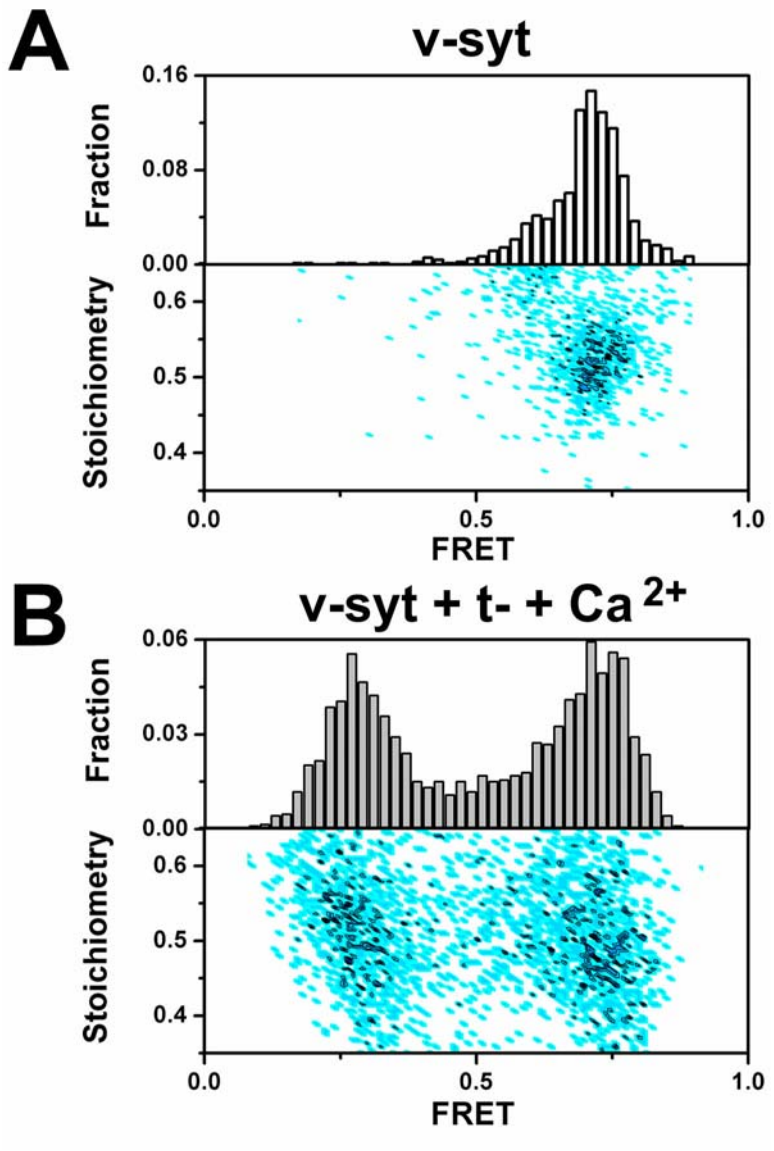

Figure 4.13. The *E* distributions with corresponding stoichiometry of v-vesicles with Syt before the reaction **(A)** and after incubating with t-vesicles plus 10 μM Ca^{2+} **(B)**. The FRET stoichiometry value around 0.5 corresponds to 1:1 donor (Cy3) and acceptor (Cy5) ratio. The low FRET peak in **(b)** with ~0.5 FRET stoichiometry value confirms the conformational change of Cy3/Cy5 probes caused by DNA hybridization.

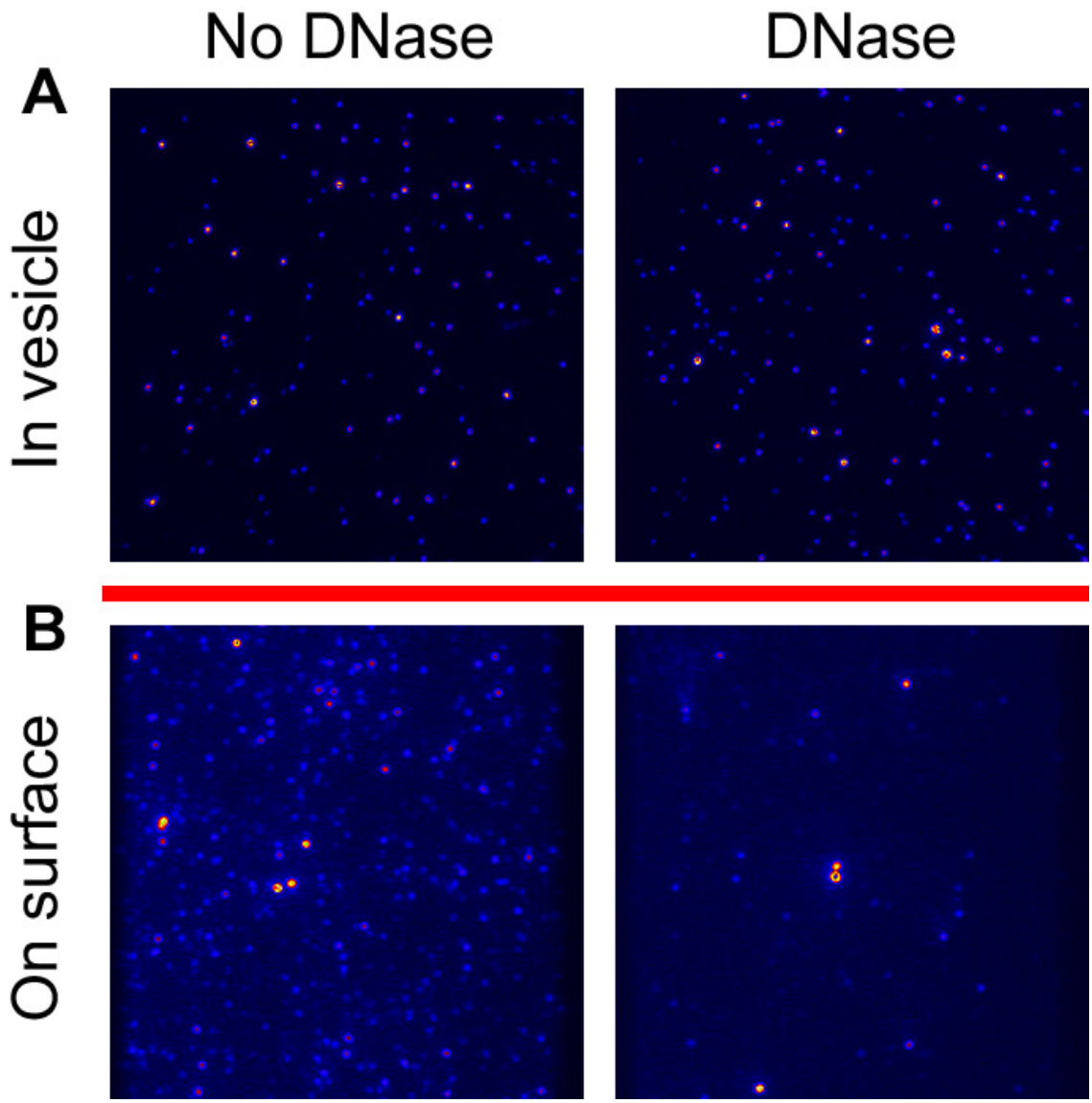

Figure 4.14. 633 nm laser excited images of acceptor channels for vesicle encapsulated **(A)** and surface immobilized **(B)** DNA probes before and after a DNase treatment. Comparing to **(B)**, the number of florescent spots in **(A)** did not change significantly, which confirms that the DNA hybridization is inside vesicles.

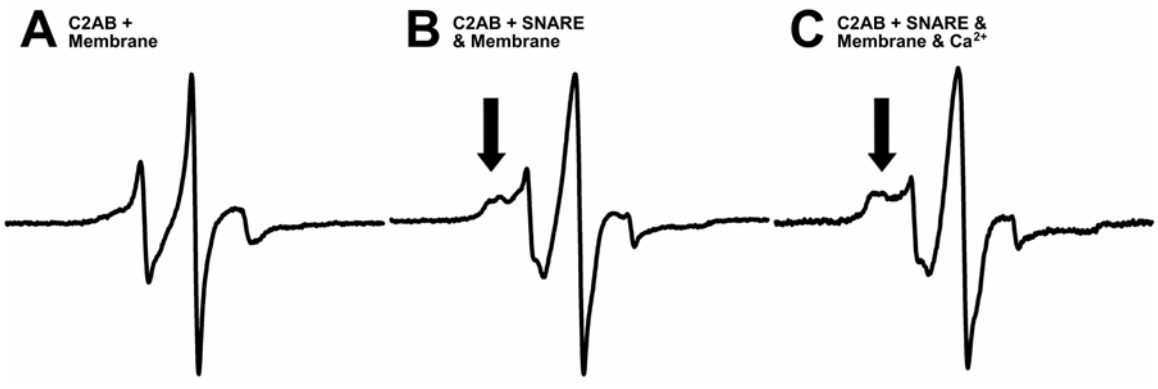

Figure 4.15. EPR spectra analysis of C2AB (I367C) with membrane **(A)**, and membrane-associated SNARE complexes in the presence **(C)** or absence **(B)** of 1 mM calcium ions. Black arrows indicate the major change of spectrum due to the protein-protein interaction.

CHAPTER 5

OUTLOOK

In order to overcome limitations of conventional methods, we have developed new techniques based on the single molecular approach using liposomes, which are artificial vesicles reconstituted with SNARE proteins.

Through our single-vesicle lipid mixing assay, we discovered the vesicle aggregation induced by C2AB/Ca^{2+}, the dual function of complexin, and the role of Munc18/SNARE-core binding mode. By using our single-vesicle content mixing assay, we found the fusion pore expansion role of yeast SNAREs and neuronal SNAREs plus synaptotagmin 1.

Our data are very encouraging and it is very likely that these studies will provide a better understanding of the SNARE-mediated membrane fusion process. New configurations based on the initial studies will be designed. Ultimately, we hope that our studies will shed light on the molecular mechanism of SNARE-mediated membrane fusion.

5.1 Remaining issues

Studying membrane fusion based on protein-reconstituted liposomes has achieved tremendous success. However, due to conflicting results [124], several issues regarding this technique have been raised, such as lipid composition, protein association rate, and protein orientation [125,126]. In order to overcome those issues, new approaches are demanded.

5.2 Future work

For single-vesicle lipid and content mixing assays described above, we are actually working on an assumption that all proteins are at the right position for inducing membrane fusion. Since all proteins are unlabeled, we are not able to tell the real story on the protein side, which is also an important part for the study of SNARE-mediated membrane fusion. Thus, in the future, I will continue working on a protein-fusion method to monitor protein-protein interactions and the content mixing simultaneously, which will give the ultimate power to study the detailed mechanism of the whole neurotransmitter release process.

Dye labeled proteins and molecular beacons will be used to probe protein-protein interactions and indicate fusion evens, respectively. The size of our liposomes is about 50 ~ 100 nm in diameter, which is smaller than the half wavelength of emission light (500 ~ 700 nm). According to the Abbe's rule of diffraction limit, direct optical observation is not able to separate signals from multiple sources within that range. In order to see multiple proteins on one liposome, a super resolution imaging technique, stochastic optical reconstruction microscopy (STORM), is required. The STORM, a single photo-switchable molecule is turned on and off, repeatedly, to measure its position accurately with ~20 nm resolution by determining the center position of the point-spread function from reconstructed images (Figure 5.1) [127,128]. Red and green lasers are usually used alternatively for turning dye molecules on and off to avoid overlapping of different fluorophores, which results a high accuracy of imaging. This technique will be adopted for our study with a modification on triggering fluorophores on and off. With a red laser

excitation in BME buffer, Cy5.5 dye undergoes a spontaneous on and off process like blinking [128]. Thus, by using a STORM image reconstruction program on images obtained from Cy5.5 labeled proteins with a red laser excitation, we should be able to locate the protein position at the sub-hundred-nanometer level.

Since STORM requires single dye illumination on one liposome for each frame, multi-dye labeled lipid mixing is not suitable for indicating fusion evens. The content mixing based on molecular beacons will be used for showing fusion events through the donor detection channel, while the acceptor detection channel is looking at Cy5.5 labeled proteins. As shown in Figure 5.2, through an image reconstruction program, we can fit the Cy5.5 labeled protein within ~100 nm range, which is the size of liposomes used in our study. Right images are reconstructed point-spread functions of three small dots (red) in left image that is one imaging spot with a red laser illumination.

The STORM technique, together with a three-color TIR setup, would be an ultimate tool to study protein-protein interactions during the SNARE-mediated membrane fusion process.

Chapter 5 Figures:

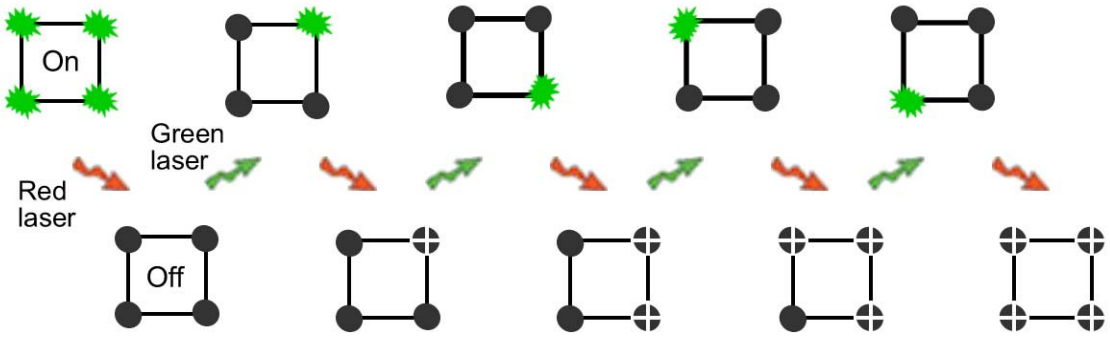

Figure 5.1. Stochastic optical reconstruction microscopy (STORM) with photo-switchable fluorophores.

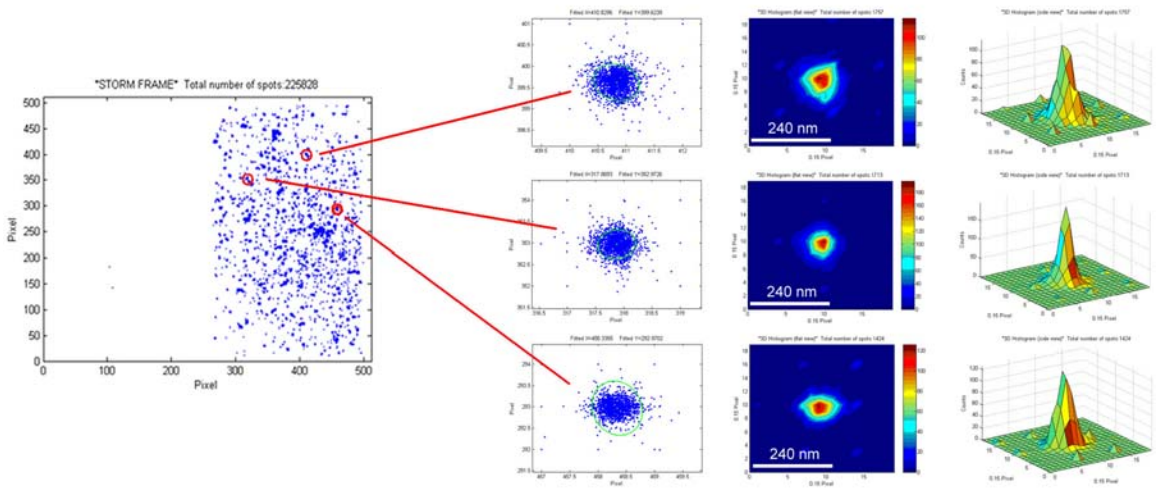

Figure 5.2. STORM testing on yeast SNARE-mediated fusion by using Cy5.5 labeled Sec9c proteins.

REFERENCES

1. Yeagle, P.L. *The Membranes of Cells* 2nd Ed., Academic Press, Inc. (1993).

2. White, J.M. Membrane fusion. *Science* **258**, 917-924 (1992).

3. Jahn, R., Lang, T. & Sudhof, T.C. Membrane fusion. *Cell* **112**, 519-533 (2003).

4. Wickner, W. & Schekman, R. Membrane fusion. *Nat. Struct. Mol. Biol.* **15**, 658-664 (2008).

5. Rizo, J. & Rosenmund, C. Synaptic vesicle fusion. *Nat. Struct. Mol. Biol.* **15**, 665-674 (2008).

6. Chernomordik, L.V. & Kozlov, M.M. Mechanics of membrane fusion. *Nat. Struct. Mol. Biol.* **15**, 675-683 (2008).

7. Weber, T., Zemelman, B.V., McNew, J.A., Westermann, B., Gmachl, M., Parlati, F., Sollner, T.H & Rothman, J.E. SNAREpins: minimal machinery for membrane fusion. *Cell* **92**, 759-772 (1998).

8. McNew, J.A., Parlati, F., Fukuda, R., Johnston, R.J., Paz, K., Paumet, F., Sollner, T.H. & Rothman, J.E. Compartmental specificity of cellular membrane fusion encoded in SNARE proteins. *Nature* **407**, 153-159 (2000).

9. Rothman, J.E. Mechanisms of intracellular protein transport. *Nature* **372**, 55-63 (1994).

10. Sollner, T., Whiteheart, S.W., Brunner, M., Erdjument-Bromage, H., Geromanos, S., Tempst, P. & Rothman, J.E. SNAP receptors implicated in vesicle targeting and fusion. *Nature* **362**, 318-324 (1993).

11. Poirier, M.A., Xiao, W., Macosko, J. C., Chan, C., Shin, Y. K. & Bennett, M. K. The synaptic SNARE complex is a parallel four-stranded helical bundle. *Nat. Struct. Biol.* **5**, 765-769 (1998).

12. Sutton, R.B., Fasshauer, D., Jahn, R. & Brunger, A.T. Crystal structure of a SNARE complex involved in synaptic exocytosis at 2.4 Å resolution. *Nature* **395**, 347-353 (1998).

13. Liu, T., Tucker, W.C., Bhalla, A., Chapman, E.R. & Weisshaar, J.C. SNARE-driven, 25-millisecond vesicle fusion in vitro. *Biophys. J.* **89**, 2458-2472 (2005).

14. Lu, X., Zhang, F., McNew, J.A. & Shin, Y.K. Membrane fusion induced by neuronal SNAREs transits through hemifusion. *J. Biol. Chem.* **280**, 30538-30541 (2005).

15. Reese, C., Heise, F. & Mayer, A. Trans-SNARE pairing can precede a hemifusion intermediate in intracellular membrane fusion. *Nature* **436**, 410-414 (2005).

16. Xu, Y., Zhang, F., Su, Z., McNew, J.A. & Shin, Y.K. Hemifusion in SNARE-mediated membrane fusion. *Nat. Struct. Mol. Biol.* **12**, 417-422 (2005).

17. Lindau, M. & Almers, W. Structure and function of fusion pores in exocytosis and ectoplasmic membrane fusion. *Curr. Opin. Cell Biol.* **7**, 509-517 (1995).

18. Han, X., Wang, C.T., Bai, J., Chapman, E.R. & Jackson, M.B. Transmembrane segments of syntaxin line the fusion pore of Ca^{2+}-triggered exocytosis. *Science* **304**, 289-292 (2004).

19. Hua, Y. & Scheller, R.H. Three SNARE complexes cooperate to mediate membrane fusion. *Proc. Natl. Acad. Sci. USA* **98**, 8065-8070 (2001).

20. Kemble, G.W., Danieli, T. & White, J.M. Lipid-anchored influenza hemagglutinin promotes hemifusion, not complete fusion. *Cell* **76**, 383-391 (1994).

21. Chernomordik, L.V., Frolov, V.A., Leikina, E., Bronk, P. & Zimmerberg, J. The pathway of membrane fusion catalyzed by influenza hemagglutinin: restriction of lipids, hemifusion, and lipidic fusion pore formation. *J. Cell Biol.* **140**, 1369-1382 (1998).

22. Armstrong, R.T., Kushnir, A.S. & White, J.M. The transmembrane domain of influenza hemagglutinin exhibits a stringent length requirement to support the hemifusion to fusion transition. *J. Cell Biol.* **151**, 425-437 (2000).

23. Zaitseva, E., Mittal, A., Griffin, D.E. & Chernomordik, L.V. Class II fusion protein of alphaviruses drives membrane fusion through the same pathway as class I proteins. *J. Cell Biol.* **169**, 167-177 (2005).

24. Yang, L. & Huang, H.W. Observation of a membrane fusion intermediate structure. *Science* **297**, 1877-1879 (2002).

25. Chernomordik, L. & Kozlov, M. Membrane hemifusion: crossing a chasm in two leaps. *Cell* **123**, 375-382 (2005).

26. Giraudo, C.G., Hu, C., You, D., Slovic, A.M., Mosharov, E.V., Sulzer, D., Melia, T.J. & Rothman, J.E. SNAREs can promote complete fusion and hemifusion as alternative outcomes. *J. Cell Biol.* **170**, 249-260 (2005).

27. Schaub, J.R., Lu, X., Doneske, B., Shin, Y.K. & McNew, J.A. Hemifusion arrest by complexin is relieved by Ca2+-synaptotagmin I. *Nat. Struct. Mol. Biol.* **13**, 748-750 (2006).

28. Chapman, E.R. Synaptotagmin: a Ca^{2+} sensor that triggers exocytosis. *Nat. Rev. Mol. Cell. Biol.* **3**, 498-508 (2002).

29. Stein, A., Radhakrishnan, A., Riedel, D., Fasshauer, D. & Jahn, R. Synaptotagmin activates membrane fusion through a Ca^{2+}-dependent trans interaction with phospholipids. *Nat. Struct. Mol. Biol.* **14**, 904-911 (2007).

30. Martens, S., Kozlov, M.M. & McMahon, H.T. How synaptotagmin promotes membrane fusion. *Science* **316**, 1205-1208 (2007).

31. Xue, M., Ma, C., Craig, T.K., Rosenmund, C & Rizo, J. The Janus-faced nature of the C2B domain is fundamental for synaptotagmin-1 function. *Nat. Struct. Mol. Biol.* **15**, 1160-1168 (2008).

32. Mahal, L.K., Sequeira, S.M., Gureasko, J.M. & Sollner, T.H. Calcium-independent stimulation of membrane fusion and SNARE pin formation by synaptotagmin I. *J. Cell Biol.* **158**, 273-282 (2002).

33. Holt, M., Riedel, D., Stein, A., Schuette, C. & Jahn, R. Synaptic vesicles are constitutively active fusion machines that function independently of Ca^{2+}. *Curr. Biol.* **18**, 715-722 (2008).

34. Diao, J., Yoon, T.-Y., Su, Z., Shin, Y.-K. & Ha, T. C2AB: a molecular glue for lipid vesicles with negatively charged surface. *Langmuir* **25**, 7177-7180 (2009).

35. Chen, X., Tomchick, D., Kovrigin, E., Arac, D., Machius, M., Sudhof, T.C. & Rizo, J. Three-dimensional structure of the complexin/SNARE complex. *Neuron* **33**, 397-409 (2002).

36. Schaub, J.R., Lu, X., Doneske, B., Shin, Y.K. & McNew, J.A. Hemifusion arrest by complexin is relieved by Ca^{2+}-synaptotagmin I. *Nat. Struct. Mol. Biol.* **13**, 748-750 (2006).

37. Tang, J., Maximov, A., Shin, O.-H., Dai, H., Rizo, J. & Sudhof, T.C. A complexin/synaptotagmin 1 switch controls fast synaptic vesicle exocytosis. *Cell* **126**, 1175-1187 (2006).

38. Giraudo, C.G., Eng, W.S., Melia, T.J. & Rothman, J.E. A clamping mechanism involved in SNARE-dependent exocytosis. *Science* **313**, 676-680 (2006).

39. Yoon, T.-Y., Lu, X., Diao, J., Lee, S.-M., Ha, T. & Shin, Y.-K. Complexin and Ca^{2+} stimulate SNARE-mediated membrane fusion. *Nat. Struct. Mol. Biol.* **15**, 707-713 (2008).

40. Jahn, R. Sec/Munc18 protein: mediators of membrane fusion moving to center stage. *Neuron* **27**, 201 (2000).

41. Rizo, J. & Sudhof, T.C. SNAREs and Munc18 in synaptic vesicle fusion. *Nat. Rev. Neurosci.* **3**, 641-653 (2002).

42. Toonen, R.F.G. & Verhage, M. Vesicle trafficking: pleasure and pain from SM genes. *Trends Cell Biol.* **13**, 177-186 (2003).

43. Toonen, R.F.G. & Verhage, M. Munc18-1 in secretion: lonely Munc joins SNARE team and takes control. *Trends Neurosci.* **30**, 564-672 (2007).

44. Khvotchev, M., Dulubova, I., Sun, J., Dai, H., Rizo, J. & Sudhof, T.C. Dual modes of Munc18-1/SNARE interactions are coupled by functionally critical binding to syntaxin-1 N terminus. *J. Neurosci.* **27**, 12147-12155 (2007).

45. Shen, J., Tareste, D.C., Paumet, F., Rothman, J.E. & Melia, T.J. Selective activation of cognate SNAREpins by Sec1/Munc18 proteins. *Cell* **128**, 183-195 (2007).

46. Dulubova, I., Khvotchev, M., Liu, S., Huryeva, I., Sudhof, T.C. & Rizo, J. Munc18-1 binds directly to the neuronal SNARE complex. *Proc. Natl. Acad. Sci. USA* **104**, 2697-2702 (2007).

47. Tareste, D., Shen, J., Melia, T.J. & Rothman, J.E. SNAREpin/Munc18 promotes adhesion and fusion of large vesicles to giant membranes. *Proc. Natl. Acad. Sci. USA* **105**, 2380-2385 (2008).

48. Shen, J., Rathore, S.S., Khandan, L. & Rothman, J.E. SNARE bundle and syntaxin N-peptide constitute a minimal complement for Munc18-1 activation of membrane fusion. *J. Cell Biol.* **190**, 55-63 (2010).

49. Diao, J., Su, Z., Lu, X., Yoon, T.-Y., Shin, Y.-K. & Ha, T. Single vesicle fusion assay reveals Munc18-1 binding to the SNARE core is sufficient for stimulating membrane fusion. *ACS Chem. Neurosci.* **1**, 168-174 (2010).

50. Chen, Y., Xu, Y., Zhang, F. & Shin, Y.-K. Constitutive versus regulated SNARE assembly: a structural basis. *EMBO J.* **23**, 681-689 (2004).

51. Forster, T. Zwischenmolekulare energiewanderung und fluoreszenz. *Ann. Physik.* **437**, 55-75 (1948).

52. Weninger, K., Bowen, M.E., Chu, S. & Brunger, A.T. Single molecule studies of SNARE complex assembly reveal parallel and anti-parallel configurations, *Proc. Natl. Acad. Sci. USA* **100**, 14800-14805 (2003).

53. Bowen, M.E., Weninger, K., Brunger, A.T. & Chu, S. Single molecule observation of liposome-bilayer fusion thermally induced by SNAREs. *Biophys. J.* **87**, 3569-3584 (2004).

54. Ha, T. Single molecule fluorescence resonance transfer. *Methods* **25**, 78-86 (2001).

55. Joo, C., Balci, H., Ishitsuka, Y., Buranachai, C. & Ha, T. Advances in single-molecule fluorescence methods for molecular biology. *Ann. Rev. Biochem.* **77**, 51-76 (2008).

56. Roy, R., Hohng, S. & Ha, T. A practical guide to single-molecule FRET. *Nat. Methods* **5**, 507-516 (2008).

57. Fix, M., Melia, T.J., Jaiswal, J.K., Rappoport, J.Z., You, D., Sollner, T.H., Rothman J.E. & Simon S.M. Imaging single membrane fusion events mediated by SNARE proteins. *Proc. Natl. Acad. Sci. USA* **101**, 7311-7316 (2004).

58. Liu, T., Tucker, W.C., Bhalla, A., Chapman, E.R. & Weisshaar, J.C. SNARE-driven, 25-millisecond vesicle fusion in vitro. *Biophys. J.* **89**, 2458-2472 (2005).

59. Domanska, M.K., Kiessling, V., Stein, A., Fasshauer, D. & Tamm, L.K. Single Vesicle millisecond fusion kinetics reveals number of SNARE complexes optimal for fast SNARE-mediated membrane fusion. *J. Biol. Chem.* **284**, 32158-32166 (2009).

60. Karatekin, E., Di Giovanni, J., Iborra, C., Coleman, J., O'Shaughnessy, B., Seagar, M. & Rothman, J.E. A fast, single-vesicle fusion assay mimics physiological SNARE requirements. *Proc. Natl. Acad. Sci. USA* **107**, 3517-3521 (2010).

61. Yoon, T.-Y., Okumus, B., Zhang, F., Shin, Y.-K. & Ha, T. Multiple intermediates in SNARE-induced membrane fusion. *Proc. Natl. Acad. Sci. USA* **103**, 19731-19736 (2006).

62. Joo, C., McKinney, S.A., Nankura, M., Rasnik, I., Myong, S. & Ha, T. Real time observation of RecA filament dynamics with single monomer resolution. *Cell* **126**, 515-527 (2006).

63. Rasnik, I., McKinney, S.A. & Ha, T. Nonblinking and long-lasting single molecule fluorescence imaging. *Nat. Methods* **3**, 891-893 (2006).

64. Hubbell, W.L., Gross, A., Langen, R. & Lietzow, M.A. Recent advances in site-directed spin labeling of proteins. *Curr. Opin. Struct. Biol.* **8**, 649-656 (1998).

65. Hubbell, W.L., Cafiso, D.S. & Altenbach, C. Identifying conformational changes with site-directed spin labeling. *Nat. Struct. Biol.* **7**, 735-739 (2000).

66. Shin, Y.-K., Levinthal, C., Levinthal, F. & Hubbell, W.L. Colicin E1 binding to membranes: time-resolved studies of spin-labeled mutants. *Science* **259**, 960-963 (1993).

67. Kim, C.S., Kweon, D.H. & Shin, Y.-K. Membrane topologies of neuronal SNARE folding intermediates. *Biochem.* **41**, 10928-10933 (2002).

68. Kweon, D.H., Kim, C.S. & Shin, Y.-K. The membrane-dipped neuronal SNARE complex: a site-directed spin labeling electron paramagnetic resonance study. *Biochem.* **41**, 9264-9268 (2002).

69. Kweon, D.H., Kim, C.S. & Shin, Y.-K. Regulation of neuronal SNARE assembly by the membrane. *Nat. Struct. Biol.* **10**, 440-447 (2003).

70. van Dijk, M. & Bonvin, A.M.J.J. 3D-DART: a DNA structure modelling server. *Nucl. Acids Res.* **37,** W235-W239 (2009).

71. Humphrey, W., Dalke, A. & Schulten, K. VMD - Visual Molecular Dynamics. *J. Molec. Graphics* **14,** 33-38 (1996).

72. MacKerell, A.D. Jr., Feig, M. & Brooks, C.L. III Extending the treatment of backbone energetics in protein force fields: limitations of gas-phase quantum mechanics in reproducing protein conformational distributions in molecular dynamics simulations. *J. Comput. Chem.* **25**, 1400-1415 (2004).

73. Phillips, J.C., Braun, R., Wang, W., Gumbart, J., Tajkhorshid, E., Villa, E., Chipot, C., Skeel, R.D., Kale, L. & Schulten, K. Scalable molecular dynamics with NAMD. *J. Comput. Chem.* **26**, 1781-1802 (2005).

74. Pabst, S., Margittai, M., Vainius, D., Langen, R., Jahn, R. & Fasshauer, D. Rapid and selective binding to the synaptic SNARE complex suggests a modulatory role of complexins in neuroexocytosis. *J. Biol. Chem.* **277**, 7838-7848 (2002).

75. Takamori, S., Holt, M., Lemke, E., Riedel, D., Urlaub, H., Schenck, S., Stenius, K., Bruegger, B., Ringler, P., Krzyzaneki, V., Mueller, S., Rammner, B., Groot, B.D., Mieskes, G., Moriyama, Y., Klingauf, J., Grubmueller, H., Heuser, J., Wieland, F. & Jahn, R. Molecular anatomy of a trafficking organelle. *Cell* **127**, 831-846 (2006).

76. Koh, T.W. & Bellen, H.J. Synaptotagmin I, a Ca^{2+} sensor for neurotransmitter release. *Trends Neurosci.* **26**, 413-422 (2003).

77. Guan, R., Dai, H. & Rizo, J. Binding of the Munc13-1 MUN domain to membrane-anchored SNARE complexes. *Biochem.* **47**, 1474-1481 (2008).

78. Thorgeirsson, T.E., Russell, C.J., King, D.S. & Shin, Y.-K. Direct determination of the membrane affinities of individual amino acids. *Biochem.* **35**, 1803-1809 (1996).

79. Archer, D.A., Graham, M.E. & Burgoyne, R.D. Complexin regulates the closure of the fusion pore during regulated vesicle exocytosis. *J. Biol. Chem.* **277**, 18249-18252 (2002).

80. Itakura, M., Misawa, H., Sekiguchi, M., Takahashi, S. & Takahashi, M. Transfection analysis of functional roles of complexin I and II in the exocytosis of two different types of secretory vesicles. *Biochem. Biophys. Res. Commun.* **265**, 691-696 (1999).

81. Xue, M., Reim, K., Chen, X., Chao, H. T., Deng, H., Rizo, J., Brose, N. & Rosenmund, C. Distinct domains of complexin I differentially regulate neurotransmitter release. *Nat. Struct. Mol. Biol.* **14**, 949-958 (2007).

82. Hanson, P.I., Roth, R., Morisaki, H., Jahn, R. & Heuser, J.E. Structure and conformational changes in NSF and its membrane receptor complexes visualized by quick-freeze/deep-etch electron microscopy. *Cell* **90**, 523-535 (1997).

83. Lin, R.C. & Scheller, R.H. Structural organization of the synaptic exocytosis core complex. *Neuron* **19**, 1087-1094 (1997).

84. Liu, W., Montana, V., Bai, J., Chapman, E.R., Mohideen, U. & Parpura, V. Single molecule mechanical probing of the SNARE protein interactions. *Biophys. J.* **91**, 744-758 (2006).

85. Li, F., Pincet, F., Perez, E., Eng, W.S., Melia, T.J., Rothman, J.E. & Tareste, D. Energetics and dynamics of SNAREpin folding across lipid bilayers. *Nat. Struct. Mol. Biol.* **14**, 890-896 (2007).

86. Abdulreda, M.H., Bhalla, A., Chapman, E.R. & Moy, V.T. Atomic force microscope spectroscopy reveals a hemifusion intermediate during soluble N-ethylmaleimide-sensitive factor-attachment protein receptors-mediated membrane fusion. *Biophys. J.* **94**, 648-655 (2008).

87. Kumaran, V. Instabilities due to charge-density-curvature coupling in charged membranes. *Phys. Rev. Lett.* **85**, 4996-4999 (2000).

88. Kim, Y.W. & Sung, W. Effects of charge fluctuation on two-membrane instability and fusion. *Phys. Rev. Lett.* **91**, 118101 (2003).

89. Toonen, R.F.G., de Vries, K.J., Zalm, R., Sudhof, T.C. & Verhage, M. Munc18-1 stabilizes syntaxin 1, but is not essential for syntaxin 1 targeting and SNARE complex formation. *J. Neurochem.* **93**, 1393-1400 (2005).

90. Lu, X., Zhang, Y. & Shin, Y.-K. Supramolecular SNARE assembly precedes hemifusion in SNARE-mediated membrane fusion. *Nat. Struct. Mol. Biol.* **15**, 700-706 (2008).

91. Rizo, J., Chen, X. & Arac, D. Unraveling the mechanisms of synaptotagmin and SNARE function in neurotransmitter release. *Trends Cell Biol.* **16**, 339-350 (2006).

92. Bai, J. & Chapman, E.R. The C2-domains of synaptotagmin-partners in exocytosis. *Trends Biochem. Sci.* **29**, 143-151 (2004).

93. Arac, D., Chen, X., Khant, H.A., Ubach, J., Ludtke, S.J., Kikkawa, M., Johnson, A.E., Chiu, W., Sudhof, T.C. & Rizo, J. Close membrane-membrane proximity induced by Ca^{2+}-dependent multivalent binding of synaptotagmin 1 to phospholipids. *Nat. Struct. Mol. Biol.* **13**, 209-217 (2006).

94. Brunger, A.T., Weninger, K., Bowen, M. & Chu, S. Single-molecule studies of the neuronal SNARE fusion machinery. *Annu. Rev. Biochem.* **78**, 903-928 (2009).

95. Klyachko, V.A. & Jackson, M.B. Capacitance steps and fusion pores of small and large-dense-core vesicles in nerve terminals. *Nature* **418**, 89-92 (2002).

96. Zhang, Q., Li, Y. & Tsien, R.W. The dynamic control of kiss-and-run and vesicular reuse probed with single nanoparticles. *Science* **323**, 1448-1453 (2009).

97. Chan, Y.H., van Lengerich, B. & Boxer, S.G. Effects of linker sequences on vesicle fusion mediated by lipid-anchored DNA oligonucleotides. *Proc. Natl. Acad. Sci. USA* **106**, 979-984 (2009).

98. Dennison, S.M., Bowen, M.E., Brunger, A.T. & Lentz, B. Neuronal SNAREs do not trigger fusion between synthetic membranes but do promote PEG-mediated membrane fusion. *Biophys. J.* **90**, 1661-1675 (2006).

99. Nickel, W., Weber, T., McNew, J.A., Parlati, F., Sollner, T.H. & Rothman, J.E. Content mixing and membrane integrity during membrane fusion driven by pairing of isolated v-SNAREs and t-SNAREs. *Proc. Natl. Acad. Sci. USA* **96**, 12571-12576 (1999).

100. Ohya, T., Miaczynska, M., Coskun, U., Lommer, B., Runge, A., Drechsel, D., Kalaidzidis, Y. & Zerial, M. Reconstitution of Rab- and SNARE-dependent membrane fusion by synthetic endosomes. *Nature* **459**, 1091-1097 (2009).

101. van den Bogaart, G., Holt, M.G., Bunt, G., Riedel, D., Wouters, F.S. & Jahn R. One SNARE complex is sufficient for membrane fusion. *Nat. Struct. Mol. Biol.* **17**, 358-364 (2010).

102. http://www.molecular-beacons.org/Introduction.html

103. Diao, J., Su, Z., Ishitsuka, Y., Lu, B., Lee, K.S., Lai, Y., Shin, Y.-K. & Ha T. A single vesicle content mixing assay for SNARE-mediated membrane fusion. *Nat. Commun.* **1**, 54 (2010).

104. Chanturiya, A. Chernomordik L.V. & Zimmerberg, J. Flickering fusion pores comparable with initial exocytotic pores occur in protein-free phospholipid bilayers. *Proc. Natl. Acad. Sci. USA* **94**, 14423-14428 (1997).

105. Jackson, M.B. Minimum membrane bending energies of fusion pores. *J. Membrane Biol.* **231**, 101-115 (2009).

106. Jackson, M.B. SNARE complex zipping as a driving force in the dilation of proteinaceous fusion pores. *J. Membrane Biol.* **235**, 89-100 (2010).

107. Bonifacino, J.S. & Glick, B.S. The mechanisms of vesicle budding and fusion. *Cell* **116**, 153-166 (2004).

108. Su, Z., Ishitsuka, Y., Ha, T. & Shin, Y.-K. The SNARE complex from yeast is partially unstructured on the membrane. *Structure* **16**, 1138-1146 (2008).

109. Chen, Y., Xu, Y., Zhang, F. & Shin, Y.-K. Constitutive versus regulated SNARE assembly: a structural basis. *EMBO J.* **23**, 681-689 (2004).

110. Pobbati, A.V., Stein, A. & Fasshauer, D. N- to C-terminal SNARE complex assembly promotes rapid membrane fusion. *Science* **313**, 673-676 (2006).

111. Weber, J.P, Reim, K. & Sorensen, J.B. Opposing functions of two sub-domains of the SNARE-complex in neurotransmission. *EMBO J.* **29**, 2477-2490 (2010).

112. Liu, W., Montana, V., Parpura, V. & Mohideen, U. Single molecule measurements of interaction free energies between the proteins within binary and ternary SNARE complexes. *J. Nanoneurosci.* **1**, 120-129 (2009).

113. Walter, A.M., Wiederhold, K., Bruns, D., Fasshauer, D. & Sorensen, J.B. Synaptobrevin N-terminally bound to syntaxin-SNAP-25 defines the primed vesicle state in regulated exocytosis. *J. Cell Biol.* **188**, 401-413 (2010).

114. Lee, H.-K., Yang, Y., Su, Z., Hyeon, C., Lee, T.-S., Lee, H.-W., Kweon, D.-H., Shin, Y.-K. & Yoon, T.-Y. Dynamic Ca^{2+}-dependent stimulation of vesicle fusion by membrane-anchored synaptotagmin 1. *Science* **328**, 760-763 (2010).

115. Wang, C.T., Lu, J.-C., Bai, J., Chang, P.Y., Martin, T.F.J., Chapman, E.R. & Jackson, M.B. Different domains of synaptotagmin control the choice between kiss-and-run and full fusion. *Nature* **424**, 943-947 (2003).

116. Bai, J.H., Wang, C.T., Richards, D.A., Jackson, M.B. & Chapman, E.R. Fusion pore dynamics are regulated by synaptotagmin/t-SNARE interactions. *Neuron* **41**, 929-942 (2004).

117. Weninger, K., Bowen, M.E., Choi, U.B., Chu, S. & Brunger, A.T. Accessory proteins stabilize the acceptor complex for synaptobrevin, the 1:1 syntaxin/SNAP-25 complex. *Structure* **16**, 308-320 (2008).

118. de Wit, H., Walter, A.M., Milosevic, I., Gulyas-Kovacs, A., Riedel, D., Sorensen, J.B. & Verhage, M. Synaptotagmin-1 docks secretory vesicles to syntaxin-1/SNAP-25 acceptor complexes. *Cell* **138**, 935-946 (2009).

119. Takahashi, N., Hatakeyama, H., Okado, H., Noguchi, J., Ohno, M. & Kasai, H. SNARE conformational changes that prepare vesicles for exocytosis. *Cell Metab.* **12**, 19-29 (2010).

120. Vrljic, M., Strop, P., Ernst, J.A., Sutton, R.B., Chu, C. & Brunger, A.T. Molecular mechanism of the synaptotagmin-SNARE interaction in Ca^{2+}-triggered vesicle fusion. *Nat. Struct. Mol. Biol.* **17**, 325-331 (2010).

121. Choi, U.B., Strop, P., Vrljic, M., Chu, S., Brunger, A.T. & Weninger, K. Single molecule FRET-derived model of the synaptogagmin 1-SNARE fusion complex. *Nat. Struct. Mol. Biol.* **17**, 318-324 (2010).

122. Rickman, C. & Davletov, B. Mechanism of calcium-independent synaptotagmin binding to target SNAREs. *J. Bio. Chem.* **278**, 5501-5504 (2003).

123. Hui, E., Johnson, C.P., Yao, J., Dunning, F.M. & Chapman, E.R. Synaptotagmin-mediated bending of the target membrane is a critical step in Ca^{2+}-regulated fusion. *Cell* **138**, 709-721 (2009).

124. Sorensen, J.B. Conflicting views on the membrane fusion machinery and the fusion pore. *Annu. Rev. Cell Dev. Biol.* **25**, 513-537 (2009).

125. Chen, X., Arac, D., Wang, T.-M., Gilpin, C.J., Zimmerberg, J. & Rizo, J. SNARE-mediated lipid mixing depends on the physical state of the vesicles. *Biophys. J.* **90**, 2062-2074 (2006).

126. Mima, J., Hickey, C., Xu, H., Jun, Y. & Wickner, W. Reconstituted membrane fusion requires regulatory lipids, SNAREs and synergistic SNARE chaperones. *EMBO J.* 27, 2031-2042 (2008).

127. Rust, M.J., Bates, M. & Zhuang, X. Sub-diffraction-limit imaging by stochastic optical reconstruction microscopy (STORM). *Nat. Methods* **3**, 793-796 (2006).

128. Bates, M., Huang, B., Dempsey, G.T. & Zhuang, X.W. Multicolor super-resolution imaging with photo-switchable fluorescent probes. *Science* **317**, 1749-1753 (2007).

AUTHOR'S BIOGRAPHY

Jiajie Diao was born in Chengdu, P.R. China. He attended Xi'an Jiaotong University in Xi'an, P.R. China and graduated with a B.S. degree in applied physics in 2001. He came to the USA to begin his graduate study at George Washington University in the summer of 2002 and joined Prof. Mark E. Reeves' lab, where he received a M.A. degree in physics. In the fall of 2005, he transferred to University of Illinois at Urbana-Champaign and joined the lab of Prof. Taekjip Ha for a Ph.D. degree in physics.